A Fluorescence based Wireless Capsule Endoscopic Tool for Screening Gastrointestinal Cancer

A Thesis Submitted to the

College of Graduate and Postdoctoral Studies

In Partial Fulfillment of the Requirements

For the Degree of Philosophy

In the Department of Electrical and Computer Engineering

University of Saskatchewan

Saskatoon

By

Mohammad Wajih Alam

PERMISSION TO USE

In presenting this thesis in partial fulfillment of the requirements for a Postgraduate degree from the University of Saskatchewan, I agree that the Libraries of this University may make it freely available for inspection. I further agree that permission for copying of this thesis in any manner, in whole or in part, for scholarly purposes may be granted by the professor or professors who supervised my thesis work or, in their absence, by the Head of the Department or the Dean of the College in which my thesis work was done. It is understood that any copying or publication or use of this thesis or parts thereof for financial gain shall not be allowed without my written permission. It is also understood that due recognition shall be given to me and to the University of Saskatchewan in any scholarly use which may be made of any material in my thesis/dissertation.

Requests for permission to copy or to make other uses of materials in this thesis in whole or part should be addressed to:

Head of the Department of Electrical and Computer Engineering
57 Campus Drive
University of Saskatchewan
Saskatoon, Saskatchewan, S7N 5A9, Canada

OR

Dean
College of Graduate and Postdoctoral Studies,
University of Saskatchewan
116 Thorvaldson Building, 110 Science Place
Saskatoon, Saskatchewan, S7N 5C9, Canada

ABSTRACT

Colorectal cancer is the second leading cause of cancer related deaths in the United States when men and women are combined. It is also the third most common type of cancer diagnosed in both women and in men. The phase at which the cancer is diagnosed is an important factor in deciding the prognosis of the patient. Despite the technological advancement in therapeutic and diagnostic field, the colorectal cancers are often spotted in advanced stage which affects the survival rate of patients adversely. Thus, early detection of cancer is important to improve the survival rate of patients.

The conventional wired endoscopic system is an invasive process in which a flexible and long cable is inserted into the digestive tube which makes the process uncomfortable and painful for the patients. This makes the patient to not want to go through the procedure, ultimately hampering the early detection process. In order to relieve the patient's suffering and visualize the gastrointestinal (GI) tract, Wireless Capsule Endoscopy (WCE) is introduced. A typical WCE is a pill-sized swallowable capsule integrated with electronics, camera, optics and wireless connectivity feature, which provides an opportunity to diagnose the GI tract through a simple and pain-free procedure. However, there are still several limitations of this technology which limits its functionality in the modern-day healthcare system. One of these challenges is related to image quality and frame rate. Higher frame rate and improved resolution increases the ability to detect more landmarks and lesions while decreasing the probability of missing important information. Although capturing of high-resolution image is now possible due to the rapid advancement in imaging technology, integrating such cameras into the world of WCE and transmitting high quality captured images would significantly affect the battery life. Therefore, a high-quality compression method is required that would reduce the impact on battery life while preserving image quality.

However, the available compression algorithms are lossy and needs complex system architecture and on-chip memory. Moreover, this technology captures thousands of images from each examination. As these capsules are not able to automate the detection of abnormality, the doctors are required to go through each frame in search of abnormality which is time-consuming and tiresome. Thus, alternate methods are needed to be explored.

Fluorescence imaging is widely used in various fields for selective and specific detection of target. In order to test the principle of fluorescence imaging, a fluorometer is designed in this work to detect breast cancer cells (MDA-MB-231) and colorectal cancer cells (HCT116). The breast cancer cells are conjugated with Green Fluorescent Protein (GFP) while the colorectal cancer cells are conjugated with IRFP702 fluorophore as explained in Chapter 4 and 5 respectively. The excitation and emission wavelength of GFP and IRFP702 fluorophores are different. The developed fluorometer can detect both breast cancer cells and colorectal cancer cells when excitation and emission components are modified to cover the excitation and emission wavelengths of respective conjugated fluorophores.

After the proof-of-concept is established, a WCE prototype is developed which utilizes the principle of fluorescence for automating the detection of colorectal cancer. The prototype is tested on porcine intestine and liquid phantom. The developed device can detect low-level of fluorescence emitted by fluorophore. This was tested by first spraying varying concentration of fluorescein (18 nM to 231μM) on top of the swine intestine and testing with the developed device. This device paves a way for pain-free, non-invasive screening for early stage detection of cancer promoting mass-screening and ultimately improving the survival rate of the patients. By utilizing the proposed capsule with targeted molecular contrast agents, which are selectively probed to the

cancerous cells, early detection of the multiple types of cancer could be possible with increased sensitivity and at a relatively low cost.

ACKNOWLEDGEMENTS

Table of Contents

LIST OF FIGURES

LIST OF TABLES

ABBREVIATIONS AND SYMBOLS

ADC	Analog to Digital Converter
BER	Bit Error Rate
BPP	Bits Per Pixel
CCD	Charge Coupled Device
CFA	Color Filter Array
CMOS	Complementary Metal-Oxide Semiconductor
CR	Compression Ratio
CRC	Colorectal Cancer
DCT	Discrete Cosine Transform
DMEM	Dulbecco's Modified Eagles Medium
DPCM	Differential Pulse Code Modulation
DVC	Distributed Video Coding
DWT	Discrete Wavelet Transform
FDA	Food Drug Administration
FIFO	First-In-First-Out
FPS	Frame Per Second
FR	Frame Rate
GFP	Green Fluorescent Protein
GI	Gastro Intestinal
HSL	Hue, Saturation, Lightness
JPEG	Joint Photographic Experts Group
LCD	Liquid Crystal Display
LDO	Low Dropout Regulators

LED	Light Emitting Diode
LPF	Low-Pass Filter
LSB	Least Significant Bit
LZ	Limpel-Ziv
LZW	Limpel-Ziv-Welch
MCE	Magnetically-Controlled Capsule Endoscope
MPEG	Moving Picture Experts Group
MRI	Magnetic Resonance Imaging
PCB	Printed Circuit Board
PD	Pixel Depth
PSNR	Peak Signal-to-Noise Ratio
PWM	Pulse Width Modulation
RF	Radio Frequency
RGB	Red, Green, Blue
ROI	Region of Interest
SB	Small Bowel
UV	Ultraviolet
VCE	Video Capsule Endoscopy
WCE	Wireless Capsule Endoscopy

1. Introduction

1.1 Research Context and Motivation

Endoscopic procedures have improved tremendously in past two decades. From the introduction of the device, Lichtleiter, in 1806 by Philipp Bozzini to the current flexible endoscopic procedure, the advanced technologies have not only made the diagnostic procedure accurate but also reduced pain for patients. The tube used in these wired endoscopic procedures are now more flexible as it utilizes advanced materials rather than using thick tube. The modern endoscopes also come with advanced tools, such as forceps. The advances in imaging technology has also introduced small cameras in the world of endoscopy, making high resolution imaging possible. Despite the drastic advancement in endoscopic procedure, the process is still painful and uncomfortable for patients. The patients are often sedated in order to reduce pain and trauma that comes with this technology. It also affects the privacy of the patient.

To solve these problems, wireless capsule endoscopy (WCE) was first introduced by Iddan *et al.* in the beginning of 21st century to examine human gastrointestinal (GI) tract. This painless and non-invasive swallowable wireless endoscopic pill enables the visualization of digestive tract without the need of anesthesia. Although this capsule removes patient's discomfort and pain that is associated with traditional endoscopic procedure, there are still many limitations (automation, image quality, battery life, frame rate, localization, etc.) of using WCE systems which hinders its application in the current medical system.

A typical WCE system consists of a pill sized electronic capsule which is 11 mm in diameter and 24-28 mm in length. In addition to these, the WCE system consists of a data logger with RF antenna and a workstation computer. The front part of a capsule constitutes of a transparent optical dome from where the lights from light emitting diodes (LEDs) illuminate the walls of the GI tract and a micro camera captures images and transmits it wirelessly to an external data logger via a transmitter. The LEDs are placed in a circular pattern around the camera for homogeneous illumination. Once a patient swallows the capsule, he/she can go on with their

normal day-to-day activities. The capsule passes through the GI tract in a passive motion through natural peristalsis from esophagus to colon. Depending on the vendor and its use, the frame rate and battery life of capsule varies. The frame rate ranges from 2 to 35 frames per second and the battery life ranges from 0.5 to 480 hour depending upon the type of capsule used [C1.1]. During the lifetime of capsule, it captures about 55,000 to 120,000 images and sends it to the data logger for storage. Most commercial capsules are not reusable. Once the process is over, the patient returns to the clinic and hands over the data logger to the physician who then connects the data logger to the workstation computer. The physician downloads the data and analyzes the captured images going frame-by-frame in search of abnormality on the vendor's specialized software. The software usually encodes the captured images into a video for the physician to review. Since the captured images are large in number, the doctor is required to go through the captured images in search of abnormality which makes this technology tiresome.
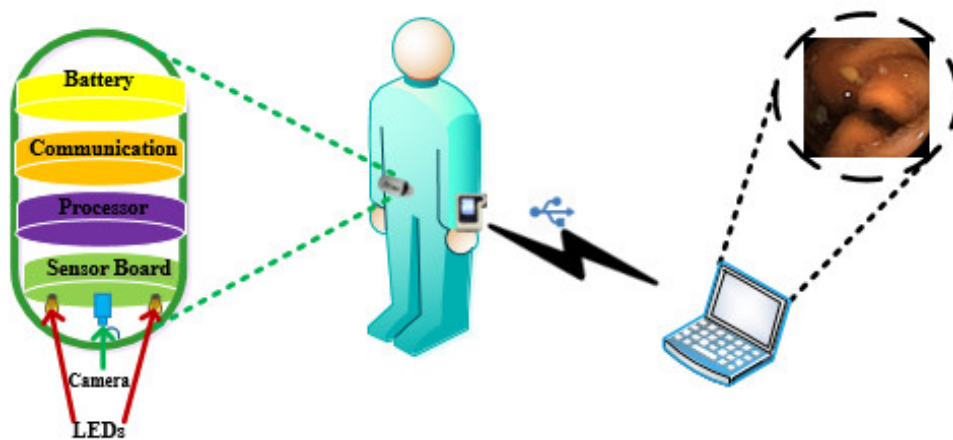
Figure 1.1 A typical WCE system

Colorectal cancer (CRC) is one of the common types of cancer diagnosed around the world and is being actively studied throughout the past few decades. It is the third most commonly diagnosed type of cancer and is also the fourth most leading cause of cancer related deaths in the world. It is estimated that about 2.2 million new cases of CRC will be diagnosed by 2030 leading to an increase of 60% [C1.2]. Study has shown that early detection and removal of the colorectal

cancer can decrease the mortality rate by up to 53% [C1.3]. The conventional processes are invasive, often demands high cost with respect to money and comfortability. Moreover, the gold standard colonoscopy directly hampers privacy of patient which is why the patients usually do not want to go to the physicians directly until the cancer is advanced to a later stage. As a result, the cancers are detected in a later stage which results in delayed and inefficient treatment. An ideal colorectal screening process is still needed which at least should have the following characteristics:

a. Should provide high diagnostic accuracy
b. Acceptable patient privacy
c. Minimize error resulting from operator
d. Avoid future health risk.
e. Should be affordable by mass population.
f. An automated system for detection.
g. Provide low health risk

In present world, an ideal procedure to screen colorectal cancer does not exist and the existing procedure does have trade-off among the above-listed characteristics. Hence, a reliable, sensitive, non-invasive colorectal screening technology would be an attractive choice for patients who are uncomfortable going through the traditional screening procedure or the patients who have medical condition which does not allow them to go through the conventional procedures. Although WCE system has been introduced to remove some limitations of existing endoscopic technology, the WCE itself has some limitations which has restricted its wide use in current healthcare system. The usual lifespan of a typical WCE capsule is about 8 hours. A typical PillCam Colon 2 capsule generates about 144,000 images over its 10-hour lifespan as it transits through the digestive system. Once the WCE process is completed in a typical scenario, a doctor is needed to sit in front of the computer analyzing each image carefully in search of abnormal frames. This makes the process uncomfortable, tiresome and time-consuming. Therefore, a system is needed by which the capsule will be able to automate the detection. If the capsule shows a positive sign of having cancer, the doctors would proceed forward with other forms of treatment which would save time and improve diagnostic accuracy. Since the patient would be comfortable to go through the process, it would also help in early detection of cancer. In this work, a WCE system will be

designed and developed which will utilize the property of fluorescence in order to automate the detection process of colorectal cancer.

1.2 Research Goals

The main goal of this research is to design and develop a prototype of a WCE system which utilizes the principle of fluorescence for screening colorectal cancer. In order to achieve this goal, following research objectives are set to achieve the goal.

1. Identify the strengths and limitation of current generation of WCE system and explore different ways by which the limitations can be addressed.
2. Build a fluorometer which utilizes the principle of fluorescence to detect breast cancer cells conjugated with a fluorophore (GFP).
3. Test the built fluorometer to detect colorectal cancer cells when conjugated with a different fluorophore (IRFP702) utilizing the principle of fluorescence. This experiment helps to realize multi-modal detection of abnormality.
4. Design and develop a WCE system utilizing the principle of fluorescence and evaluate different combination of sensors, electronic components, and dye which covers the excitation and emission range of the selected fluorophore.
5. Investigate the optimum arrangement of electronic and optical component so that the device is in capsular form. The capsule should be affordable by mass population and minimize error resulting from operator.
6. Evaluate the performance of the fluorescence based wireless endoscopic pill in a more realistic scenario, animal testing of the capsule (*ex-vivo*) is performed on swine intestine.

1.3 Organization of the Thesis

The thesis is organized in a manuscript-based style. The first chapter of the thesis presents the overview of WCE system, motivation of the thesis, and objectives of the research. The main content and contributions of the thesis are included in the form of published manuscripts. The remainder of the thesis is organized as follows.

Chapter 2 presents relevant research background and works that have proposed wireless capsule endoscopic and non-wireless based solutions for colorectal cancer. The manuscript in Chapter 3 presents the compression algorithms utilized in present WCE systems and presents a possible solutions and trade-offs in choosing the compression algorithm for efficient operation of WCE system. This helps to better realize the limitation present in current imaging-based capsule. Finally, summary and future recommendations are presented in Chapter 3.

The manuscript in Chapter 4 describes the development of a low-cost fluorometer to detect breast cancer cells conjugated with GFP. This work helps to realize the importance of utilizing principle of fluorescence for selective and specific detection of breast cancer cells. The manuscript in Chapter 5 presents the development of fluorometer to detect colorectal cancer conjugated with IRFP702. This chapter helps to realize the possibility of multi-modal detection of cancer cells by slight modification in the detection and excitation components based on conjugated fluorophore.

The manuscript in Chapter 6 presents the development of a WCE system for screening colorectal region utilizing the principle of fluorescence. This device is tested ex-vivo on swine intestine and liquid phantom with various concentration of fluorophore. Finally, summary of accomplishment and future recommendations are presented in Chapter 7.

References

[C1.1] Alam, M.W.; Sohag, M.H.A.; Khan, A.H.; Sultana, T.; Wahid, K.A. IoT-Based Intelligent Capsule Endoscopy System: A Technical Review. In Intelligent Data Analysis for Biomedical Applications; Hemanth, J., Gupta, D., Balas, V.E., Eds.; Elsevier: Amsterdam, The Netherlands, 2019; pp. 1–20, ISBN 978-0-12-815553-0.

[C1.2] Arnold, M.; Sierra, MS., Laversanne M.; Soerjomataram, I.; Jemal, A.; Bray, F. Global patterns and trends in colorectal cancer incidence and mortality. Gut 2017;66:683-691.

[C1.3] "Colonoscopy reduces deaths" [Online]. Available: https://www.cancer.gov/types/colorectal/research/colonoscopy-reduces-deaths. [Accessed: 05-July-2020].

2. Research Background

About 20 million people in Canada and 70 million people in United States of America suffer from diseases related to digestive system annually [C2.1, C2.2]. Hence the tools and techniques that are used to diagnose GI disorders are becoming important and popular. Over the last couple of decades, many tools and techniques have been introduced to assist physicians in diagnosing patients who are suffering from diseases related to digestive system. However, these procedures require skilled manpower, needs sedation and brings patient discomfort. The endoscopic procedures are considered invasive and painful as well. Thus, there was a need to introduce a reliable technology which was non-invasive and could enable visualization of GI tract accurately. In this context, a WCE system was introduced which offered non-invasive imaging of GI tract without the need of surgery or painful procedure.

The first commercial endoscopic capsule was developed by Given Imaging (Yoqneam, Israel) in the mid-1990s and was termed as PillCam. This capsule was approved by Food and Drug Administration (FDA) in the year 2001 [C2.3]. Given Imaging further enhanced this project and developed few more specific targeted capsules to detect the disease in colon, small intestine and oesophagus. These capsules were termed as: PillCam Colon, PillCam (SB, SB2 & SB3) and PillCam ESO respectively. More than a million capsule endoscopy systems have already been used in clinics worldwide and more than 1000 peer-reviewed publications have now appeared in literature which shows its growing popularity. Most of these WCE systems are composed of three parts: a non-reusable capsule, data logger and a workstation computer as shown in Fig. 1. The WCE capsules weighs in between 3.3-6 grams, the size ranges in between 10-11mm diameter and 24-32 mm in length, and the operating time varies from 8-12 hours depending upon the vendor. Although these capsules are bigger in size than a regular capsule, these capsules are small enough that they can be swallowed. A typical capsule consists of an imaging module (CCD or CMOS camera), illumination modules (4-6 white LEDs per camera), batteries, telemetry system (transmitter), etc. The capsule can generate about 50,000-120,000 image based on the manufacturer. In addition to radio frequency, other medium can also be used for communication, such as: ultrasound, human body or magnetic field. The data logger is connected to a sensor array

which is fixed on the patient's abdomen via adhesive pads. In PillCam SB3 capsule, entire sensor array is enclosed in a belt which can be worn around patient's waist.

Following the trend of PillCam, there were several other companies which developed capsules (Patency capsule [C2.4], EndoCapsule [C2.5], CapsoCam [C2.6], MiroCam [C2.7], OMOM capsule [C2.8]) and are now available commercially in the market. Each capsule from different manufacturer has its own strengths and weaknesses. PillCam Colon is a specialized capsule endoscopy system especially designed to screen colorectal region. The latest version of PillCam Colon 2 is slightly larger than PillCam SB capsule measuring 11.6 x 31.5mm. It consists of two image sensors. The field of view is increased in this version which covers 172 degrees [C2.9]. However, increasing the field of view resulted in low resolution of images. This capsule captures images at 4 frame per second when in stationary and at 35 frame per second when in motion [C2.10] i.e. the camera captures a minimum of 144,000 frames during its lifetime when capturing at 4 frames per second. The images are received and saved by data logger through an antenna-led array. The clinician downloads the data to the computer after the process is over for post-processing. This is a promising capsule but further improvements as well as studies are needed before it can replace colonoscopy. Currently, this capsule is mostly used for patients who had incomplete history of colonoscopy or for those patients who don't want to go through the process of other endoscopic procedure [C2.11].

Although the endoscopic system which uses white light imaging can now provide high resolution of images, the post-processing heavily relies on the expertise of a physician who is going through frames in order to find the abnormalities. Such analysis requires the patient to have very distinct morphological changes in order to be diagnosed accurately. The distinct morphological changes often appear very late, thus hampering the overall diagnostic process. Despite tremendous advancement of therapeutic and diagnostic possibilities, colorectal cancer in patients are often detected in advanced stage and the survival rate for such patients is 14%. However, if the same cancer was diagnosed at an early stage, the chances of survival can increase to 90% [C2.12]. In addition to having a difficult access to GI tract, the long period of time without any specific symptom for cancer further makes it problematic to detect such cancer at its early stage [C2.13]. It has always been difficult to distinguish between tumor and inflammation at its early stage which leads to diagnostic delay. Defining the border of tumor at its advanced stage clinically is also

7

problematic. That is why, the surgeons still greatly rely on histopathological and biopsies outcome which is again time-consuming.

New techniques, based on the principle of light, are needed to be introduced to the world of endoscopy system to improve the abnormality detection rate. Fluorescence imaging has already proved to be efficient in diagnosing early gastric cancer over white light imaging technology with greater sensitivity and efficiency. Fluorescence imaging is an exciting and popular technique used by modern biologists as it allows them to differentiate between different objects of interest. Because of its intrinsic selectivity, it is now one of the most important part of microscopy in the field of biology where specific molecules, like fluorophores, absorb light at certain wavelength and emits at a different higher wavelength. Due to its large spectral range, it is often possible to image different cellular, subcellular and molecular structures at the same time. Also, different fluorescent products (like, green fluorescent protein) allows biologists to genetically tag protein of living beings. These promising non-invasive imaging techniques should be able to distinguish between benign and malignant cell, normal and tumor cell, and between inflammation and early cancer cell. When introduced to capsule endoscopy system, these techniques will further be able to aid in the localization and provide instant diagnosis of abnormal tissues and hence provide better image contrast, resolution and detailed information. As such, the development of fluorescent imaging technique is a growing field for the detection of early cancerous cell which can provide real-time information about the location, size and metastasis of tumor cell. It does so by providing specific contrast between cancer and normal cell. The change in contrast between normal and tumor cell is due to the biochemical and morphological changes in these tissues which alters the optical properties and leads to specific tissue based autofluorescence. Targeted fluorescence can also be achieved with the help of fluorescent probes where an external labelling agent (For example, fluorescein or Green Fluorescent Protein) is introduced inside the body intravenously to target specific cancer cells. This fluorescence imaging technique has proved to be very useful for the detection of early cancer with great accuracy and sensitivity in comparison to white light imaging. Fluorescence guided endoscopy has already shown some promising result as this technique has resulted in the increase in detection rate of tumors by 30% and caused reduced in tumor recurrence by 20% [C2.14]. A system to automate detection of colorectal cancer utilizing the principle of fluorescence with a WCE system is still an open topic for research.

References

[C2.1] "Digestive Conditions - Canadian Digestive Health Foundation." [Online]. Available: https://cdhf.ca/digestive-disorders/. [Accessed: 19-April-2020].

[C2.2] "Digestve Diseases statistics for the United States" [Online]. Available: https://www.niddk.nih.gov/health-information/health-statistics/digestive-diseases [Accessed: 19-April-2020].

[C2.3] P. V Waghmare, C. V Panchal, and B. N. Poul, "Swallowable wireless capsular endoscopy: A novel breakthrough in the biomedical industry and future progress," *Int. J. Pharm. Sci. Res.*, vol. 4, no. 11, pp. 4133–4144, 2013.

[C2.4] Á.´ Caunedo-Álvarez, J. Romero-Vazquez, and J. M. Herrerias-Gutierrez, "Patency© and agile© capsules," *World J. Gastroenterol.*, vol. 14, no. 34, pp. 5269–5273, 2008.

[C2.5] "EndoCapsule." [Online]. Available: https://medical.olympusamerica.com/. [Accessed: 14-April-2020].

[C2.6] "CapsoCam Endoscopy system" [Online]. Available: https://capsovision.com/us/. [Accessed: 14-April-2020].

[C2.7] "Intromedic MiroCam Capsule Endoscope System" [Online]. Available: https://www.intromedic.com:549/eng/item/item_010100_view.asp?search_kind=&gotopag e=1&no=3. [Accessed: 14-April-2020].

[C2.8] "OMOM Capsule Endoscopy System" [Online]. Available: http://english.jinshangroup.com/capsuleendoscopy.html [Accessed: 14-April-2020].

[C2.9] M. E. R. Cristiano Spada, Fabio De Vincentis, Paola Cesaro, Cesare Hassan and A. Z. and G. C. Leonardo Minelli Grazioli, Santiago Bolivar, "Accuracy and safety of second-generation PillCam COLON capsule for colorectal polyp detection," *Therap. Adv. Gastroenterol.*, vol. 5, no. 3, pp. 173–178, 2012.

[C2.10] S. N. Adler and Y. C. Metzger, "PillCam COLON capsule endoscopy: recent advances and new insights," *Therap. Adv. Gastroenterol.*, vol. 4, no. 4, pp. 265–268, 2011.

[C2.11] S. Noh Hong, S.-H. Kang, H. Joo Jang, and M. B. Wallace, "Recent Advance in Colon Capsule Endoscopy: What's New?," *Clin Endosc*, vol. 51, pp. 334–343, 2018.

[C2.12] "Colorectal Cancer: Statistics | Cancer.Net." [Online]. Available: https://www.cancer.net/cancer-types/colorectal-cancer/statistics. [Accessed: 03-April-2020]

[C2.13] "Colorectal Cancer: Symptoms and Signs | Cancer.Net." [Online]. Available: https://www.cancer.net/cancer-types/colorectal-cancer/symptoms-and-signs. [Accessed: 03-April-2020].

[C2.14] M-A. D'Hallewin, L. Bezdetnaya, F. Guillemin, "Fluorescence detection of bladder cancer: A review", European Urology, Vol. 42 (5), pp. 417-425.

3. Are Current Advances of Compression Algorithms for Capsule Endoscopy Enough? A Technical Review

The majority of commercially available WCE system is image based. It is important to know the pros and cons of existing system to find the research gap and propose a solution. This chapter reviews the compression algorithms that are used in WCE systems and presents its advantages and disadvantages. WCE has paved a way for painless diagnosis and introduces a possibility of screening entire GI tract, promoting mass screening. However, there are still several challenges of this technology: low frame rate, low image quality, low data-rate for telemetry, inability to perform automatic detection of abnormalities, etc. Increasing resolution and frame rate of the WCE system significantly increases power consumption during RF transmission. Absence of efficient compression also affects on-chip memory, system architecture, and battery life of the system. It is found from this review that the search for an efficient compression algorithm that can overcome the challenges still remains open. It is also concluded that alternative approaches should be explored for automating the detection of abnormality using this technology. The commercial capsule SB2 and SB3 were also tested on horse to know the limitation of existing WCE system which is presented in a published manuscript and not included in this thesis [3A].

[3A] Julia B. Montgomery, Jose L. Bracamonte, Mohammad Wajih Alam, Alimul H. Khan, Shahed K. Mohammed, Khan A. Wahid. Is there an application for wireless capsule endoscopy in horses?. Can Vet J. 2017;58(12):1321–1325.

The analysis and findings of this chapter is reported in the below mentioned published journal manuscript. The student contributed to literature review, writing the original draft and revision of the manuscript.

M. W. Alam, M. M. Hasan, S. K. Mohammed, F. Deeba and K. A. Wahid, "Are Current Advances of Compression Algorithms for Capsule Endoscopy Enough? A Technical Review," in IEEE Reviews in Biomedical Engineering, vol. 10, pp. 26-43, 2017.

Are Current Advances of Compression Algorithms for Capsule Endoscopy Enough? A Technical Review

Mohammad Wajih Alam, Md. Mehedi Hasan, Shahed Khan Mohammed, Farah Deeba, and Khan A. Wahid

Abstract

The recent technological advances in capsule endoscopy system have revolutionized the healthcare system by introducing new techniques and functionalities to diagnose gastrointestinal tract. These techniques improve diagnostic accuracy and reduce the risk of hospitalization. Although many benefits of capsule endoscopy are known, there are still limitations including lower battery life, higher bandwidth, poor image quality and lower frame rate, which have restricted its wide use. In order to solve these limitations, the importance of a low-cost compression algorithm, that produces higher frame rate with better image quality and yet consumes lower bandwidth and transmission power, is paramount. While several review papers have been published describing the capability of capsule endoscope in terms of its functionality and emerging features, an extensive review on the compression algorithms from past and for future applications is still of great interest. Hence, in this review, we aim to address the issue by exploring the characteristics of endoscopic images, analyzing the strengths and weaknesses of useful compression techniques, and making suggestions for possible future adaptation.

Index Terms

Compression algorithm, capsule endoscopy, endoscopic images, image processing, image reconstruction

3.1 Introduction

In order to diagnose gastrointestinal (GI) abnormalities, such as obscure GI bleeding, Crohn's disease, celiac disease, etc., endoscopic procedures play a vital role by enabling the view of human GI including the esophagus, large bowel, colon, and parts of the small intestine [C3.1]–[C3.4]. The typically used conventional endoscopy system, known as wired endoscopy, creates discomfort for patients as it requires a flexible and long cable to be pushed into the digestive tube [C3.5], [C3.6], making the patient endure a painful and uncomfortable procedure. Moreover, wired endoscopy cannot reach certain areas of the GI tract, such as a significant part of the small bowel [C3.3], [C3.7]. In order to relieve patients' suffering and view the entire small intestine, wireless capsule endoscopy (WCE) or video capsule endoscopy (VCE) are options used in modern days. WCE is a promising technology, integrated with a camera and wireless connectivity feature, which provides an opportunity to diagnose the entire GI tract through a simple, noninvasive, and pain-free procedure.

| *a* | *b* | *c* | *d* |
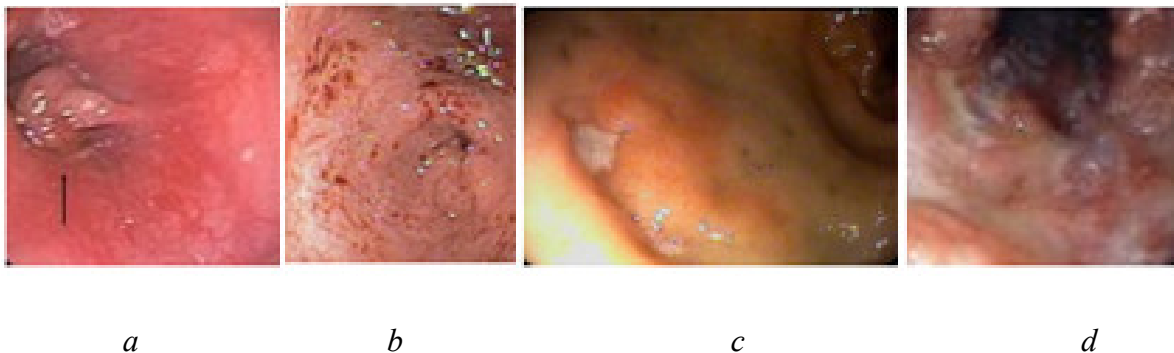
Figure 3.1 Endoscopic images: (a) esophageal polyp, (b) severe antral gastritis in stomach, (c) duodenal ulcer, and (d) crohn's disease in ileum (Courtesy: NASPGHAN) [3.15]

Despite many advantages of WCE, this technology still has several limitations [C3.8], [C3.9]. In 2000, a commercial product known as PillCam was introduced by Given Imaging Ltd., Israel [C3.3], [C3.10], [C3.11]. Today, there are many commercial capsules with similar functionalities. The image quality and the frame rate of current generation WCE capsules are inferior compared to that of wired endoscopy; a frame rate of 2–6 frames per second (fps) is usually achieved in PillCam (see Section II) where 10 fps is desired for diagnosis [C3.9]. Some sample

endoscopic images with different diseases are shown in Fig. 3.1. The image resolution needs to be enhanced as the diagnostic is error-prone due to the low resolution of the captured images [C3.12]. Increasing the resolution causes a significant increase in power consumption during radio frequency (RF) transmission. Moreover, the on-chip memory and complex system architecture also add to power consumption [C3.12]. Hence, capsule battery life is another critical constraint, which should supply enough power to run for more than 16 h [C3.6], [C3.12] and is essential for increased completion rates [C3.13], [C3.14] in the absence of efficient compression.

a   *b*
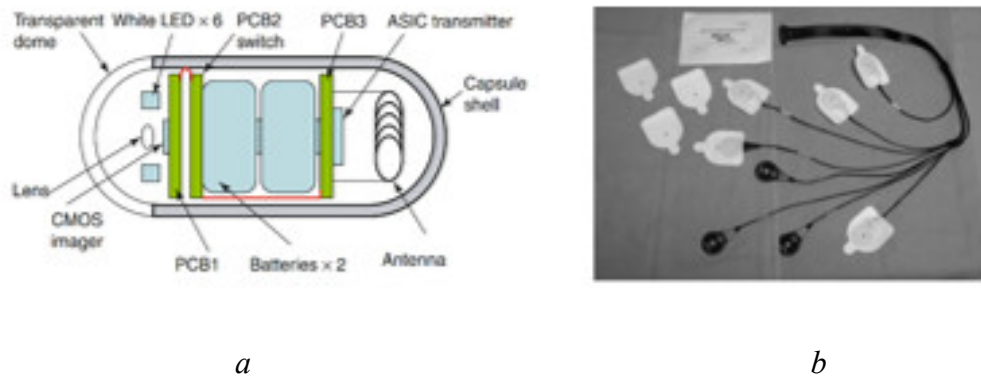
Figure 3.2 Endoscopic capsule: (a) schematic view of the capsule and its components [C3.16], and (b) recording unit and sensors [C3.2].

Figure 3.3 Commercial capsule endoscopes [C3.16]. Left to right: Agile patency capsule, PillCam SB2, EndoCapsule, CapsoCam, MiroCam, OMOM capsule, PillCam ESO, and PillCam COLON2.

Therefore, to satisfy the requirement of high image resolution along with high frame rate while keeping the power consumption low, image compression must be applied [C3.112]. There have been a significant number of works on the optimization of the image compression algorithms for saving power consumption as well as for improving visual image quality. This paper provides a technical review of all state-of-the-art image and data compression algorithms used in capsule endoscope systems with an attempt to help researchers in finding the optimum parameters and compression methodology.

3.2   Wireless Capsule Endoscopy System

3.2.1 Capsule System

Conventionally, a capsule endoscope system comprises three parts: the ingestible capsule, a portable image-recording belt or jacket, and a workstation computer with image processing software (see Fig. 3.2). The swallowable electronic capsule captures images during its transit through the GI tract, processes the images, and then transmits the data to a data-receiving unit through an RF channel. In the image-recording subsystem, almost every system uses eight body leads/antennas (except three leads in esophageal operation and 14 leads in the OMOM capsule system). The body leads are attached to the abdomen and the chest, which helps in the detection of the position of the capsule. In the workstation computer, powerful software is used to process the recorded images [C3.2]. Fig. 3.3 shows several commercially available endoscopy capsules while Table 3.1 presents technical specifications of those capsules.

3.2.2 Commercially Available Capsules

Most commercially available WCE systems use image compression techniques embedded in the capsule hardware. Although much information about the specific compression algorithm is not available, the patents published by the inventors provide some information about the compression algorithm adopted by them. Given Imaging is a pioneer in the field of capsular endoscopy and commercializes solutions for different parts of GI tracts, for example, the PillCam SB for the small intestine, PillCam ESO for esophageal imaging, and PillCam COLON for the

large intestine. All these products use a complementary metal-oxide semiconductor (CMOS) image sensor as the imager but differ mainly in frame rate, resolution, and battery life as shown in Table 3.1. Initially, Given Imaging proposed a system [C3.17] comprising a data compression unit, which would compress the image data using a JPEG or MPEG compression algorithm. Later, it proposed an in vivo compression system [C3.18], where mosaic image data are transformed into another color space (Y, Cb, Cr, Gdiff) and then directly compressed by a compression module, which is integral to the imager, by implementing fast efficient and lossless image compression system (FELICS) compression. A compression ratio (CR) of 4–8 can be achieved by adopting this algorithm. It has also proposed an alternate method of compression [C3.20] where subsequent images will be compared, and then only the differences between the images would be transmitted, rather than each image. Another proposal explores the possibility of variable frame rates for different parts of the GI tract, where compression will be adopted in the case of a higher frame rate. In addition, a spatially varying dilution pattern has been proposed taking into account the nonuniform resolution of the endoscopic image due to the adopted optical system in a capsule endoscope [C3.21].

Olympus Corporation proposed a conventional compression algorithm [C3.22] for a capsule endoscope, where pixels interpolation from the raw data is followed by a compression algorithm. Innurvation Inc. has brought out a new concept [C3.23] of variable resolution and/or variable magnification scanning system which implicitly reduces data by varying frame rate and resolution, depending on the speed of the capsule. In the case of low-resolution images, data are compressed by combining groups of pixels. However, MiroCam capsules do not use data compression and RF for wireless data transmission [C3.24].

Though it obviates the requirement for a high-frequency modulation process and antenna driving, according to the survey [C3.25], the speed of body area network in endoscopic applications is around 2 Mbps, which limits its operation at 3 fps. Recently, Ankon magnetically-controlled capsule endoscope (MCE) system developed NaviCam, which additionally includes a guidance magnet robot; this robot provides five degrees of control freedom, including two rotational and three translational. The resolution of the image is 480 × 480 and frame rate is 2 fps. In order to achieve higher frame rates, all these existing capsules need a higher compression rate (CR).

Table 3.1 Commercial endoscopic capsules

Device	Company	Frames per second	Battery life	Dimension (mm)	Approval status	Image sensor	Compression
PillCam SB	Given Imaging	2	6-8 h	11 × 26	FDA (2001)	CMOS	Yes
PillCam SB2		2	8 h	11 × 26	FDA (2007)	CMOS	Yes
Pillcam SB3		Adaptive (2-6)	12 h	11 × 26	FDA (2013)	CMOS	Yes
PillCam ESO		14	20 min	11 ×26	FDA (2004)	CMOS	Yes
PillCam ESO 2		18	20 min	11 ×26	FDA (2007)	CMOS	Yes
PillCam Colon		4	10 h	11 × 31	CE (2006)	CMOS	Yes
EndoCapsule	Olympus	2	8-10 h	11 × 26	FDA (2007)	CCD	Yes
MiroCam	Intromedic	3	10-12 h	10.8 × 24	CE (2007) FDA(2012)	CMOS	No
OMOM	Jinshan	2	7 – 9 h	10.8 x 24.5	CE (2007)	CMOS	Yes
CapsoCam SV1	CapsoVision	12-20	15 h	13 × 27.9	N/A	CMOS	No
NaviCam	Ankon Technologies	2	-	11 × 31	SFDA (2013)	CMOS	Yes

h – hours; FDA -Food and Drug Administration; CE - Conformité Européene; SFDA - State Food and Drug Administration; CMOS –Complementary metal-oxide semiconductor and so on in Table 3.1.

3.3   Compression Requirements for WCE

Since the primary objective of WCE is to diagnose the human GI tract for anomalies by a physician from WCE images [C3.26], the image quality is one of the primary concerns for the

development of any compression scheme [C3.27]. However, the limited power supply and low transmission rate appeal for a high-quality compression method that can reduce the transmitted data while preserving a high image quality [C3.28].

The resources saved in this process can make the addition of auxiliary capabilities (drug delivery, locomotion, speed control) viable. The low frame rate, unpredictable motion, and low tolerance to image distortion along with limited resources make the hardware implementation of a motion-compensated compression scheme inappropriate for WCE. On the other hand, conventional lossless compression systems are not feasible due to the associated high memory requirement and high computational cost [C3.29]. The consequent increase in the silicon area and power consumption due to the image compressor generates a significant overhead to the system, making it very challenging to design a suitable image compression system capable of providing a high CR and high image quality while being power- and area-efficient [C3.29]. Based on these facts, the following requirements can be set.

a. For diagnostic accuracy, the quality of image reconstruction is critical [C3.27]. It has been reported that a minimum peak signal-to-noise ratio (PSNR) of 35 dB in reconstructed image quality is required for accurate diagnosis [C3.30], [C3.31] of the typical medical images. However, any information about the shape and texture of an object in the images may not be accurately reflected in the PSNR of the endoscopic images. So, a higher PSNR is desirable.

b. A study [C3.32] suggests that a higher frame rate increases the ability to detect more landmarks, lesions, frame per landmark/lesion, and decreases the probability of missing vital signs. A lower frame rate hinders the real-time video streaming of a smooth motion, which is highly desirable for a correct diagnosis. A frame rate of at least 10 fps [C3.33] is strongly expected for endoscopic diagnosis so that the capsule does not miss any important information. Some studies also suggested 15 fps [C3.34] as the necessary frame rate for endoscopic images. Frame rate should be higher in the areas such as esophagus where the capsule moves at a higher speed. However, a frame rate of 25 fps is needed to achieve the smoothness quality of classic wired endoscopy [C3.9].

c. The bandwidth of the transceiver of the capsule endoscopic system is limited. A recent transceiver can transmit information at 2 Mbps maximum, though a 1 Mbps transceiver is more prevalent in capsule endoscopy to reduce the power requirement. So, in order to maintain the compressed data rate at less than 2 or 1 Mbps (whichever is used), the CR must be higher.

Table 3.2 shows the calculation of CR for different commercial systems and an ideal system. The uncompressed data rate is proportional to frame rate, resolution, and pixel depth. In order to achieve an adequate frame rate, the compression ratio must be increased.

For a system that requires 10 fps for 512 × 512 images in 8-bit raw image format, in order to transmit using a 2 or 1 Mbps transceiver, the CR must be more than 10 or 20, i.e., CR should be more than 95% or 90%, respectively, as shown in Table 3.2. Thus, a compression algorithm should achieve at least 90–95% CR in conjunction with optimized reconstructed images to improve the current diagnostic efficiency and achieve a real-time capability.

The CR can be defined as the ratio of total bits before compression to total bits after compression. However, there is no specific standard available in the literature for calculating CR. Hence, we list the methods for calculating CR in this section.

Generally, in the literature, there are three types of data available from where CR can be calculated as explained below:

a. In some papers, CR is given in percentage (%). We took the CR data directly from the paper and reported it in our table.

b. In some papers, CR is given in bits per pixel. Here, we calculated CR using the following formula:

$$CR = \left(1 - \frac{Compressed\ bits\ per\ pixel(\text{i.e., bpp } taken\ from\ paper)}{Uncompressed\ bits\ per\ pixel(\text{i.e., } 8\ bits)}\right) x\ 100\% \tag{3.1}$$

c. In some papers, CR is given in ratio only. For example, CR = 20:1. In such cases, we calculated it using the following formula:

$$CR = \left(1 - \frac{1}{Compression\ ratio\ (\text{i.e., ratio taken from the paper})}\right) x\ 100\% \qquad (3.2)$$

d. The capsule must consume low power while operating. A typical WCE needs about 30 mW [C3.35] of electrical power to operate, among which power is mainly consumed by the CMOS image sensor, light emitting diodes, and RF transceiver [C3.36]. In order to be able to last for a sufficient time inside the GI tract, the images obtained should be compressed so that the data that need to be sent wirelessly are reduced as transmitting images generally consume more than 60% of the power [C3.37], [C3.38]. Hence, compression engines must be simple, low cost, and should help in reducing overall the capsule power consumption.

Any image compression algorithm with high complexity should not be chosen to limit the power consumption. So, the focus should be on developing algorithms with low complexity.

e. It is important to limit the memory needed for compression because that requires a large silicon area and power. Therefore, the capsule should not store the data on the chip, rather transmit all the data instantly. So, the compression algorithm should have the capability to do real-time processing of images and videos.

Table 3.2 Compression ratio calculation for WCE system

Criteria	PillCam SB2	MiroCam	OMOM	EndoCapsule	NaviCam	Expected values
Frame rate (FR) [frame per sec (fps)]	2	3	2	2	2	10
Resolution (R) (pixels)	256 x 256	320 x 320	320x320	512x512	480x480	512 x 512
Pixel depth (PD) (Bits per pixel)	-	-	-	-	-	8
Uncompressed data rate = $FR \times R \times PD$ * (Mbps)	1	2.34	1.56	4	3.52	20
Uncompressed data rate with 10fps (Mbps)	5	7.81	7.81	20	17.58	20
Minimum compression ratio required for a 2Mbps/1Mbps transmitter with 10 fps	2.5/5 (60%/80%)	3.9/7.81 (74.36%/87.20%)	3.9/7.81 (74.36%/87.20%)	10/20 (90% / 95%)	8.79/17.58 (88.62%/94.31%)	10/20 (90%/ 95%)

*Assuming that image sensor produces images with 8-bits raw image format.

f.   Commercial capsules and most other capsules in research still do not work in a pure real-time video mode or provide a high frame rate. Video compression includes interframe calculations. In video compression, the algorithm takes into account the fact that consecutive frames contain redundant information, and thus it would be more efficient to

consider the information of the previous frame when sending the current frame. For example, motion JPEG does not send the fixed background information again. However, this kind of setup is still not used due to two reasons [C3.33]. First, we need to store at least one entire image until the second image arrives in, which requires a significant amount of memory. Second, the frame rate is still slow, and the camera position changes before capturing the next frame when the perspective changes; thus, there is much less redundant information between two succeeding frames. Though it is possible to find a relation between two frames by transforming into the frequency domain, doing that would increase the computational complexity.

.

3.4   WCE Compression System

A typical WCE compression system consists of a color space converter, compression filter, quantizer, and an entropy encoder as shown in Fig. 3.4. Many compressors available today utilize a color space transformer in order to find the most dominating and useful component in the image and treat them in a special way. The next stage consists of a compression engine that is based on predictive or transform coding. It is followed by a quantizing and encoding stage after which the compressed binary data stream is generated, which can be transmitted wirelessly. However, there are some systems that do not use any color space converter or quantizer in order to reduce computational burden or to have a lossless system. Therefore, in this section, the WCE usage of the main stages such as color space converter, compression filter, and entropy encoders will be discussed, which will be followed by a detailed discussion of two main types of compression filters.

Input image → Color Space Converter → Compression filter (predictive or transform) → Quantizer → Entropy encoder → Compressed image
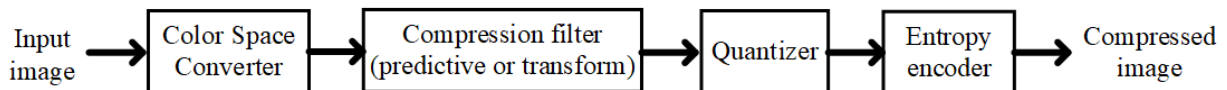
Figure 3.4 Typical WCE compression system

22

3.4.1 Color Space Conversion

The images produced by a general image sensor include red (R), green (G), and blue (B) components. A color space is a method by which we can specify, create, visualize, and define a color [C3.39]. The selection of the color space depends on the image and its application because, in some images, one of the description metrics might be able to furnish more information than other metrics, while, in other images, that metric might not be so useful. Depending on the purpose, there are many color spaces, such as, RGB, CMYK (cyan magenta yellow black), HSL (hue saturation and lightness), (luminance-chrominance), and CIE (International Commission on Illumination). Since the luminance components dominate the endoscopic images and range widely from low to high values, luminance-chrominance-based color spaces are widely used in endoscopic image compression. Due to the limited variation of chrominance components, these components are usually discarded in lossy compressions.

3.4.1.1 YUV Color Space

Some researchers proposing the prediction-based algorithms [C3.33], [C3.40] take advantage of typical endoscopic image characteristics and utilize prediction-based techniques to limit the bandwidth required to transmit the endoscopic video. Before applying the prediction, it is also quite common to use color space transformation (especially in YUV) [C3.33], discarding some U and V components while selectively sending a single set of Y and V components [C3.33]. The RGB to YUV color space conversion formula in standard JPEG2000 is presented in [C3.41], which involves floating point calculation. The algorithm [C3.33] converts it into the following equivalent integer-based calculation to reduce computational complexity:

$$
\begin{aligned}
Y &= \frac{R}{4} + \frac{G}{2} + \frac{B}{8} \\
U &= 128 - \frac{G}{2} + \frac{B}{2} \\
V &= 128 + \frac{R}{2} - \frac{G}{2}
\end{aligned}
\tag{3.3}
$$

23

3.4.1.2 YEF Color Space

YEF color space is also a luminance-based color space [C3.26], [C3.42], which is common in the differential pulse code modulation (DPCM) based algorithms. Experiments show that YEF color space shows some additional properties compared to YUV and YC_gC_o [C3.42]. Since, in most cases, the intensity distribution of green in endoscopic images is very similar to that of the blue component while the intensity distribution of Y has a similar pattern to the green and blue components, subtracting green and blue from Y will produce differential pixel values of almost an equal number and reduce the entropy of the chrominance space, resulting in a higher compression ratio in the chrominance plane. The relationship of the color space transformation is as follows:

$$Y = \frac{R}{4} + \frac{G}{2} + \frac{B}{4}$$

$$E = \frac{Y}{2} - \frac{G}{2} + 128 = \frac{R}{8} - \frac{G}{4} + \frac{B}{8} + 128$$

$$F = \frac{Y}{2} - \left(\frac{3B}{8} + \frac{G}{8}\right) + 128 = \frac{R}{8} + \frac{G}{8} - \frac{B}{4} + 128$$

(3.4)

3.4.1.3 YC$_g$C$_o$ Color Space

In discrete cosine transform (DCT) based algorithms, the color space transformation is also skipped in order to save power dissipation, except [C3.43] which uses YC_gC_o the color space transformation of input Bayer color filter array (CFA) images. YC_gC_o components can be found by the following formula, which is originally designed for the H.264 video coding standard [C3.44]:

$$Y = \frac{1}{2}\left(G + \frac{(R+B)}{2}\right)$$

$$C_g = \frac{1}{2}\left(G - \frac{(R+B)}{2}\right)$$

$$C_o = \frac{(R-B)}{2}$$

(3.5)

24

3.4.2 Compression Filters

All the image compression algorithms for capsule endoscopy can be categorized into two types: based on the quality of the reconstructed image and based on the way the algorithm works.

3.4.2.1 Lossless, Near-Lossless, and Lossy Algorithms

Based on the quality of the reconstructed image, the image compression algorithms can be divided into two categories: lossy algorithms and lossless/near-lossless algorithms. In lossless compression, it is possible to reconstruct the image exactly like the original one, while in near-lossless compression a certain degree of distortion is accepted, provided that there is no loss of valuable information [C3.45], [C3.46]. The principle of lossless compression is the reduction of redundancy in the image by exploiting the spatial correlation and appropriate digital coding [C3.33]. But as per Clunie's observation in [C3.47] on a large number of compression algorithms, the best compression ratio stays below 4 for gray-scale images, while it is below 12 for color images [C3.33]. On the other hand, lossy compression might reduce the information content of the image [C3.128] though it might not directly affect the resolution [C3.33]. Most of the lossless and near-lossless algorithms are based on the predictive coding such as JPEG-LS and DPCM, while lossy algorithms are based on transform codings such as DCT and discrete wavelet transform (DWT).

3.4.2.2 Predictive and Transform Coding

Similar to the compression of any two-dimensional data, methods in the art of compressing WCE images can be classified into two categories: time-domain or space encoding and transform-domain encoding. Time-domain techniques are based on prediction-comparison. The assumption is that dependence is innate among the pixels in the image data. In predictive coding, such dependence can be removed by a good estimator, which converts the data into a format so that there is almost no dependence among neighboring pixels [C3.48]. Generally, these include delta modulation, DPCM [C3.49], or JPEG-LS-based techniques, though the endoscopic researchers mostly consider DPCM, JPEG-LS, and simple predictive coding. These methods are mostly

lossless and near-lossless with a few exceptions. A detailed review on most of the predictive coding based WCE algorithms is given in Section V.

On the other hand, in a transform-domain method or transform coding, a block of pixels is decomposed into a set of coefficients and the compression is achieved by eliminating insignificant coefficients or by reducing the number of levels of quantization in the transform domain [C3.48]. The compression is lossy and requires higher computation compared to predictive coding, but the CR is higher as well. A detailed review of most of the transform coding based WCE algorithms is presented in Section VI.

The main challenge in WCE is ability to decrease the power consumption as well as overall area of the capsule while maintaining satisfactory reconstructed quality of the image. Hence, the focus should be on proposing a low-complexity image compression algorithm by analyzing the unique properties of the obtained endoscopic image keeping in mind the trade-offs of both lossless and lossy compression algorithms.

3.4.3 Entropy Encodings for WCE

This section lists encodings that are typically used in capsule endoscopy for converting compressed signals into the binary bit stream.

3.4.3.1 Zero-Coding

A zero coding is useful in capsule endoscopy and can drastically reduce the image size when a prediction-based algorithm creates a large number of zeros as errors. In zero coding, zeros are grouped following each other, and the number of zeros is coded. For example, a set of six zeros [0 0 0 0 0 0] is coded as [0 6]; this saves four words. This coding is used in the prediction-based algorithm [C3.33] followed by Huffman coding.

3.4.3.2 Huffman Coding

Huffman coding [C3.50] is a variable-length coding, which is a widely used entropy encoding scheme in capsule endoscopy [C3.33] and various applications. The main concept of Huffman coding is that the code depends on the probability of occurrence of the symbol. The symbol with less probability is coded with a longer digit number, while that with the higher probability is coded with a small number of digits. The Huffman table contains all dictionary information of digital representation of each symbol.

3.4.3.3 Golomb–Rice Coding

Golomb–Rice coding [C3.51], [C3.52] is an adaptive variable-length coding and, therefore, useful for the prediction-based algorithm after getting the difference between the actual signal and predicted signal; the values of the differences are either zero or close to zero, which makes a variable length coding very useful. This coding gives the optimum code length for the geometric distribution [C3.51]. When this coding is applied to the differences, which can be either positive or negative, the differences are converted into positive numbers by changing the ranges since the Golomb–Rice coding works only for positive numbers. The basic principle [C3.52], [C3.53] for converting a value into code is to divide the value by a divisor and find the quotient and remainder of the division. In the code, the quotient is first written in unary notation, followed by a stop bit "1," followed by the remainder. For example, if the divisor is 4, 11 can be coded as 00 1 11 because the quotient is 2 and the remainder is 3. For different applications, the value of divisor will be different, and the optimum value of divisor is found by setting different divisors and achieved compression ratios.

3.4.3.4 Lempel–Ziv Encoding

The Lempel–Ziv encoding [C3.54], [C3.55] is an adaptive dictionary data compression technique. This coding considers repetition in symbols and the sequences are parsed into distinct phrases. The dictionary is built in a single pass while at the same time also encoding the data. Interestingly, the dictionary is not needed to transmit to the store because the decoder can build up

the dictionary. A detailed description on how to encode using this method can be found in the report [C3.56]. This encoding is mostly used in DCT-based WCE compression techniques such as [C3.5], [C3.12], [C3.57], and [C3.58].

3.4.3.5 Lempel–Ziv Welch Encoding

This is the modified version of Lempel–Ziv coding [C3.59]. Unlike Lempel–Ziv encoding, this encoding uses a dictionary with predefined symbols. Only at the time of compression, the codeword is made from those symbols, thus providing a high compression ratio. This encoding is used by Li and Deng [C3.60] in the DCT-based algorithm along with subsampling green and blue components.

3.5   Predictive Coding based Algorithms

Predictive coding based techniques are one of the two types of algorithms that are used in a capsule endoscopy system as discussed earlier. The methods are mostly near-lossless and lossless and include JPEG-LS, simple or general predictive technologies, and DPCM-based methods. These compression algorithms reconstruct the full information that was present in the original image, i.e., the pixel information does not change/remains similar after the image is reconstructed. Hence, these algorithms are able to provide a compression ratio of only about 1:2 to 1:3 [C3.61], which is not enough when compared with transform coding based algorithms, leading to more power consumption and hence affecting the battery life of a WCE capsule. The advantage is that full pixel information is reconstructed bit by bit and the restored image is visually similar to the original image. The following section describes predictive coding based algorithms in detail for compression of WCE images.
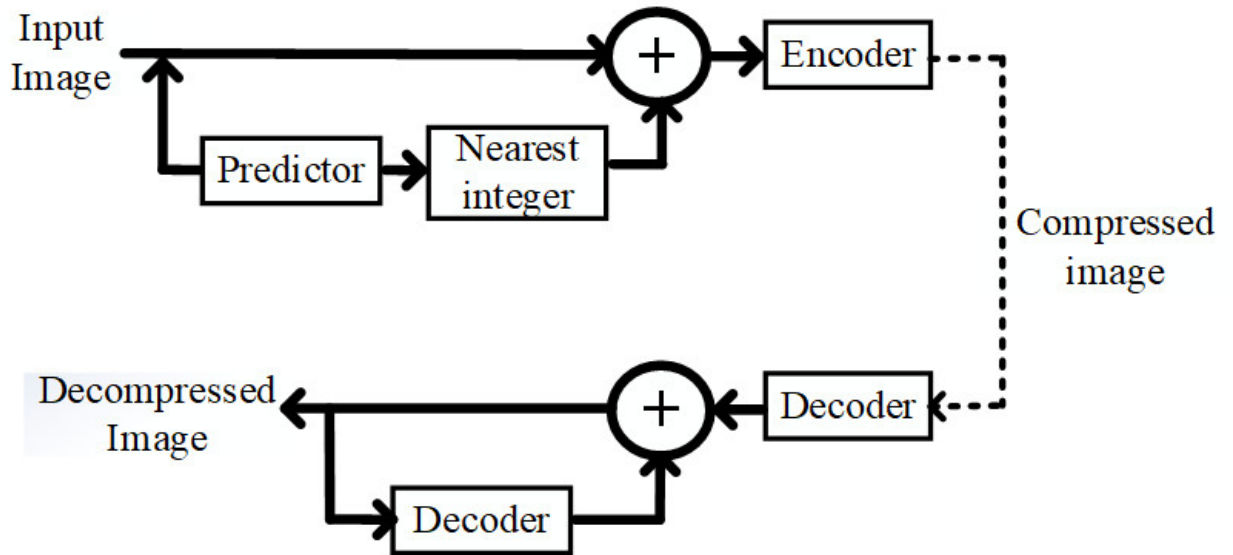
Figure 3.5 Typical model for lossless prediction based compression and decompression.

3.5.1 General or Simple Prediction based Algorithms

3.5.1.1 Principle

The main principle of this type of lossless image compression technique is based on the detection of lossless redundancy. It is true that except JPEG2000 [C3.62], which uses wavelet transform, most of the present methods of image compressions use some form of prediction. In this section, we will discuss the methods that are explicitly based on the prediction [C3.63]. Usually, in order to compress prediction and store error (the difference between the pixel and its predictions), they are converted into the bitstream with the help of encoding methods such as Huffman [C3.50], Golomb [C3.51], Rice [C3.52], or arithmetic coding [C3.64]. Normally, the prediction is done using the value of previously visited neighbor pixels. Fig. 3.5 shows a lossless predictive coding, which consists of both an encoder and a decoder. Both of them contain a similar predictor. As shown in Fig. 3.5, before the input pixel is encoded, a predictor generates a corresponding predictive integer value. Some algorithms such as JPEG-LS [C3.65], CALIC [C3.66], TMW [C3.67], EDP [C3.68], [C3.69], adaptive lossless technique such as [C3.63], spatial prediction technique [C3.70], and DPCM use the prediction-based algorithm.

3.5.1.2 Prediction Formula and Encoding

It is shown empirically by Clunie [C3.47] that the most accurate estimations for the predictor in medical images can be obtained by subtracting the neighboring pixel values rather than averaging them. So, one of the formulas used is previous pixel minus previous pixel above plus corner pixel (of above and left), as shown in Fig. 3.6(a). Another formula is previous pixel plus pixel above minus corner pixel, as shown in Fig. 3.6(b).
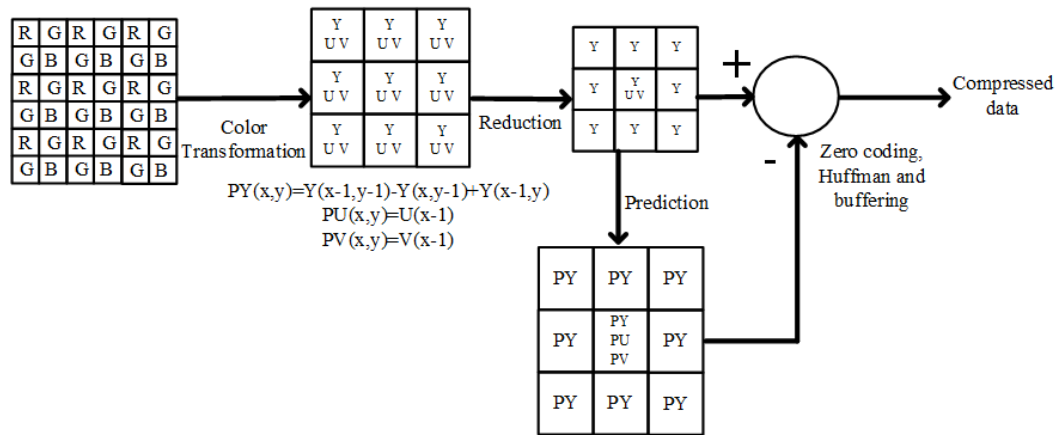
a
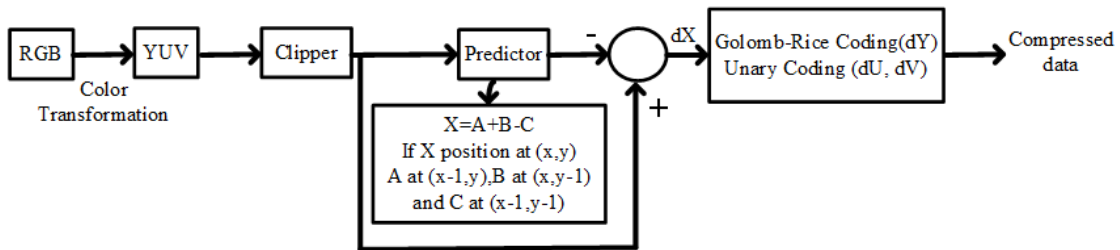
b

Figure 3.6 General prediction based near-lossless image compression techniques: (a) [C3.33] and (b) in [C3.40]

The prediction error can be coded in many ways. The method used in [C3.33] is zero coding followed by Huffman coding and buffering. Alternatively, using Golomb–Rice coding for Y and unary coding for U and V components is another option to encode the difference errors, which is considered in [C3.40]. Unary coding is found when the divisor is set to zero in Golomb–Rice coding.

3.5.1.3 Future of Prediction-based Techniques

There is room to improve prediction-based algorithms and utilize them in capsule endoscopy. There is a trade-off between CR and PSNR (see Table 3.4). It is possible to work on finding a better color space transformation, which is both integer-based and completely orthogonal. Reduction of U and V components might be an option when lossy or near-lossless compression is the target with a higher CR. For prediction, future researchers also have room to consider a wide range of neighboring components. It would also be interesting to experiment with different encoding techniques as well.

3.5.2 JPEG-LS-based Algorithms

All of the JPEG-LS-based compression schemes for WCE have two principle components: JPEG-LS engine and a preprocessing stage, which consists of a low-pass filter (LPF) and transformation. JPEG-LS-based compression algorithms provide the highest lossless CR and compression speed for the medical images that have a similar background [C3.72]. In this section, first a general principle of the JPEG-LS compression engine will be demonstrated and then the role of the preprocessing stage will be discussed.

3.5.2.1 Principles

JPEG-LS, a lossless compression method based on the LOCO-I algorithm [C3.71], consists of two independent and distinct phases called modeling and encoding [C3.65]. In JPEG-LS, the spatial redundancy in the image is reduced by a prediction model called the median edge detector, where a simple edge detection algorithm predicts the value of the next pixel, and instead of sending

the absolute value, only the prediction residue is sent, resulting in a reduction in entropy. Furthermore, JPEG-LS utilizes a simple fixed context modeller focusing on a narrow band of applications for modeling of the residue. Later, a suitable choice of an encoder from a collection of Golomb coder reduces the coding redundancy. JPEG-LS further improves the performance by using run-length coding for flat regions. A block diagram of the JPEG-LS encoder is shown in Fig. 3.7. A detailed description of the JPEG-LS algorithm can be found in [C3.65]. By focusing on a narrow band of applications, JPEG-LS can achieve comparable performance to alternative lossless compression methods having high complexity. Due to these reasons, JPEG-LS is often used for compression in digital imaging and communication in medicine [C3.73].
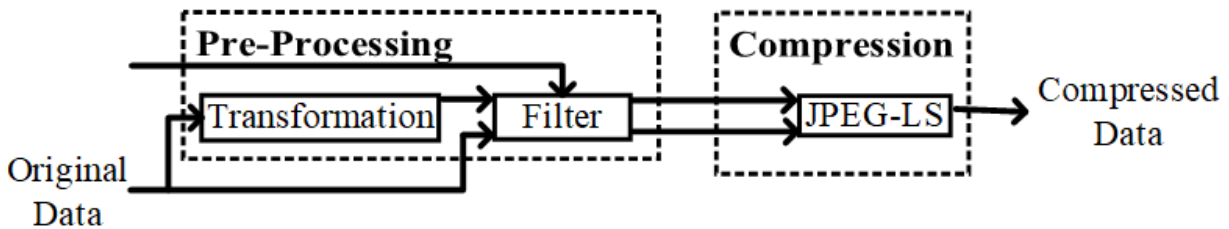
Figure 3.7 Typical block diagram of JPEG-LS

The compression schemes can be divided into two categories: compression first schemes and interpolation first scheme.

3.5.2.2 Compression First Schemes

Most digital cameras use a single image sensor to capture the color image, where to capture a different portion of wavelength a special mechanism called Bayer CFA [C3.74] is coated over the image sensor to record only one of the three components at each pixel position [C3.75]. Due to its power constraint, most of the WCE uses CFA to reduce power consumption.

The resultant CFA image is generally (especially for the interpolation first scheme) interpolated via a demosaicing stage and then forwarded to the lossless or lossy image compression

stage such as JPEG-LS [see Fig. 3.8(a)]. However, the demosaicing stage increases the redundancy in information as the resultant R, G, and B components have a significant correlation between them, ultimately reducing the compression performance [C3.75], [C3.76] , [C3.112]. Moving the interpolation stage after the compression stage can improve the compression performance by avoiding the increase in redundancy due to interpolation. However, the discontinuity between the color components in a CFA image introduces a new problem for compression. Using structure separation and transformation, the individual color components can be organized contagiously, but the resultant high-frequency component generated between them can attenuate the CR [C3.76]. So, an LPF is generally incorporated in the transformation stage to reduce the high-frequency components. The general structure of such compression first schemes is shown in Fig. 3.8(b). All of the compression systems in the literature based on JPEG-LS have used the same JPEG-LS scheme with modification in the preprocessing stage [C3.37], [C3.77]–[C3.82], except [C3.28].
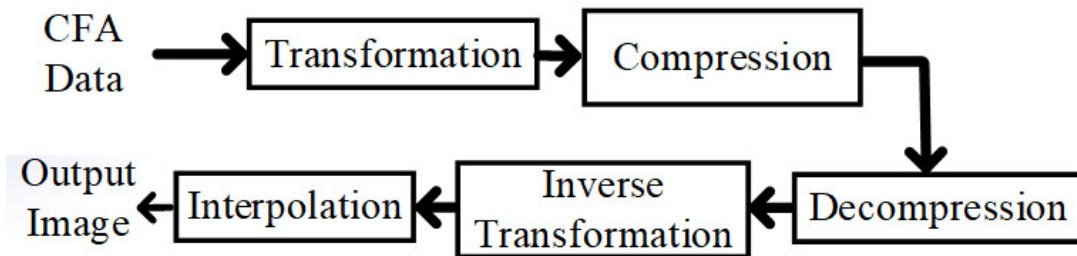
a
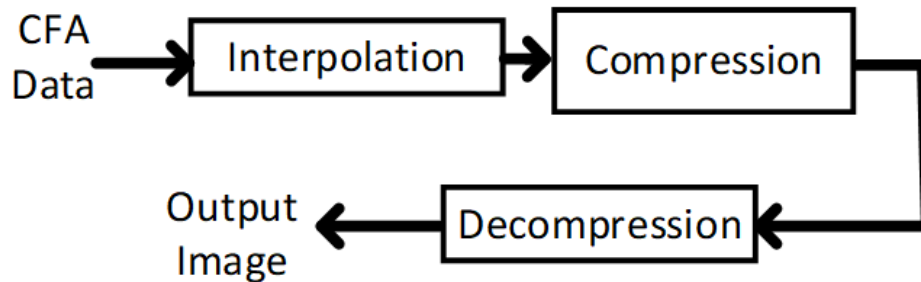
Figure 3.8 (a) Compression first scheme and (b) interpolation first scheme.

3.5.2.3 Preprocessing in Compression First Schemes

Preprocessing of the CFA raw data is a major component before sending it to the compression engine, as shown in Fig. 3.7. In order to avoid losing information in this process and retransform the image into the original CFA form, the transformation should be perfectly reversible, and the reverse transform procedure should be simple. In this section, the two major components of the preprocessing stage are discussed in detail.

Transformation: The CFA image has twice the number of G components as R or B components. The G components are organized in a quincunx form. The CFA image can be separated into two rectangular grids: one grid containing all the G components and the other grid containing the R and B components [C3.76].

Although all the works in the literature on the JPEG-based compression system for WCE have quincunx to rectangle transformation for the G components, most of the works do not transform the grid containing the R and B components. The transformation stage comes after the LPF stage in most of these works [C3.78]–[C3.81], except in [C3.37] and [C3.82], where the transformation stage antecedes the LPF.

Low-Pass Filtering: Motivated by the fact that CFA images contain higher frequency components than the color image, an LPF is incorporated in the preprocessing stage to reduce aliasing. However, to be suitable for use in the lossless or near-lossless scheme, the filtering process must be perfectly reconstructable, and the reconstruction process must be simple. To this end, most of the works in the literature have used some modification of the moving average filter for its simple reconstruction process. The LPF of the two grids can be done using the same filter, reducing the complexity in the transmitter [C3.37], [C3.82]. Some works have used a separate filter for two grids to take into account the difference in characteristics between them [C3.78] – [C3.81]. Some filters have used the raster scan or the progressive scan nature of the CFA filter to design the filter, which reduces the memory requirement significantly [C3.37], [C3.81], [C3.82]. A brief overview of all the LPFs used in the literature is presented in Table 3.3. Quality control and region of interest (ROI) parameters can be incorporated into the LPF stage, which can further improve the compression performance by providing lossless compression for ROI while providing lossy compression for another region. For example, the compression scheme presented in [C3.37], [C3.77] – [C3.80], and [C3.82] has the capability to incorporate quality control in the

LPF. However, the ROI detection scheme suitable for such system was not discussed in any of the works.

3.5.2.4 Interpolation First Scheme

Although most of the work in the literature is based on the compression first scheme, the interpolation first scheme is exploited in few works. By using a suitable casual interpolation template, such method can improve the compression performance by increasing the spatial correlation of adjacent pixels [C3.28]. The resultant increase in correlation reduces the CR but gives a better accuracy in terms of distortion due to prediction.

3.5.2.5 Future of JPEG-LS based Algorithms

There are thousands of frames in a video. However, only a few frames might be of interest to the gastroenterologist. The automated extraction of an ROI is advantageous to both gastroenterologists as well as for CR, which can provide the high-quality compression to the ROI while providing low-quality compression to other frames. In the future, the researchers in this field can focus more on automatic extraction of the ROI, and on its incorporation into a JPEG-LS compression system. Several researchers in medical imaging are now employing the interframe coding with JPEG-LS, for improving the compression performance of the system, by taking into account the high temporal redundancy. To our knowledge, such an algorithm has not yet been employed for the WCE system. In the future, more focus should be given in utilizing the temporal redundancy along with the spatial redundancy, to reduce the power and memory requirement of the WCE videos. Another prospective research area of performance improvement is the search for a casual interpolation template and a prediction model, which can reflect different characteristics, especially characteristics that carry significant diagnostic importance, in the WCE image.

3.5.3. DPCM-based Techniques

3.5.3.1 Principles

DPCM [C3.83]–[C3.86] is a widely known procedure for differential quantization of communication signals. As the luminance of images dominates in the case of endoscopic images, a prediction-based technique is preferable for the wireless endoscopy [C3.26], [C3.42],[C3.87].

3.5.3.2 Subsampling

Due to the absence of a bluish color object in the GI tract, the variation in U component in the endoscopic image is less than that of V component. This phenomenon makes subsampling more favorable when using YUV color space. Subsampling might not result in pure lossless compression though it is possible to achieve a near-lossless mode. For example, in [C3.26], subsampling is used in YUV color space, where the Y, U, and V components are subsampled in the ratio of 8:1:2. The resulting compression can work in the near-lossless mode.

3.5.3.3 Future of DPCM-based Algorithms

DPCM-based algorithms are promising because they can work in both lossless and acceptable lossy modes. In the lossy mode, this provides one of the highest CRs among all prediction-based techniques. In the lossless or near-lossless mode, the CR is better than JPEG-LS-based algorithms. However, a careful choice of color space, subsampling, and encoding can provide, promising results to achieve a high CR allowing high frame rates. Specially, a better prediction filter should be achieved instead of subtracting from the previous pixel. Moreover, a DPCM such as [C3.87] including a color space transformation and subsampling might give a higher CR with an acceptable quality of the image, which can be used in future endoscopic systems. Also, DPCM between consecutive frames has a good prospect for achieving a higher frame rate.

Table 3.3 Filters used in different JPEG-LS compression schemes

Study	Separate Filter for G and B, R	LPF before Transformation	Filter Used
Xie *et al.* [C3.77]	No	No	Moving Average with span=1 in vertical and horizontal direction
Xie *et al.* [C3.78]	Yes	Yes	Not Specified
Xie *et al.* [C3.79], [C3.80]	Yes	Yes	$Hg = \begin{pmatrix} 0 & 0 & 0 & 0 & 0 \\ 0 & -1 & 0 & 0 & 0 \\ -1 & 0 & 4 & 0 & 0 \\ 0 & -1 & 0 & 0 & 0 \\ 0 & 0 & 0 & 0 & 0 \end{pmatrix}$ and $H_{rb} = \frac{1}{4} \begin{pmatrix} 1 & 1 & 0 \\ 1 & 1 & 0 \\ 0 & 0 & 0 \end{pmatrix}$
Xie *et al.* [C3.82]	No	No	$H_{gbr} = \frac{1}{4} \begin{pmatrix} 1 & 1 & 1 \\ 0 & 1 & 0 \\ 0 & 0 & 0 \end{pmatrix}$
Li *et al.* [C3.81]	Yes	Yes	$Fg(i,j) = \begin{cases} \dfrac{0(i,j)+F(i-1,j-1)+F(i,j-2)+F(i-1,j-3)+1}{4}, i \in even \\ \dfrac{0(i,j)+F(i-1,j-1)+F(i,j-2)+F(i-1,j-1)+1}{4}, i \in odd \end{cases}$ $F(i,j) = \begin{cases} \dfrac{0(i,j)+F(i-1,j-1)+F(i,j-2)+F(i-1,j-3)+1}{4}, i \in even \\ \dfrac{0(i,j)+F(i-1,j-1)+F(i,j-2)+F(i-1,j+1)+1}{4}, i \in odd \end{cases}$
Chen *et al.* [C3.37]	No	Yes	$P'_{(X,Y)} = \frac{1}{4}\left(\left(P_{(X,Y)} + P'_{(X-1,Y-1)} +1\right) + \left(P'_{(X-1,Y)} + P'_{(X,Y-1)} +1\right)\right)$
Liu *et al.* [C3.28]	Interpolation First Scheme		Causal Interpolation Template

3.6 Transform Coding based Algorithms

Transform-domain-based algorithms are based on the utilization of interpixel correlation, and this produces a less correlated transformed version of the image. Most of the transform coding techniques utilized in WCE are based on DCT and a few on DWT. DCT is the core of the JPEG image compression standard, while modern JPEG2000 uses DWT as its core because of a high CR while maintaining the quality. Most of the transform codings employed in WCE work in the lossy mode and many of them provide a high CR (more than 85%). Although this technique does not recover fully encoded data, a transform coding based algorithm may be fit for endoscopic

application by recovering only the useful information while achieving higher compression. In terms of endoscopic application, it may be possible to generate images that are perceptually similar, which may/may not hamper the diagnostic accuracy by using the algorithms that are based on transform coding. The amount of compression that is to be applied on an image might depend on several different factors, such as target disease, target body part, etc. Thus, transform coding based algorithms are chosen when higher compression is needed, and the amount of compression can be determined based on the ability of a human to distinguish between compressed and original images.

3.6.1. DCT-based Techniques

3.6.1.1 Basic Principles

DCT [C3.88] is mostly employed as a lossy compression scheme. It is widely used in many image and video compression codecs [C3.89] – [C3.108]. A typical DCT takes 8×8 grayscale block and applies compression. The same process is repeated for each color channel.

DCT is employed in the JPEG standard [C3.109] and often used for the compression of WCE images [C3.5], [C3.12], [C3.57], [C3.58], [C3.115], [C3.116]. A typical algorithm usually includes demosaicing of the raw image (optional), color space transformation, two-dimensional (2-D) forward transformation, and quantization followed by an entropy encoding. In all these implementations, image pixels are accessed in 4×4 or 8×8 blocks from the image sensors.

The DCT is much more-well established than the wavelet transforms but still requires complex calculations, which can be a burden for WCE application [C3.110], [C3.111]. Hence, a simplified integer version of DCT (also known as iDCT) is becoming popular [C3.8], [C3.109], [C3.111], [C3.114]. Quantization can be redundant in this version of DCT as this transform already represents loss. iDCT has already proved to be effective in WCE application [C3.8] at the cost of temporary storages as the frames are divided into 8×8 blocks. One of the advantages of iDCT is that the quantization part can be removed partly as it is embedded within DCT transformation. However, at a lower bit rate, this algorithm produces significant artifacts in reconstructed frames, which results in the poor quality of images [C3.113].

3.6.1.2 Demosaicing and Subsampling

As the resolution of demosaiced images for WCE is still low and some important spots can be unintentionally omitted [C3.57], all the DCT-based compression techniques skip these steps. Moreover, the color space transformation is also skipped in order to save power dissipation, except [C3.43], which uses Y–Cg–Co color space transformation of input Bayer CFA images.

It is shown experimentally with 414 endoscopic images in [C3.87] that the red component dominates the green and blue components, and more accurately the green components dominate the blue components in an average endoscopic image while luminance (Y) is similar and close to the red components. This fact opens the opportunity of subsampling in RGB color space as well. Lin *et al.* [C3.5], [C3.58] and Li and Deng [C3.60] used this opportunity and subsampled the G and B components in 2:1 ratio. As blue components are less than the green component and less important in decision-making, the blue component can be subsampled further, for example, in 4:1 ratio. Thus, a simple coder can provide optimum image compression by utilizing the best color transformation, acquiring the unique properties of an endoscopic CFA image [C3.112].

3.6.1.3 DCT Application and Quantization

DCT-based compression techniques are lossy since they use quantization to increase CR. For 2-D DCT forward transformation, in [C3.57], an 8×8 DCT is applied on R, G1, G2, and B signals separately, followed by a modified quantization table [C3.116] to reduce hardware cost and quantization error. A 4×4 DCT is used in [C3.8], [C3.12], [C3.43], [C3.60], and [C3.117]. When subsampling is used in [C3.5] and [C3.58] for a 2:1 subsampled component, a 4×4 DCT is used while no DCT transformation is used for a 4:1 subsampled blue component. The subsampling based GICam [C3.5], [C3.58] uses the RGB quantization table [C3.116] and modifies it to save the computation of demosaicing and color space transformation, which, in turn, saves the power consumption in preprocessing steps and reduces the computational loads. Wahid *et al.* [C3.12] used a standardized JPEG quantization table for arithmetic integer quantization, which was extracted from [C3.109]. In many cases [C3.60], [C3.117], a quantization table is used where the table components are a power of 2 since the multiplication by the components can be achieved easily by shift operation in circuits.

3.6.1.4 Encoding

Limpel–Ziv (LZ) coding [C3.55] is quite common in DCT-based compression for entropy encoding. This is due to the fact that it does not need complex computation and look-up tables. It also consumes less power and uses a smaller silicon size than the other candidates, such as the Huffman encoding and the arithmetic coding [C3.57]. However, Tajallipour and Wahid [C3.118] explored four different types of entropy encoding such as Huffman encoding, LZ, Limpel–Ziv–Welch (LZW), and LZW–Flush encoding and found a better CR with Huffman and LZW, while Huffman requires more memory and LSW and LZ require a larger dictionary and library size. Since the hardware resource is limited in WCE, LZW-flush is a considerable option.

3.6.2 DWT-based Techniques

Since the mid-1980s, a number of compression algorithms have emerged based on wavelet theory [C3.119], which leads to a higher CR with fewer image artifacts. For the first time, Turcza *et al.* [C3.120] proposed DWT-based image transformation for WCE application in the year 2007, where integer approximations of DCT/DWT transformations are used. Although DCT transform results in a higher CR but a loss of information in reconstructed images (also called blocking effect), DWT does not have this limitation and can be easily used in image compression algorithms, such as standard JPEG2000 [C3.120]. In wavelet transformation, an image is analyzed by passing it through an analysis filter bank followed by a decimation operation [C3.121]. This analysis filter bank, consisting of an LPF and a high-pass filter at each decomposition stage, is suitable for image compression. Among many types of wavelets, the Haar wavelet is the simplest and offers low-cost implementation, which is suitable for WCE application. This wavelet was used in the capsule by Thoné *et al.* [C3.34]. Wavelet transform divides a signal into high-frequency and low-frequency components using two different filters. In the next level, low-pass components are again split into two components. This is called sub-band coding. For Haar wavelets, LPF and high-pass filters, $h(z)$ and $g(z)$, respectively, are very straightforward:

$$h(z) = \frac{1}{\sqrt{2}}(1 + z^{-1})$$

$$g(z) = \frac{1}{\sqrt{2}}(1 - z^{-1})$$

(3.6)

Thoné *et al.* [C3.34] proposed a compression algorithm for WCE based on Haar wavelet transformation. Because of limited color content in the endoscopic image, YCbCr color space is used, and only the Y component is followed by Haar transform and quantization by removing N least significant bits (LSBs). This is followed by standard zigzag run-length coding, delta coding of the dc components, and fixed Huffman table encoding. The achieved PSNR is better for a higher CR (>25) when compared to DCT-based compression techniques, including [C3.33], [C3.120], and [C3.122].

3.7 Video Coding Algorithms

In this section, a short comparison between image and video coding algorithms is presented. A typical video coding representation consists of an audio coder, video coder, and an image coder. An audio coder is not of interest for WCE application. However, a video coder is of importance. As discussed earlier, an image coder exploits the correlation between pixels. In contrast, a video coder exploits the correlation between frames and works on reducing the size of each frame. A commercial endoscopic capsule such as PillCam, developed by Given Imaging, and most other algorithms proposed and developed till date in the literature still provide a low frame rate. As discussed earlier, these capsules provide a low-resolution image at a relatively low frame rate by using conventional coding schemes (JPEG), which operate at low complexity. In order to provide a high frame rate, video coding algorithms, which are based on interframe correlation, can be one of the solutions. In the literature of capsule endoscopy, two techniques are used so far for video coding: AVC/H264 [C3.123] and distributed video coding (DVC) [C3.38]. Although implementing the state-of-the-art video compression techniques might be able to provide a high CR, the main challenge is that those algorithms are computationally expensive and require complex hardware, thus consuming more power, which a capsule cannot afford. Hence, video coding algorithms can be considered when the developed hardware (longer battery life, miniaturized size, etc.) can allow a more complex algorithm to be implemented in the system.

3.7.1 Modified H264

A typical AVC/H/264 video compression technique utilizes the YCbCr color space for intraframe prediction and motion estimation for interframe prediction, through which both spatial and temporal redundancies are reduced from the plane [C3.124]. The difficulty in implementing computationally expensive motion estimation along with a low frame rate associated with WCE makes the intraframe prediction mode infeasible for WCE. To avoid the demosaicing and interpolation of the Bayer CFA data, researchers modified the interframe prediction mode to work directly on raw Bayer CFA data [C3.123]. In [C3.123], in order to save power and computational expenses, RGB color space is used instead. Based on the fact that the GI tract is cardinal, the intraframe prediction mode is fixed to 4×4 dc mode since the 4×4 block mode is found better than the 8×8 block mode with a little decrease in quality. Rate-distortion optimization is turned off, since based on the experiment, this does not reduce the quality of the image as well. However, this algorithm can provide 82% compression in the lossy mode (PSNR 36.24 dB).

3.7.2 Distributed Video Coding (DVC)
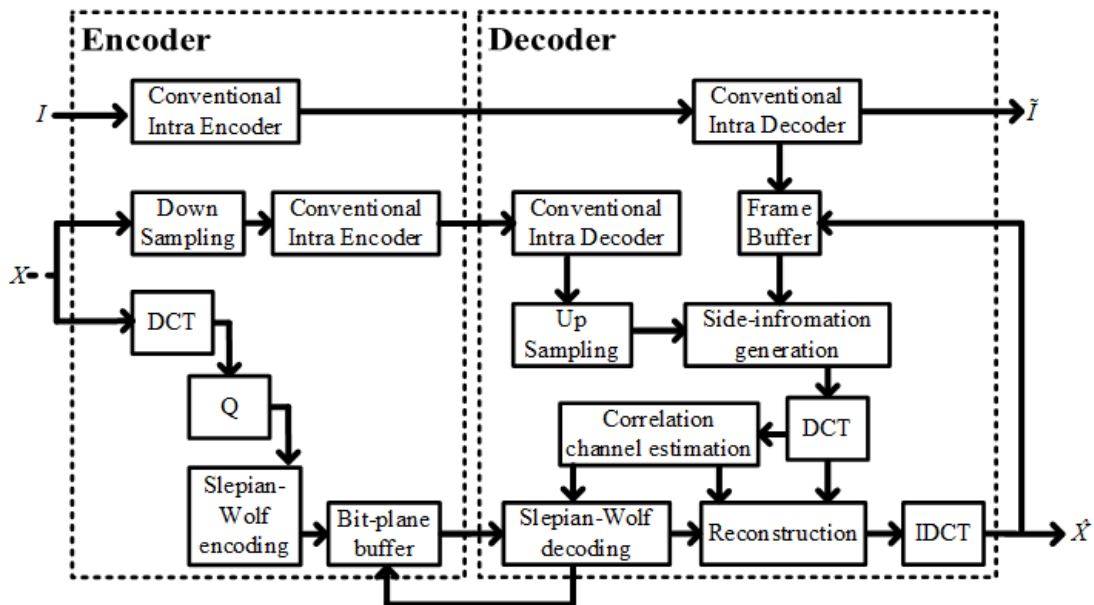
Figure 3.9 Block diagram of a typical DVC technique

Based on the theory of distributed lossless coding proposed by Slepian and Wolf [C3.125] and the extension of the Slepian–Wolf theorem for lossy compression by Wyner–Ziv (WZ) [C3.126], DVC enables separate encoding and joint decoding of video signals. By shifting the highly expensive motion compensation unit from the encoder, DVC ensures a simple encoder system with low power. So, for an application such as an endoscopic capsule demanding a power and area constraint transmitter with high compression efficiency, DVC constitutes an ideal alternative to a conventional intraframe coding method such as MJPEG.

The DVC encoder first divides the video frames into key and WZ frames. The key frames are transmitted through a conventional intra-encoder, while the WZ frames are encoded utilizing a Slepian–Wolf encoder. For an endoscopic capsule, a hash-based transform domain is utilized for the generation of side-information (see Fig. 3.9) [C3.127]. At the decoder the key frames are conventionally decoded using a conventional decoder; the hash information, which is a down-sampled version of the WZ frames, is integrated with the key frame to produce the side-information. Later, the side-information and the encoded WZ frames are utilized to decode the video frames. The proposed method reported a 40% reduction of the encoding computational time compared to H.264/AVC Intra with PSNR improvement up to 0.77 dB [C3.127]. DVC facilitates employment of side-information prediction using a database of available endoscopic images and consequently can achieve a higher CR. Such scheme was exploited by [C3.38], where they have created a database in the decoder side to predict the side-information using the dc value coming from the transmitter and reported it to outperform the MJPEG. The method used to calculate CR is not clearly explained in [C3.38]. As such, CR is calculated in this paper at PSNR = 39 dB for [C3.38] by:

$$Compression\ ratio = \frac{Total\ bits\ before\ compression}{Total\ bits\ after\ compression} = \frac{256*256*2*8}{50000} = 20.97 \qquad (3.7)$$

and

$$CR = \left(1 - \frac{1}{Compression\ ratio}\right) x\ 100\% = 95.23\% \qquad (3.8)$$

43

Table 3.4 Summary of compression for WCE

Study	CM	CoM	Sub-category/ features	Specific information	Color space	Hardware Implementation or Simulation of Hardware	CR (%)	PSNR (dB)	Average power in active mode (mW)	FR	BL
Xie *et al.*(2004) [C3.78]	JPEG-LS	LL and NL	Compression first	LPF before transmission	RGB (Bayer)	Simulation at 0.18 um CMOS process	56.25 to 13.75	46.37 to ∞	9.8 (SR)	15	-
Xie *et al.* (2005) [C3.79]	JPEG-LS	NL	Compression first	LPF before transmission	RGB (Bayer)	FPGA verification/ASIC layout at UMC 0.18 um CMOS	**72.75**	**46.89**	8.2 (SR)	0-7	10.3
Xie *et al.* (2005) [C3.80]	JPEG-LS	NL	Compression first	LPF before transmission	RGB (Bayer)	ASIC 0.18 um CMOS process	**72.75**	**46.89**	14.5	0-8	15
Xie *et al.* (2007) [C3.82]	JPEG-LS	NL	Compression first	LPF before transmission	RGB (Bayer)	ASIC 0.18 um CMOS process	73.5 to 13.75	46.37 to ∞	7.5	8	-
Li *et al.*(2007) [C3.81]	JPEG-LS	NL	Compression first	LPF before transmission	RGB (Bayer)	Simulation with UMC 0.18 um 1P6M CMOS	54.13	46.43	7.1	-	-
Chen *et al.*(2009) [C3.37]	JPEG-LS	NL	Compression first	LPF before transmission	RGB (Bayer)	ASIC UMC 0.18 um 1P6M CMOS	54.13	46.43	1.3	0-2	6-8
Chen *et. al.* (2016) [C3.128]	JPEG-LS	NL	Prediction	GR Encoder	CFA (RGB)	FPGA board, 0.18um and 90nm TSMC CMOS	49.75	46.43	3.1	30	-

44

Table 3.4 (continued)

Liu *et al.* (2015*)* [C3.28]	JPEG-LS	NL	Interpolation First Scheme	No LPF	RGB (Bayer)	ASIC 0.18 um CMOS	56.89	46.31	-	-	-
Liu *et. al.* (2016) [C3.72]	JPEG-LS	NL	Interpolation First Scheme	No LPF	RGB (Bayer)	ASIC 0.18 um CMOS	72.89	46.21	11.7	24	WPT
Hu *et al.* (2009) [C3.87]	DPCM	Lossy	-	Haar wavelet encoding	RGB	-	**89.27**	37.16	-	-	-
Khan *et al.*(2011) [C3.26]	DPCM	NL	Subsampled input based	GR Encoder	YUV (8:1:2)	Simulation	**80.2**	48.2	-	2	-
Khan *et al.* (2014) [C3.42]	DPCM	LL	Image clipping included	GR Encoder	YEF	FPGA Capsule	**78**	∞	1.63	2	8.5
Mohammed *et. al.* (2017) [C3.112]	DPCM	LL	Compression first	GR and Unary clipping	CFA (YLMN)	Simulation in Verilog	55.87	∞	0.94	-	-
Turgis *et al.*(2005) [C3.33]	General Prediction	Lossy	-	Zero coding, Huffman coding	YUV	ASIC 0.25 um CMOS process	**95**	-	7.5	10	-
Khan *et al.* (2011) [C3.40]	General prediction	LL	Image clipping included	GR and unary encoder	YUV	Simulation in VHDL	**72**	∞	-	2.2	-
Fante *et. al.* (2015) [C3.29]	DPCM	Lossy	Demosaicking-First	GR	YUV	ASIC UMC 130nm CMOS	**90.35**	40.66	0.592	2	-
		LL					73.62	∞	0.034		

Table 3.4 (continued)

Lin *et al.* (2006) [C3.57]	DCT	Lossy	-	LZ	YcbCr	Software verification in FPGA	79.65	32.51	14.92 (SR)	2	-
Lin *et al.* (2006) [29]	DCT	Lossy	2:1 Subsampled for G and 4:1 subsample for B	LZ	RGB	FPGA Verification	79.62	32.18	9.17	2	-
Lin *et al.* (2011) [C3.5]	DCT	Lossy	2:1 subsampling for G and B components	LZ	Y-Co-Cg	FPGA Verification	82.28	**40.73**	**5.29**	**2**	-
Turcza *et al.*(2011) [C3.43]	DCT	Lossy	-	DPCM along with variable length Huffman codes	Y-Co-Cg	FPGA system	**90.80**	36.01 (CFA) 35.36 (RGB)	10.2 / 12.5	12 / 24	-
Turcza *et al.*(2006) [C3.8]	DCT	Lossy	-	Variable length Huffman codes	Y-Co-Cg	No implementation	96.87 / 95.89	36.49 / 35.00	-	-	-
Wahid *et al.* (2008) [C3.12]	DCT	Lossy	-	LZ encoding	RGB	Simulation	**87.13**	32.95	10 (SR)	-	12 (ER)
Li et al. (2009) [C3.60]	DCT	NL / Lossy	2:1 subsampling for G and B components	LZW Encoding	RGB	No HW implementation	**75.41** / **87.18**	**47.67** / 39.71	-	-	-
Gu *et al.* (2012) [C3.117]	DCT	Lossy	-	Huffman Encoding	RGB	No HW implementation	**86**	39.2	-	-	-

Table 3.4 (continued)

Turcza *et. al* (2017) [C3.146]	DCT with Predictive	Near-lossless	-	GR Encoder	CFA (RGB)	Verilog UMC 180 nm CMOS	74.35	46.68	0.106	2	-
Thone *et al.* (2010) [C3.34]	DWT	Lossy	Har wavelet transform	RLE and Huffman Encoding	YCbCr	FPGA validation	**96**	35-38	-	-	-
Dung *et al.*(2008) [C3.123]	Simplified AVC/H. 264	Lossy	Intra-frame prediction (Video)	-	RGB	FPGA validation	**82.1**	36.24	0.92	2	-
Boudechiche *et al.* (2014) [C3.38]	DVC	Lossy	-	-	RGB	No HW implementation	**95.23**	39	-	-	-
Wu *et. al.* (2009) [C3.145]	Compressed sensing	Lossy	-	-	YUV	No HW implementation	**80** / **50**	22.04 / 31.02	-	-	-

CM: Compression Method; CoM: Compression Mode; CR: Compression Rate; PSNR: Peak Signal-to-noise ratio; FR: Frame Rate; BL: Battery Life; SR: Simulation result; ER: Estimated result; WPT: Wireless Power Transmission, LL: lossless, NL: near-lossless, GR: Golomb-Rice.

3.8 Analysis and Discussion

Table 3.4 summarizes most of the compression algorithms proposed for WCE till date. Similar types of algorithms are grouped together and shown by a particular shade of color in the table. From this table, we can have a comprehensive view of the existing compression schemes.

3.8.1. Analysis of the Existing Algorithms

Lossless or near-lossless compression such as JPEG-LS-based systems provides good image quality at the expense of a low CR. The best CR achieved using a JPEG-LS-based system is 72.75% by Xie *et al.* [C3.80], which is still low. Also, the transmission can consume a significant amount of power in JPEG-LS. Hence, it is vital to search for an alternative. Moreover, JPEG-LS-based algorithms use the established standard JPEG-LS engine with other preprocessing. The JPEG-LS engine itself is complicated and computationally expensive, which requires much more power. The image compressor modified with the standard JPEG-LS [C3.72] can be used to avoid unnecessary calculation, reducing memory usage while saving considerable power. So, the research should focus more on a customized light compression engine rather than a standard engine. However, lossless algorithms based on DPCM or general prediction provide a perfect reconstruction of the image, which can help in very accurate diagnosis. However, the CR is still not enough (highest value is 78% by Khan and Wahid [C3.42]) to reach a minimum of 10 fps.

High compression is possible by a transform coding technique such as DCT-based techniques. Some of the research works that achieved higher CRs are 90.80% by Turcza and Duplaga [C3.43], 87.13% by Wahid *et al.* [C3.12], 87.18% by Li and Deng [C3.60], and 86% by Gu *et al.* [C3.117]. In spite of high CR, all of the DCT-based compressions are lossy except the algorithm by Li and Deng [C3.60], which also offers near-lossless compression (PSNR 47.67) with a CR of 75.41%, which is better than most JPEG-LS-based compression methods. Li *et al.* used RGB subsampling at 2:1:1 before application of DCT and used LZ coding to find a better CR though the system is not implemented in any capsule yet. It might be a good idea to explore this technique in the capsule environment. A DCT-based algorithm requires buffer memory to store the pixel matrix, which makes it less favorable for hardware implementation. This requirement of buffer memory can be minimized by including large output first-in-first-out (FIFO) [C3.129], which can be a good choice considering the trade-off among the CR, required buffer size, and the image reconstruction quality.

On another note, the utilization of PSNR as the measure of quality metric may not always reflect the actual quality perceived by the end product, i.e., the diagnostic yield of the image. In designing these compression systems, a large portion of the literature has neglected the subjective quality perceived by the physician. As a result, particularly for lossy compression schemes, a

resultant image may discard important diagnostic information but still may output a good PSNR. This gap between the compression designer and physician is preventing us from devising a highly optimized compression algorithm with high diagnostic efficacy.

In spite of the problems described before, a few compression algorithms are promising. Some lossy algorithms, which have a comparatively acceptable PSNR (>35 dB) in diagnosis, provide enough compression (>90%) to achieve 10 fps in order to not miss any ROI in the GI tract. Such algorithms use the DWT-based technique by Thoné *et al*. [C3.34], DCT-based technique by Turcza and Duplaga [C3.43], and DPCM-based technique by Hu *et al*. [C3.87] and Fante *et al*. [C3.29], Turcza and Duplaga [C3.146] proposed an image compressor that combines transform coding (DCT) with predictive coding in CFA images to get a higher CR along with better image quality for WCE applications. Though the exact cost and power requirement could not be accessed for each of them to get the exact battery life at a high frame rate, these algorithms provide the hope to achieve the requirement of the expected compression algorithms for WCE.

On the other hand, lossless and near-lossless algorithms, which can be useful in endoscopy in a region where a high frame rate can be waived off by the physicians, are the DPCM-based algorithms by Khan and Wahid [C3.42] providing 78% compression in the lossless mode and by Khan and Wahid [C3.26] providing 80.2% compression in the near-lossless mode. Also, removing context and combining run mode with regular mode reduces complexity and improves CR and makes it efficient for very large scale integration implementation [C3.128]. Though the CR is not enough for a high frame rate, these works might be able to provide guidelines to achieve an optimum compression in lossless and near-lossless modes for future researchers.

3.8.2. Outstanding Problems

Despite rapid development in capsule endoscopy technology, there are still many outstanding problems that require further improvement. Sometimes capsules fail to capture the crucial image of the GI tract region. This is because of two reasons: 1) the locomotion is currently driven by natural peristalsis since the physicians are unable to control the capsule's motion and orientation. 2) The limitation of frames per second, for which the capsule may fail to capture an important region. The second problem is relevant to this review; due to the limitation of frame

rate, many landmarks or lesions can be missed in between two consecutive frames and some of them might be interesting to the physicians.

Also, most of the existing commercial capsules and capsules in research use a CMOS camera, which takes low power and a standard image of general depth. In order to use the capsule to diagnose diseases, which requires information of tissue depth, for example, to diagnose cancer, tumor, lesion, etc., it is important to use a charge coupled devices (CCD) camera, which creates images with infrared information in addition to RGB pixels thus making it heavy. To be able to achieve this, sufficient research is needed on CCD images to compress them.

Modern commercial capsules last for around 9–15 h [C3.130]. They should be able to operate for more than 16 h if there is any situation in the GI tract that makes the capsule slower. Operating for 24 h continuously while maintaining a high frame rate with a high-quality image still remains a goal. Also, as a capsule might remain for around 24 h [C3.6], [C3.12] in the human body as well, in that case, a higher battery life is crucial. Here, a low-power, low-complexity compression algorithm has a significant role as well.

Most of the capsules do not transmit real-time videos, though many can transmit real-time images at a nonvideo frame rate. It first stores the data in memory, which consumes silicon space and thus consumes power to write and read the data before transmitting. Also, real-time endoscopy, which can bring more benefits to diagnosis, is not possible in any of the commercial capsules due to a low frame rate. A higher CR with high-quality yields is necessary for that. Moreover, the future endoscopy would be tele-operated capsule endoscopy with active locomotion, where a large amount of video information will be needed to transmit so that the physician can inspect in real-time.

Some researchers used the established standard JPEG-LS engine with other preprocessing. The JPEG-LS engine itself is complicated and computationally expensive, which requires much more power. Also, the CR is not higher though it can offer near-lossless compression. Redundancy between frames is common, especially in the case of a higher frame rate or video. To date, there has been very little research [C3.123], [C3.38] on WCE compression algorithms, which take frame redundancy into account though these do not provide enough CR with acceptable PSNRs.

3.8.3. Future Directions

It is obvious that we need extensive research work to achieve a high CR with an acceptable quality of image. Hence, in this section, we propose some recommendation for achieving these goals. Though generally color space transformation is lossy and irreversible, they are very useful for the endoscopic image. Lossy algorithms, which are based on DCT with a luminance-based color space transformation and subsampling of color components, provide a higher CR with marginally acceptable quality of images. So, an integer-based but totally orthogonal color space transformation is needed where most of the information can be captured in the luma (or Y) component since an integer-based and orthogonal color space transformation is easily reversible, hence resulting in better lossless ratios and low hardware computational cost. Furthermore, endoscopic images are usually dominant in red color, and subtracting these blue and green components from luma will reduce the entropy, and, thus, higher compression in chrominance planes can be achieved.

However, defining the acceptable measure of image quality that can be considered standard for lossy compression is challenging and yet to be done. The future research on DCT-based WCE should be focused more on improving the image quality.

It is necessary to avoid any complex hardware that is based on JPEG-LS. Rather, simplified algorithms should be used. DPCM, simplified DCT, simple DWT, etc., are some of the techniques that can be explored to find better compression since some algorithms based on those principles achieved a higher CR with an acceptable quality of the image. Lifting based DWT based techniques might be useful since these would be computationally less expensive compared to the matrix-based DCT. In the case of a higher order wavelet-based DWT, which can ensure better compression efficiency, a lifting based technique can be used, which simplifies the implementation [C3.132].

On the other hand, a lossless or near-lossless technique, which is based on DPCM along with an appropriate color space transformation and subsampling followed by an appropriate variable length entropy such as the Golomb–Rice coder, provides excellent quality images with low compression. DPCM might also be useful for interframe compression for higher frame rates. In most scenarios, there might not be so much differences between two consecutive frames. But,

the DPCM-based method, which compromises on the quality, is able to provide video frame rate compression; this method utilizes Har wavelet encoding along with DPCM.

Future generations of video capsules are supposed to transmit at higher frame rates while maintaining high video quality and an increased battery life. Therefore, they will require efficient video compression at the lowest possible computational cost [C3.133]. Dung *et al.*[C3.123] used a simplified format of the AVC/H.264 video encoder, which is discussed in Section VII-A. However, this lossy compression system decreases the power significantly with a reasonable CR, though it is not experimented with a higher frame rate. So, experimenting this with a higher frame rate can be a future option where a lossy compression is enough for the application. One of the main constraints to introduce a video coding algorithm in capsule endoscopy is that the encoder must be lightweight with modest computational capacity with limited battery life. Distributed source coding [C3.125] based WZ video coding (DVC) [C3.126] as mentioned in [C3.133] – [C3.135] could be a promising solution. Though this is not explored enough, many researchers recommend this technique for WCE as a promising way to enable an interframe encoder to achieve a high frame rate with light hardware [C3.135], [C3.136].

A capsule endoscopic camera, which can provide a wider field view, is an option that can be used in the future to increase the field of view [C3.137]. However, the images obtained are heavier than normal images and need to be compressed even more. One important future direction is the devising of an objective quality metric that can mimic the subjective evaluation from a physician. A comprehensive understanding of the features that the gastroenterologist monitors from endoscopic images and features being neglected by them can provide guidance toward developing a more optimized compression scheme. As more capsules will capture CCD images, which contain infrared information, it is important to utilize the available knowledge of capsule compression for CCD images in order to come up with suitable algorithms. In addition the multispectral imaging and spectral compression techniques also need to be explored, which have promising applications in WCE in the near future.

Moreover, the current generation of capsule endoscopes is dependent on the potential of the clinician to diagnose by going through each frame of video obtained from the capsule during post processing, which is inefficient and time-consuming. Hence, along with the combination of efficient compression algorithms, the future of the capsule endoscope is more promising as it tends

to utilize the property of light to make an instant diagnosis of abnormal tissue via promising imaging techniques, which include optical biopsy [C3.138], fluorescence microscopy [C3.139], molecular imaging [C3.140], auto detection, and localization of abnormalities [C3.131], and hence provide better image contrast, resolution, and detailed information. Also, the lack of movement control of capsule [C3.141] is another drawback the present endoscope system has. In the near future, the physicians will be able to control the locomotion [C3.141], [C3.142] of capsule and better diagnose the affected area with improved precision. It will also help in drug delivery [C3.142], [C3.143] to the targeted areas. Also, research to enhance the functionality of VCE software is another area that needs to be considered. The VCE software should be able to reduce diagnostic errors by automating and localizing detection of hemorrhage, lesion, and other abnormalities while providing enhanced video quality [C3.144] and hence help reduce the scanning time for the physicians during post processing of the captured data.

3.9 Conclusion

WCE has enabled the way for painless diagnosis, screening the entire GI tract, and encouraging patients have GI tract medical examinations, thus paving the way for mass screening. However, there are still many challenges related to commercial WCE that hinder its wide application, including low frame rate, low battery life, limited power resources, low image quality, low data-rate for telemetry, inability to perform automatic detection of abnormalities, etc. Despite the research into the implementation of other functionalities in WCE, the imaging unit plays a core part of the whole system to generate higher image quality and a higher frame rate while keeping bandwidth and power consumption low.

In this paper, we reviewed the major compression algorithm that is used in WCE application and presented its advantages and disadvantages. An appropriate compression algorithm can be chosen based on 1) the medical requirement of diagnosis, and 2) other electronic components that are used in the capsule. It is evident from this review that the search for an efficient compression algorithm that can overcome all challenges still remains open. An irreversible compression algorithm (lossy) shows good promise and needs to be explored more. The achievable compression depends not only on the compression algorithm, but also on the target body part, disease, and the nature of investigation. There is constant technological advancement

of WCE happening, but still there are many outstanding challenges. The urge to have an ideal real-time smart capsule in order to provide a proper and rapid diagnosis of many GI diseases, including cancer and specific characteristics of endoscopic images, still leaves an open area for specialized compression research.

References

[C3.1] K. M. Reavis and W. S. Melvin, "Advanced endoscopic technologies," *Surgical Endoscopy*, vol. 22, pp. 1533–1546, 2008.

[C3.2] M. R. Basar, F. Malek, K. M. Juni, M. S. Idris, and M. I. M. Saleh, "Ingestible wireless capsule technology: A review of development and future indication," *International Journal of Antennas and Propagation*, vol. 2012, no. 807165, pp. 1–14, 2012.

[C3.3] G. Ciuti, A. Menciassi and P. Dario, "Capsule Endoscopy: From Current Achievements to Open Challenges," *IEEE Reviews in Biomedical Engineering*, vol. 4, pp. 59-72, 2011.

[C3.4] R. Salmore, "Our heritage: A history of gastroenterology and gastroenterology nursing," *Gastroenterology Nursing*, vol. 21, no. 2, pp. 40–43, 1998.

[C3.5] M-C. Lin and L-R. Dung, "A Subsample-Based Low-Power Image Compressor for Capsule Gastrointestinal Endoscopy," *EURASIP Journal on Advances in Signal Processing*, vol. 2011, no. 257095, pp. 1-15, 2011.

[C3.6] G. Iddan, G. Meron, A. Glukhovsky, and P. Swain, "Wireless capsule endoscopy," *Nature*, vol. 405 (6785), pp. 417, 2000.

[C3.7] A. Loeve, P. Breedveld, and J. Dankelman, "Scopes too flexible and too stiff," *IEEE Pulse*, vol. 1, no. 6, pp. 2154–2287, Dec. 2010.

[C3.8] P. Turcza and M. Duplaga, "Low-power image compression for wireless capsule endoscopy," *2007 IEEE International Workshop on Imaging Systems and Techniques*, Krakow, pp. 1-4, 2007.

[C3.9] M. Mylonaki, A. Fritscher-Ravens, and P. Swain, "Wireless capsule endoscopy: A comparison with push enteroscopy in patients with gastroscopy and colonoscopy negative gastrointestinal bleeding," *Gut*, vol. 52, no. 8, pp. 1122–1126, 2003.

[C3.10] A. Moglia, A. Menciassi, M. O. Schurr, and P. Dario, "Wireless capsule endoscopy: From diagnostic devices to multipurpose robotic systems," *Biomedical Microdevices*, vol. 9, no. 2, pp. 235–243, 2007.

[C3.11] G. Iddan and P. Swain, "History and development of capsule endoscopy," *Gastrointestinal Endoscopy Clinic*, vol. 14, pp. 1–9, 2004.

[C3.12] K. Wahid, S. Ko, and D. Teng, "Efficient hardware implementation of an image compressor for wireless capsule endoscopy applications," *2008 IEEE International Joint Conference on Neural Networks (IEEE World Congress on Computational Intelligence)*, Hong Kong, pp. 2761-2765, 2008.

[C3.13] A. Moglia, A. Menciassi, and P. Dario, "Recent patents on wireless capsule endoscopy," *Recent Patents on Biomedical Engineering*, vol. 1, pp. 24–33, 2008.

[C3.14] G. Ou, N. Shahidi, C. Galorport, et al., "Effect of longer battery life on small bowel capsule endoscopy," *World Journal of Gastroenterology*, Vol. 21, pp. 2677-2682, 2015.

[C3.15] "Endoscopy Photo Gallery." [Online]. Available: http://www.naspghan.org/content/97/en/endoscopy-photo-gallery. [Accessed: 22-Jul-2017].

[C3.16] M. Keuchel, F. Hagenmüller, and H. Tajiri, *Video capsule endoscopy: A Reference Guide and Atlas*. Springer, 1st edition, 2014.

[C3.17] A. Glukhovsky, D. Avni, and G. Meron, "Diagnostic device using data compression," Patent WO 2003010967 A1, Feb 6, 2003.

[C3.18] O. Zinaty and E. Horn, "In-vivo imaging device providing data compression," US patent US9113846 B2, Aug 25, 2015.

[C3.19] P. G. Howard and J. S. Vitter, "Fast and efficient lossless image compression," *[Proceedings] DCC `93: Data Compression Conference, Snowbird*, UT, pp. 351-360, 1993.

[C3.20] D. Avni, G. Meron, E. Horn, O. Zinaty, and A. Glukhovsky, "Diagnostic device, system and method for reduced data transmission," US patent US7664174 B2, 2010.

[C3.21] E. Horn, "Device, system, and method for reducing image data captured in-vivo," Patent US7336833 B2, Jun 30, 2008.

[C3.22] T. Shigemori and A. Matsui, "Body-cavity image observation apparatus", US patent US8038608 B2, Oct 18, 2011.

[C3.23] W. R. Bandy *et al.*, "Ingestible endoscopic optical scanning device," US patent US8529441 B2, Sep. 10, 2013.

[C3.24] S. Bang *et al.*, "First clinical trial of the 'MiRo' capsule endoscope by using a novel transmission technology: electric-field propagation," *Gastrointestinal Endoscopy*, vol. 69, no. 2, pp. 253–259, 2009.

[C3.25] S. Ullah, P. Khan, N. Ullah, S. Saleem, H. Higgins, and K. S. Kwak, "A Review of Wireless Body Area Networks for Medical Applications," *International Journal of Communications, Network and System Sciences*, vol. 2, pp. 797–803, 2009.

[C3.26] T. H. Khan and K. A. Wahid, "Low Power and Low Complexity Compressor for Video Capsule Endoscopy," *IEEE Transactions on Circuits and Systems for Video Technology*, vol. 21, no. 10, pp. 1534–1546, 2011.

[C3.27] A. Menciassi, G. Ciuti and C. Cavallotti, "Future developments of video capsule endoscopy: Hardware," *Video capsule endoscopy: A reference guide and atlas*, 1st ed., Springer, pp. 543-556, 2014.

[C3.28] G. Liu, G. Yan, S. Zhao, and S. Kuang, "A complexity-efficient and one-pass image compression algorithm for wireless capsule endoscopy," *Technology and Health Care*, vol. 23 (s2), pp. S239–S247, 2015.

[C3.29] K. A. Fante, B. Bhaumik, and S. Chatterjee, "Design and Implementation of Computationally Efficient Image Compressor for Wireless Capsule Endoscopy," *Circuits, Systems, and Signal Processing*, Vol. 35 (5), pp. 1677-1703, 2015.

[C3.30] R. S. H. Istepanian, N. Philip, M. G. Martini, N. Amso, and P. Shorvon, "Subjective and objective quality assessment in wireless teleultrasonography imaging," *30th Annual International IEEE EMBS Conference, Vancouver, Canada,* pp. 5346–5349, 2008.

[C3.31] P. C. Cosman, R. M. Gray, and R. A. Olshen, "Evaluating quality of compressed medical images: SNR, subjective rating, and diagnostic accuracy," *Proceedings of the IEEE*, vol. 82(6), pp. 919–932, Jun 1994.

[C3.32] I. Fernandez-Urien *et al.*, "Capsule endoscopy capture rate: Has 4 frames-per-second any impact over 2 frames-per-second?," *World Journal of Gastroenterology*, vol. 20(39), pp. 14472–14478, Oct. 2014.

[C3.33] D. Turgis and R. Puers, "Image compression in video radio transmission for capsule endoscopy," *Sensors and Actuators A: Physical*, pp. 129–136, Sep. 2005.

[C3.34] J. Thoné, J. Verlinden, and R. Puers, "An efficient hardware-optimized compression algorithm for wireless capsule endoscopy image transmission," *Procedia Engineering.*, vol. 5, pp. 208–211, 2010.

[C3.35] M. R. Basar, M. Y. Ahmad, J. Cho, and F. Ibrahim, "Application of Wireless Power Transmission Systems in Wireless Capsule Endoscopy: An Overview," *Sensors* , vol. 14(6), pp. 10929-10951, 2014.

[C3.36] Q. Angermann, A. Histace, O. Romain, X. Dray, A. Pinna, B. Granado, "Smart videocapsule for early diagnosis of colorectal cancer: toward embedded image analysis" in *Computational Intelligence in Digital and Network Designs and Applications*, 1st edition, Springer, pp. 325-350, 2015.

[C3.37] X. Chen, X. Zhang, L. Zhang, N. Qi, H. Jiang, and Z. Wang, "A wireless capsule endoscopic system with a low-power controlling and processing ASIC," *IEEE Asian Solid-State Circuits Conference,* 3-5 Nov, Japan, pp. 321–324, 2008.

[C3.38] D. E. Boudechiche, S. Benierbah, and M. Khamadja, "A new approach to generate side information for distributed video coding in capsule endoscopy", *2014 6th International Symposium on Communications, Control and Signal Processing,* Greece, pp. 124–127, Aug 2014.

[C3.39] A. Ford and A. Roberts, "Colour space conversions," *Westminster University, London*, 1998. [Online]. Available: http://herakles.fav.zcu.cz/research/night_road/westminster.pdf [Accessed on: 22-July-2017].

[C3.40] T. H. Khan and K. a. Wahid, "Lossless and Low-Power Image Compressor for Wireless Capsule Endoscopy," *VLSI Deign*, vol. 2011, pp. 1–12, 2011.

[C3.41] C. Christopoulos, A. Skodras, and T. Ebrahimi, "The JPEG2000 still image coding system: an overview," *IEEE Transactions on Consumer Electronics*, vol. 46, no. 4, pp. 1103–1127, 2000.

[C3.42] T. H. Khan and K. A. Wahid, "Design of a Lossless Image Compression System for Video Capsule Endoscopy and Its Performance in In-Vivo Trials," *Sensors*, vol. 14(11), pp. 20779–20799, 2014.

[C3.43] P. Turcza and M. Duplaga, "Low power FPGA-based image processing core for wireless capsule endoscopy," *Sensors and Actuators A: Physical*, vol. 172, no. 2, pp. 552–560, Dec. 2011.

[C3.44] G. J. Sullivan, P. N. Topiwala, and A. Luthra, "The H. 264/AVC advanced video coding standard: Overview and introduction to the fidelity range extensions,"*, Presented at the SPIE conference on Applications of digital image processing XXVII*, pp. 454–474, Nov 2004.

[C3.45] L. Ke and M. W. Marcellin, "Near-lossless image compression: minimum-entropy, constrained-error DPCM," *IEEE Transactions on Image Processing*, vol. 7(2), pp. 225–228, 1998.

[C3.46] W. B. Pennebaker and J. L. Mitchell, *JPEG: Still Image Data Compression Standard*. Kluwer Academic Publishers, Norwell, 1950.

[C3.47] D.A. Clunie, "Lossless compression of grayscale medical images: effectiveness of traditional and state of the art approaches," *Proc. SPIE, Vol. 3980*, pp. 74–84, Feb 2000.

[C3.48] H. Kobayashi and L. R. Bahl, "Image data compression by predictive coding I: Prediction algorithms," *IBM Journal of Research and Development*, vol. 18, no. 2, pp. 164–171, 1974.

[C3.49] H. R. Schindler, "Delta modulation", *IEEE Spectrum,* Vol. 7(10), pp. 69-78, 1970.

[C3.50] D. A. Huffman, "A Method for the Construction of Minimum-Redundancy Codes," *Proceedings of the IRE*, vol. 40, no. 9. pp. 1098–1101, 1952.

[C3.51] S. W. Golomb, "Run-length encodings," *IEEE Transactions on Information Theory*, vol. 12, no. 3, pp. 399-401, 1966.

[C3.52] R. Rice and J. Plaunt, "Adaptive Variable-Length Coding for Efficient Compression of Spacecraft Television Data," *IEEE Transactions on Communication Technology*, vol. 19, no. 6, pp. 889-897, Dec. 1971.

[C3.53] V. Quotient and R. Code, "Golomb-Rice Coding." [Online]. Available: https://urchin.earth.li/~twic/Golomb-Rice_Coding.html. [Accessed: 21-July-2017]

[C3.54] J. Ziv and A. Lempel, "Compression of individual sequences via variable-rate coding," *IEEE Transactions on Infromation Theory.*, vol. 24, no. 5, pp. 530–536, 1978.

[C3.55] J. Ziv and A. Lempel, "A universal algorithm for sequential data compression," *IEEE Transactions on Information Theory*, vol. 23, no. 3. pp. 337–343, 1977.

[C3.56] C. Zeeh, "The Lempel Ziv Algorithm," [Online]. Available: https://tuxtina.de/files/seminar/LempelZiv.pdf, Stuttgart, 2003, [Accessed: 21-July, 2017]

[C3.57] M-C. Lin, L-R. Dung, and P-K. Weng, "An ultra-low-power image compressor for capsule endoscope.," *Biomedical Engineering Online*, vol. 5 (14), Feb 2006.

[C3.58] M-C. Lin, L-R. Dung, and P-K. Weng, "A cardinal image compressor for capsule endoscope*", IEEE Biomedical Circuits and Systems Conference*, London, pp. 146–149, 2006.

[C3.59] H. C. Kotze and G. J. Kuhn, "An evaluation of the Lempel-Ziv-Welch data compression algorithm," *COMSIG 1989 Proceedings: Southern African Conference on Communications and Signal Processing,* Stellenbosch, pp. 65-69, 1989.

[C3.60] J. Li and Y. Deng, "Fast Compression Algorithms for Capsule Endoscope Images," *2nd International Congress on Image and Signal Processing*, Tianjin, pp. 1-4, 2009.

[C3.61] H. K. Huang, *PACS and Imaging Informatics: Basic Principles and Applications*, 2nd ed, Wiley-Blackwell, Hoboken, 2010.

[C3.62] S. Fößel, "JPEG 2000 for Digital Cinema," in *The JPEG 2000 Suite*, John Wiley & Sons, Ltd, pp. 249–272, 2009.

[C3.63] R. Jovanovic and R. A. Lorentz, "Adaptive Lossless Prediction based Image Compression," *Applied Mathematics & Information Sciences*, vol. 8, no. 1, pp. 153-160, 2014.

[C3.64] I. H. Witten, R. M. Neal, and J. G. Cleary, "Arithmetic Coding for Data Compression," *Commun. ACM*, vol. 30, no. 6, pp. 520–540, Jun. 1987.

[C3.65] M. J. Weinberger, G. Seroussi, and G. Sapiro, "The LOCO-I lossless image compression algorithm: principles and standardization into JPEG-LS," *IEEE Transactions on Image Processing*, vol. 9, no. 8. pp. 1309–1324, 2000.

[C3.66] C. T. H. Baker, G. A. Bocharov, and C. A. H. Paul, "Mathematical Modelling of the Interleukin-2 T-Cell System: A Comparative Study of Approaches Based on Ordinary and Delay Differential Equation," *Journal of Theoretical Medicine*, vol. 1, no. 2, pp. 117–128, 1997.

[C3.67] B. Meyer and P. Tischer, "TMW - a new method for lossless image compression," in *Proc. of the 1997 International Picture Coding Symposium (PCS97)*, pp. 533–538, Sep 1997.

[C3.68] X. Li and M. T. Orchard, "Edge-directed prediction for lossless compression of natural images," *IEEE Transactions on Image Processing*, vol. 10, no. 6. pp. 813–817, Jun 2001.

[C3.69] X. Li and M. T. Orchard, "Edge directed prediction for lossless compression of natural images," *Proceedings 1999 International Conference on Image Processing (Cat. 99CH36348),* Vol. 4*, Kobe, pp. 58-62, 1999.

[C3.70] C. Kuo, T. Chou, and T. Wang, "An efficient spatial prediction-based image compression scheme," *in IEEE Transactions on Circuits and Systems for Video Technology,* vol. 12, no. 10, pp. 850-856, Oct 2002.

[C3.71] M. J. Weinberger, G. Seroussi, and G. Sapiro, "LOCO-I: a low complexity, context-based, lossless image compression algorithm," *Data Compression Conference, 1996.* DCC '96. Proceedings, Snowbird, UT, pp. 140-149, 1996.

[C3.72] G. Liu, G. Yan, B. Zhu and L. Lu, "Design of a video capsule endoscopy system with low-power ASIC for monitoring gastrointestinal tract", *Medical & Biological Engineering & Computing*, vol. 54, no. 11, pp. 1779-1791, Nov. 2016.

[C3.73] V. K. Bairagi, "Symmetry-Based Biomedical Image Compression," *Journal of Digital Imaging*, vol. 28, no. 6, pp. 718–726, Dec 2015.

[C3.74] B. E. Bayer, "Color Imaging Array," US patent US3971 065 A, Jul 20, 1976.

[C3.75] S-Y. Lee and A. Ortega, "A novel approach of image compression in digital cameras with a Bayer color filter array," *Proceedings 2001 International Conference on Image Processing (Cat. No.01CH37205),* Thessaloniki, vol.3, pp. 482-485, 2001.

[C3.76] C. C. Koh, J. Mukherjee, and S. K. Mitra, "New efficient methods of image compression in digital cameras with color filter array," *IEEE Transactions on Consumer Electronics,* vol. 49, no. 4, pp. 1448-1456, Nov. 2003.

[C3.77] X. Xie *et al.*, "A new approach for near-lossless and lossless image compression with Bayer color filter arrays," *Third International Conference on Image and Graphics (ICIG'04)*, Hong Kong, China, pp. 357-360, 2004.

[C3.78] X. Xie *et al.*, "A novel low power IC design for bi-directional digital wireless endoscopy capsule system," in *IEEE International Workshop on Biomedical Circuits and Systems*, pp. S1/8-S5-8, 2004.

[C3.79] X. Xie, G. Li, X. Chen, L. Liu, C. Zhang, and Z. Wang, "A Low Power Digital IC Design Inside the Wireless Endoscopy Capsule," *2005 IEEE Asian Solid-State Circuits Conference*, Hsinchu, pp. 217-220, 2005.

[C3.80] X. Xie, G. Li, X. Chen, X. Li, and Z. Wang, "A Low-Power Digital IC Design Inside the Wireless Endoscopic Capsule," *IEEE Journal of Solid-State Circuits*, vol. 41, no. 11, pp. 2390-2400, Nov. 2006.

[C3.81] X. Li, X. Xie, X. Chen, G. Li, Z. Wang, and H. Chen, "Design and Implementation of a Low Complexity Near-lossless Image Compression Method for Wireless Endoscopy Capsule System," *2007 IEEE International Symposium on Circuits and Systems*, New Orleans, LA, pp. 1321-1324, 2007.

[C3.82] X. Xie, G. L. Li, and Z. H. Wang, "A Near-Lossless Image Compression Algorithm Suitable for Hardware Design in Wireless Endoscopy System," *EURASIP Journal on Advances in Signal Processing*, vol. 2007, no. 1, pp. 1-13, Dec. 2006.

[C3.83] C. C. Cutler, "Differential quantization of communication signals," US patent US2605361 A, Jul 29, 1952.

[C3.84] K. Feher, "Digital Signal Processing (DSP) Techniques," *Telecommunications Measurements, Analysis, and Instrumentation*, Atlanta: Noble Publishing Corporation, pp. 75–76, 1996.

[C3.85] W. Kowalk, "DPCM - Differential Pulse Code Modulation", University of Oldenburg, 2002 [Online]. Available: http://einstein.informatik.uni-oldenburg.de/rechnernetze/dpcm.htm. [Accessed on: 22 July, 2017].

[C3.86] W-H. Steeb, "Quantization," *Mathematical Tools in Signal Processing with C++ & Java Simulations*, Singapore: World Scientific, pp. 14, 2005.

[C3.87] C. Hu, M. Q. H. Meng, L. Liu, Y. Pan, and Z. Liu, "Image representation and compression for capsule endoscope robot," *2009 International Conference on Information and Automation*, Zhuhai, Macau, pp. 506-511, 2009.

[C3.88] N. Ahmed, T. Natarajan, and K. R. Rao, "Discrete Cosine Transform," *IEEE Transactions on Computers,* vol. C-23, no. 1, pp. 90-93, Jan. 1974.

[C3.89] A. B. Watson, "Image Compression Using the Discrete Cosine Transform," *Mathematica Journal*, vol. 4, no. 1, pp. 81–88, 1994.

[C3.90] A. M. Raid, W. M. Khedr, M. A. El-dosuky, and W. Ahmed, "Jpeg Image Compression Using Discrete Cosine Transform - A Survey," *International Journal of Computer Science & Engineering Survey*, vol. 5, no. 2, pp. 39–47, 2014.

[C3.91] K. Cabeen and P. Gent, "Image Compression and Discrete Cosine Transform", [Online]. Available: http://www.lokminglui.com/dct.pdf. [Accessed on: 22 July, 2017].

[C3.92] N. R. Thota and S. K. Devireddy, "Image Compression Using Discrete Cosine Transform," *Georgian Electronic Scientific Journal: Computer Science and Telecommunication*, vol. 3, no. 17, pp. 35–42, 2008.

[C3.93] K. R. Rao and P. Yip, *Discrete cosine transform: algorithms, advantages, applications*. San Diego: Academic press, 2014.

[C3.94] S. J. Sasson, "Method and apparatus for performing image compression using discrete cosine transform," US patent US5189526 A, Feb-23, 1993.

[C3.95] A. S. Lewis and G. Knowles, "Image compression using the 2-D wavelet transform," *IEEE Transactions on Image Processing*, vol. 1, no. 2, pp. 244-250, Apr 1992.

[C3.96] W-H. Chen, H. Smith, and S. Fralick, "A Fast Computational Algorithm for the Discrete Cosine Transform," *IEEE Transactions on Communications*, vol. 25, no. 9, pp. 1004-1009, Sep 1977.

[C3.97] E. W. Jacobs, Y. Fisher, and R. D. Boss, "Image compression: A study of the iterated transform method," *Signal Processing*, vol. 29, no. 3, pp. 251–263, 1992.

[C3.98] N. B. Nill, "A visual model weighted cosine transform for image compression and quality assessment," *IEEE Transactions on Communications,* vol. 33, no. 6, pp. 551-557, Jun 1985.

[C3.99] J. Robinson and V. Kecman, "Combining support vector machine learning with the discrete cosine transform in image compression," *IEEE Transactions on Neural Networks*, vol. 14, no. 4, pp. 950-958, July 2003.

[C3.100] Y. Yang, N. P. Galatsanos, and A. K. Katsaggelos, "Regularized reconstruction to reduce blocking artifacts of block discrete cosine transform compressed images," *IEEE Transactions on Circuits and Systems for Video Technology,* vol. 3, no. 6, pp. 421-432, Dec 1993.

[C3.101] G. Strang, "The discrete cosine transform," *SIAM Rev.*, vol. 41, no. 1, pp. 135–147, 1999.

[C3.102] Y. Zhao and B. Yuan, "Image compression using fractals and discrete cosine transform," *Electronics Letters*, vol. 30, no. 6, pp. 474, 1994.

[C3.103] A. J. Ahumada Jr and H. A. Peterson, "Luminance-model-based DCT quantization for color image compression," Proc. SPIE 1666, Human Vision, Visual Processing, and Digital Display III, pp. 365-374, Aug 1992.

[C3.104] R. A. DeVore, B. Jawerth, and B. J. Lucier, "Image compression through wavelet transform coding," *IEEE Transactions on Information Theory,* vol. 38, no. 2, pp. 719-746, March 1992.

[C3.105] S. A. Khayam, "The discrete cosine transform (DCT): theory and application," *Dept. Elect. Comput. Eng., Michigan State Univ.,* Lansing, MI, USA, Tech. Rep. ECE 802-602, 2003.

[C3.106] E. Elharar, A. Stern, O. Hadar, and B. Javidi, "A hybrid compression method for integral images using discrete wavelet transform and discrete cosine transform," *Journal of Display Technology*, vol. 3, no. 3, pp. 321-325, Sept. 2007.

[C3.107] W. B. Pennebaker and J. L. Mitchell, *JPEG: Still Image Data Compression Standard.* Springer US, 1st edition, 1993.

[C3.108] N. I. Cho and S. K. Mitra, "Warped discrete cosine transform and its application in image compression*", IEEE Transactions on Circuits and Systems for Video Technology*, vol. 10, no. 8, pp. 1364-1373, Dec 2000.

[C3.109] G. K. Wallace, "The JPEG still picture compression standard," *Communications of the ACM - Special issue on digital multimedia systems*, vol. 34, no. 4, pp. 30–44, April 1991.

[C3.110] S. Aisyah and J. S. Mandeep, "Image processing using DCT and wavelet transform*", Optoelectronics and Advanced Materials-Rapid Communications*, Vol. 6, no. 1-2, pp. 29-35, 2012.

[C3.111] A. Mostafa, K. Wahid and S-B. Ko, "An Efficient YCgCo-based Image Compression Algorithm for Capsule Endoscopy", *Proceedings of 14th International Conference on Computer and Information Technology (ICCIT 2011)*, Dhaka, pp. 219-222, 2011.

[C3.112] S. K. Mohammed, KMM. Rahman and K. A. Wahid, "Lossless compression in Bayer Color Filter Array for capsule endoscopy", *IEEE Access*, vol. PP, no. 99, pp. 1-1, 2017.

[C3.113] A. Perkis, "Visual Compression*," presented at the TTT4135: Multimedia signal processing, lecture*, NTNU, Trondheim, 2016.

[C3.114] N. Jarray, M. Elhajj and A. Zitouni, "An optimized DCT compressor based on Cordic-Loeffler approach for wireless endoscopic capsule", International Journal of Advanced and Applied Sciences, Vol. 4, no. 7, pp. 59-65, 2017.

[C3.115] P. Turcza and M. Duplaga, "Hardware-Efficient Low-Power Image Processing System for Wireless Capsule Endoscopy," *IEEE Journal of Biomedical and Health Informatics,* , vol. 17, no. 6, pp. 1046–1056, 2013.

[C3.116] H. A. Peterson, H. Peng, J. H. Morgan, and W. B. Pennebaker, "Quantization of color image components in the DCT domain," *Proc. SPIE 1453, Human Vision, Visual Processing, and Digital Display II*, vol. 1453, pp. 210–222, 1991.

[C3.117] Y. Gu, X. Xie, Z. Wang, G. Li, and T. Sun, "Two-stage wireless capsule image compression with low complexity and high quality," *Electronics Letters*, vol. 48, no. 25, pp. 1588–1589, Dec. 2012.

[C3.118] R. Tajallipour and K. Wahid, "Efficient data encoder for low-power capsule endoscopy application," *10th International Conference on Information Sciences Signal Processing and their Applications (ISSPA)*, pp. 512–515, 2010.

[C3.119] Y. Q. Shi and H. Sun, *Image and video compression for multimedia engineering: Fundamentals, algorithms, and standards*. CRC press, 1999.

[C3.120] P. Turcza, T. Zieliński, and M. Duplaga, "Low complexity image coding algorithm for capsule endoscopy with Bayer color filter array," *Signal Processing Algorithms, Architectures, Arrangements, and Applications SPA 2007*. Poznan, pp. 27-32, 2007.

[C3.121] S. Lawson and J. Zhu, "Image compression using wavelets and JPEG2000: a tutorial," *Electronics & Communication Engineering Journal,* vol. 14, no. 3, pp. 112-121, Jun 2002.

[C3.122] P. Turcza, T. Zieliński, and M. Duplaga, "Hardware Implementation Aspects of New Low Complexity Image Coding Algorithm for Wireless Capsule Endoscopy," International Conference on *Computational Science – ICCS 2008,* vol. 5101, Springer Berlin Heidelberg, pp. 476–485, 2008.

[C3.123] L-R Dung, Y-Y Wu, H-C Lai and P-K Weng "A modified H.264 intra-frame video encoder for capsule endoscope," *2008 IEEE Biomedical Circuits and Systems Conference*, Baltimore, MD, pp. 61-64, 2008.

[C3.124] T. Wiegand, G. J. Sullivan, G. Bjontegaard, and A. Luthra, "Overview of the H.264/AVC video coding standard," *IEEE Transactions on Circuits and Systems for Video Technology,* vol. 13, no. 7, pp. 560-576, July 2003.

[C3.125] D. Slepian and J. K. Wolf, "Noiseless coding of correlated information sources," *IEEE Transactions on Information Theory*, vol. 19, no. 4, pp. 471–480, 1973.

[C3.126] A. D. Wyner and J. Ziv, "The rate-distortion function for source coding with side information at the decoder," *IEEE Transactions on Information Theory*, vol. 22, no. 1, pp. 1–10, 1976.

[C3.127] N. Deligiannis *et al.*, "Distributed Coding of Endoscopic Video," *IEEE International Conference On Image Processing*, pp. 1853–1856, 2011.

[C3.128] S. L. Chen, T. Y. Liu, C. W. Shen and M. C. Tuan, "VLSI Implementation of a Cost-Efficient Near-Lossless CFA Image Compressor for Wireless Capsule Endoscopy," *IEEE Access*, vol. 4, no. , pp. 10235-10245, 2016.

[C3.129] P. Turcza and M. Duplaga, "Energy-efficient image compression algorithm for high-frame rate multi-view wireless capsule endoscopy," *Journal of Real-Time Image Processing*, pp. 1-13, 2016.

[C3.130] M. D. Jensen, J. B. Brodersen, and J. Kjeldsen, "Capsule endoscopy for the diagnosis and follow up of Crohn's disease: a comprehensive review of current status," *Annals of Gastroenterology, Vol. 30, No 2*, pp. 168-178, 2017.

[C3.131] F. Deeba, S. K. Mohammed, F. M. Bui and K. A. Wahid, "Efficacy Evaluation of SAVE for the Diagnosis of Superficial Neoplastic Lesion," in *IEEE Journal of Translational Engineering in Health and Medicine*, vol. 5, pp. 1-12, 2017.

[C3.132] I. Daubechies and W. Sweldens, "Factoring wavelet transforms into lifting steps," *Journal of Fourier Analysis and Applications*, vol. 4, no. 3, pp. 247–269, 1998.

[C3.133] N. Deligiannis *et al.*, "Wyner-Ziv video coding for wireless lightweight multimedia applications," *EURASIP Journal on Wireless Communications and Networking*, vol. 2012, no. 1, pp. 106, 2012.

[C3.134] F. Pereira, L. Torres, C. Guillemot, T. Ebrahimi, R. Leonardi, and S. Klomp, "Distributed Video Coding: Selecting the most promising application scenarios," *Signal Processing: Image Communication.*, vol. 23, no. 5, pp. 339–352, 2008.

[C3.135] L. Stankovic, V. Stankovic, and S. Cheng, "Distributed compression: Overview of current and emerging multimedia applications," *Proceedings of the 18th IEEE International Conference on Image Processing (ICIP),* New York, pp. 1801–1804, 2011.

[C3.136] R. Cohen, "Feedback-less Distributed Video Coding and its Application in Compressing Endoscopy Videos," M.S. Thesis, Department of Electrical Engineering, Technion–Israel Institute of Technology, Haifa, Israel, 2012.

[C3.137] G. Wilson and K. H. Wang, "In vivo image capturing system including capsule enclosing a camera," US patent US8773500 B2, Jul 2014.

[C3.138] T. D. Wang and J. Van Dam, "Optical biopsy: A new frontier in endoscopic detection and diagnosis," *Clinical Gastroenterology and Hepatology*, vol. 2, no. 9. pp. 744–753, 2004.

[C3.139] M. A. Al-Rawhani *et al.*, "Wireless fluorescence capsule for endoscopy using single photon-based detection," *Scientific Reports*, vol. 5, no. 18591, Dec. 2015.

[C3.140] M. Goetz and T. D. Wang, "Molecular Imaging in Gastrointestinal Endoscopy," *Gastroenterology*, vol. 138, no. 3, pp. 828-833, Mar 2010.

[C3.141] A. Koulaouzidis, D. K. Iakovidis, A. Karargyris, and E. Rondonotti, "Wireless endoscopy in 2020: Will it still be a capsule?," *World Journal of Gastroenterology*, vol. 21, no. 17, pp. 5119–5130, May 2015.

[C3.142] K. Twomey and J. Marchesi, "Swallowable capsule technology: current perspectives and future directions," *Endoscopy*, vol. 41, no. 4, pp. 357–362, Apr. 2009.

[C3.143] F. Munoz, G. Alici, and W. Li, "A review of drug delivery systems for capsule endoscopy," *Advanced Drug Delivery Reviews*, vol. 71, pp. 77–85, May 2014.

[C3.144] D. K. Iakovidis and A. Koulaouzidis, "Software for enhanced video capsule endoscopy: challenges for essential progress," *Nature Reviews Gastroenterology and Hepatology*, vol. 12, no. 3, pp. 172–186, Mar. 2015.

[C3.145] J. Wu and Y. Li, "Low-complexity video compression for capsule endoscope based on compressed sensing theory," *2009 Annual International Conference of the IEEE Engineering in Medicine and Biology Society,* Minneapolis, MN, pp. 3727-3730, 2009.

[C3.146] P. Turcza and M. Duplaga, "Near-lossless energy-efficient image compression algorithm for wireless capsule endoscopy", *Biomedical Signal Processing and Control*, vol. 38, pp. 1-8, Sep. 2017.

4. Development of a Low-Cost and Portable Smart Fluorometer for Detecting Breast Cancer Cells

In Chapter 3, the current generation of WCE capsules and their compression algorithms were reviewed. Using the camera affects power consumption, battery life, frame rate, etc. As the search for efficient compression algorithm is still open, it was concluded that alternative approaches to detect abnormality should be explored. Fluorescence imaging is widely used in the various fields for selective and specific detection for different objects of interest. In order to test the principle of fluorescence imaging, a working prototype is necessary. In this work, a fluorometer is designed and developed from off-the-shelf components to test the principle of fluorescence. The built fluorometer was tested to detect the breast cancer cells which was conjugated with Green Fluorescent Protein (GFP). This device was used to differentiate between breast cancer cells and control cells. This work describes a way to detect fluorescence without camera, utilizing minimum components. This device presents a low-cost solution for selective and specific detection of breast cancer cells. Prior to this, a fluorescence microscope [4A] was developed to detect breast cancer cells.

[4A] Md. Mehedi Hasan, Mohammad Wajih Alam, Khan. A. Wahid, Sayem Miah, and Kiven Erique Lukong, "A Low-Cost digital microscope with real-Time fluorescent imaging capability," PLoS One, vol. 11, no. 12, p. e0167863, Dec. 2016.

The analysis and findings of this chapter is reported in the below mentioned published journal manuscript. The student has contributed in conceptualization, methodology, analysis, writing the original draft and revision of the manuscript.

Mohammad Wajih Alam, Khan A. Wahid, Raghuveera Kumar Goel, and Kiven Erique Lukong, "Development of a low-cost and portable smart fluorometer for detecting breast cancer cells," Biomed. Opt. Express 10, 399-410 (2019)

Development of a Low-Cost and Portable Smart Fluorometer for Detecting Breast Cancer Cells

Mohammad Wajih Alam, Khan A. Wahid, Raghuveera Kumar Goel, and Kiven Erique Lukong

Abstract

Instruments that allow the detection of fluorescence signal are invaluable tools for biomedical and clinical researchers. The technique is widely used in cell biology to microscopically detect target proteins of interest in mammalian cells. Importantly, fluorescence microscopy finds major applications in cancer biology where cancer cells are chemically labelled for detection. However, conventional fluorescence detection instruments such as fluorescence imaging microscopes are expensive, not portable and entail potentially high maintenance costs. Here we describe the design, development and applicability of a low-cost and portable fluorometer for the detection of fluorescence signal emitted from a model breast cancer cell line, engineered to stably express the green fluorescent protein (GFP). This device utilizes a flashlight which works in the visible range as an excitation source and a photodiode as the detector. It also utilizes an emission filter to mainly allow the fluorescence signal to reach the detector while eliminating the use of an excitation filter and dichroic mirror, hence, making the device compact, low-cost, portable and lightweight. The custom-built sample chamber is fabricated with a 3D printer to house the detector circuitry. We demonstrate that the developed fluorometer is able to distinguish between the cancer cell expressing GFP and the control cell. The fluorometer we developed exhibits immense potential for future applicability in the selective detection of fluorescently-labelled breast cancer cells.

4.1 Introduction

Fluorescence microscopy which is based on the principle of fluorescence imaging is a powerful tool used by many biologists as well as chemists to monitor cell dynamics and molecules in the field of biology and chemistry. These commercial fluorescent microscopes offer various advantages: live cell imaging, wide field-of-view, sensitive sophisticated cameras for high resolution images, etc. The fluorescently labelled proteins of interest help researchers to investigate any cellular process and aid in extracting meaningful information. However, these microscopes [C4.1, C4.2] are expensive as they utilize sophisticated optics making it affordable only by hospitals/research lab with healthy financial resources. Moreover, operating these microscopes requires trained operator [C4.3] who has an in-depth understanding of the microscope and knows how to optimize the components of microscope to control the wavelength, exposure and hence, retrieve data. A few low-cost fluorescent microscopes [C4.4–C4.6] were also developed to make it accessible to a greater audience from developing countries but low resolution hinders their application.

Fluorimeters, on the other hand, are commonly used in laboratory/controlled environment as well as in nature to observe/monitor the fluorescent signals emitted from the subject of interest [C4.7–C4.11]. Monitoring these signals usually helps to identify the presence of specific molecules in the object of interest. However, these fluorimeters are usually costly and bulky, and require multiple sophisticated equipment and lab environment. Furthermore, the measurements from these devices may also be susceptible to unreliable variation caused due to the changing environment/atmosphere, sensors, instrument design as well as the calibration of the equipment/parts. Hence, it is still a challenge to build a device from off-the-shelf components which do not require sophisticated equipment or environment.

Breast cancer is the most common form of cancer affecting women with 1 in 8 women expected to be diagnosed with the disease during her lifetime [C4.12]. Canadian cancer statistics project breast cancer to be the second-leading cause of cancer-related deaths among women [C4.13]. In 2017, 26,300 new cases of female breast cancer cases leading to 5000 estimated deaths, were reported in Canada [C4.14]. Though breast cancer mortality rates have declined over the years primarily due to improvements in therapy, early and effective screening is essential to lower the overall incidence and associated mortalities. The most common clinical procedures employed

for diagnosing breast cancer include X-ray mammography [C4.15] and Magnetic Resonance Imaging (MRI) [C4.16]. These equipment are large in size, sophisticated, expensive and are accompanied by high costs of operation and maintenance. The application of these diagnostic equipment in a clinical setting is therefore substantially dependent on financial factors and may not necessarily be feasible for use in low-income or developing countries. Therefore, it is imperative that alternate tools and equipment be developed to implement more economical procedures for breast cancer detection.

The use of fluorescence imaging techniques as a clinically viable alternative to detect cancer cells in vivo has gained significant momentum over the years. Several studies have described the detection of cancer cells in vivo by labelling the cells either with a selective cancer cell-permeable fluorescent chemical/dye or a fluorophore targeting a cancer-specific protein of interest [C4.17–C4.19]. However, the ultrasensitive imaging instruments used for the detection of the fluorescence signal are expensive and the entire imaging process is extensively dependent on sophisticated hardware and dedicated software. This therefore warrants the need for the development of a cost-effective instrument as a means to detect fluorescence signals in the cellular and physiological range.

In this work, we designed and fabricated a low-cost, compact, sensitive and portable fluorometer for the detection of fluorescently-labelled breast cancer cells. We present a fluorescence detection system in which the excitation source and the detector (photodiode) are placed on the opposite sides of the sample in a straight line as shown in Fig. 4.1 to detect breast cancer cells.
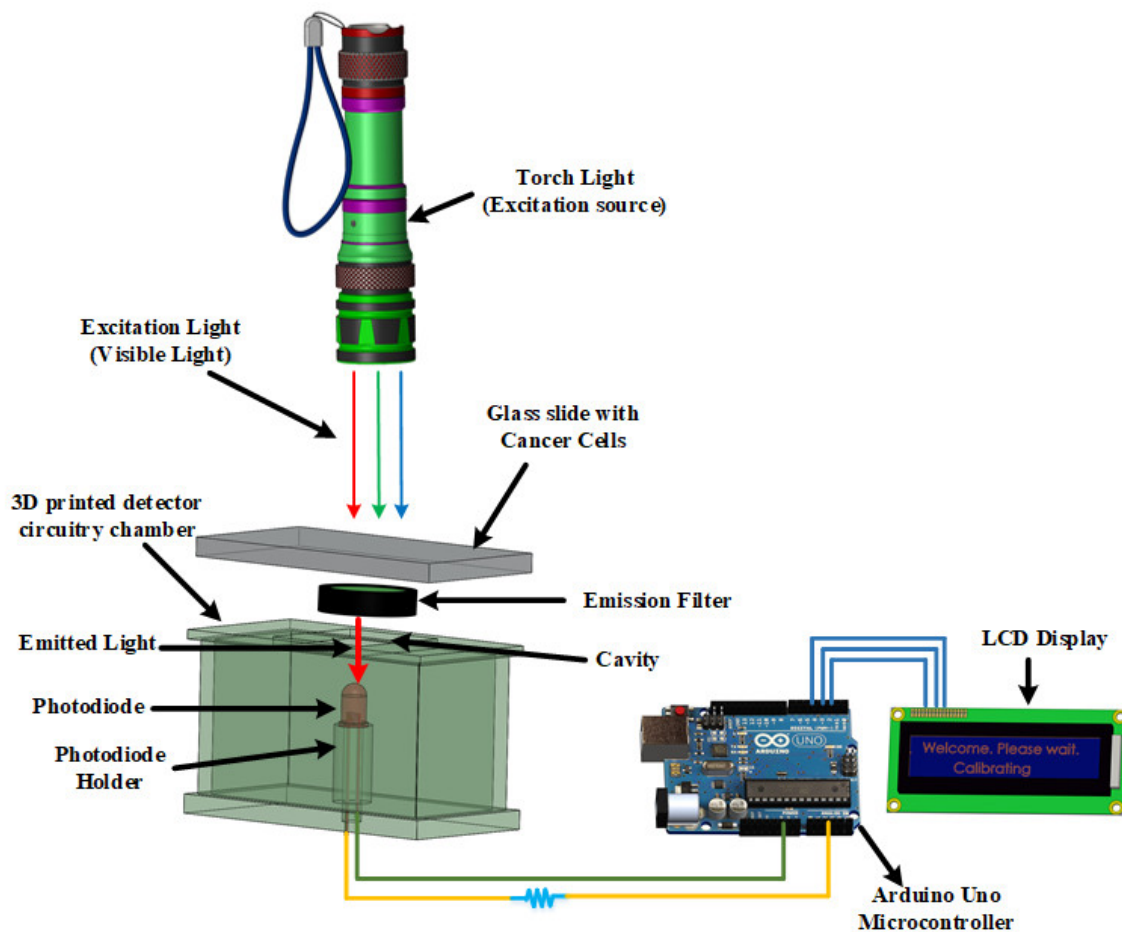
Figure 4.1 A graphical illustration and working principle of the developed device

4.2 Materials and Methods

The developed device consists of a flashlight (Ultrafire C8) which works in visible range, a photodiode (Mouser, 720-SFH203) to detect fluorescent signal, a microcontroller (Arduino Uno) to read and transmit the data and a LCD screen to display message as major components. The photodiode was chosen based on its spectral characteristics. It responds in the range of 400nm-1,100nm and has a short switching time of 5ns. This makes it an ideal candidate for use in this device. Fig. 4.1 shows the operating principle and the overall block diagram of the system where mainly the excited fluorescence signal is allowed to reach the photodiode with the help of an emission filter, thereby, improving the reliability of the system. The flashlight uses Cree XR-E Q5 type emitter which has 3 switching mode (high, low and strobe). The flashlight was operated in high mode for this experiment. The dimension of flashlight is 14.5cm x 4.5cm x4.5cm and have a luminous flux of 200 lm [C4.20, C4.21]. Fig. 4.2 shows a list of

73

off-the-shelf components that are required to assemble this device successfully. The detector circuitry is placed inside the sample chamber which is printed with 3D printer (CR-10). The complete dimension of the sample chamber is shown in Fig. 4.3. The sample chamber is black in color (Fig. 4.2(a)) in order to reduce interference.

(a)   (b)   (c)   (d)   (e)   (f)
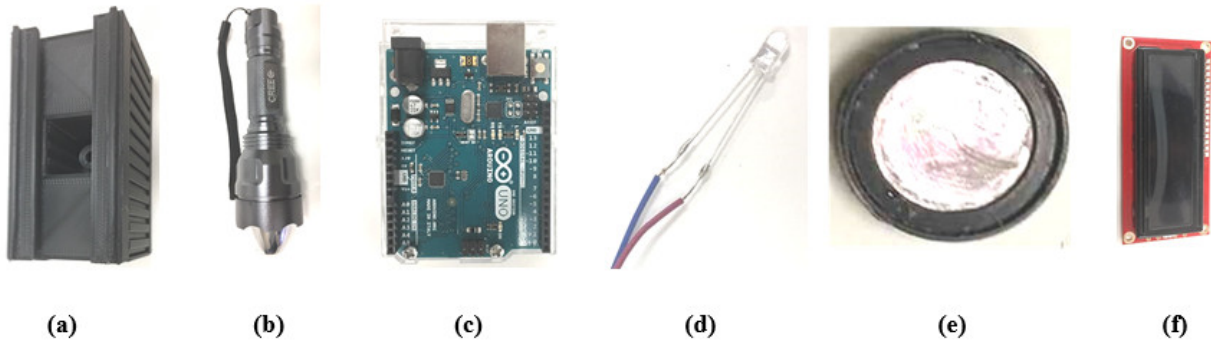
Figure 4.2 Off-the-shelf components needed to build the prototype (a) 3D printed sample chamber (b) flashlight (c) arduino uno microcontroller (d) photodiode (e) emission Filter (f) LCD display. (The images are not to scale)

(a)   (b)   (c)
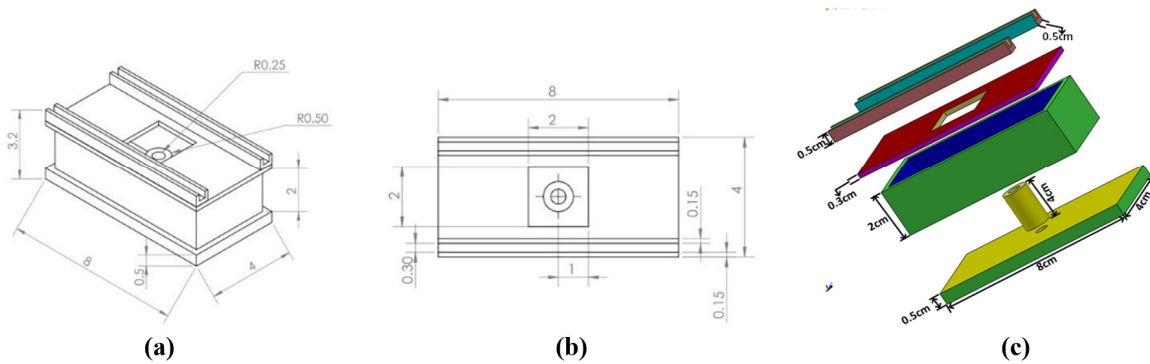
Figure 4.3 Detail dimension of the sample chamber which houses the detector circuitry. (a) isometric View (b) top view (c) 3-dimensional exploded view (all dimensions are in cm).

Immortalized human breast cancer cells were used to test the fluorometer prototype. The human breast cancer cell line, MDA-MB-231 was procured from ATCC (American Type Culture Collection, USA). These cells are cultured as a monolayer in vitro. The cells were cultured at 37°C in Dulbecco's Modified Eagles Medium (DMEM) high glucose media (SH30243.01, Hyclone) supplemented with 10% Fetal Bovine Serum (FBS). The gene encoding the Green Fluorescent Protein (GFP) was stably introduced in these cells via retroviral transduction. Briefly, the gene encoding GFP was first cloned into the retroviral plasmid, pLPC. The plasmid was then transfected in the HEK293 Amphotropic retrovirus packaging cell line, using a 1% Polyethyleneimine (PEI) solution as the transfection reagent. 24-48 hours post-transfection, the culture media containing the retrovirus was harvested and used to transduce the MDA-MB-231 cells. The transduced cells were selected with puromycin and GFP expression in the live cells was confirmed via fluorescence microscopy using a commercial Olympus inverted IX51 fluorescence microscope (Olympus, USA). It should be noted that like all immortalized mammalian (human) cell lines used in biomedical research, the MDA MB-231 cell line is cultured and grows as a monolayer in vitro, using petridishes and coverslips. Furthermore, the MDA MB-231 cells are morphologically homogenous and therefore have a uniform cell size. Changes in cellular shape are observed in instances where the cells undergo proliferation and migration [C4.22]. This however accounts for little variability in the overall cellular population due to homogeneity in growth characteristics. For imaging the cells, the cells were seeded on coverslips (Cat. # 12-540C, FisherScientific, USA) in 6-well culture dishes and cultured overnight as described above. The cells were then fixed using 1% paraformaldehyde (PFA) and the coverslips were mounted on microscope glass slides (Cat. # 12-552-3, FisherScientific, USA). The commercial glass slides and coverslips used have standard dimensions of 75 mm x 25 mm (length x width) and 25 mm x 25 mm (length x width) respectively. The thickness of the glass slides and coverslips were 1 mm and 0.25 mm respectively. Additionally, the thickness of the commercially procured glass slides and cover slips used in this study is highly uniform (identical). These materials are used extensively for imaging purposes and are manufactured with precision to ensure that the products are identical in dimensions. Such precision ensures rigorous reproducibility in the context of imaging quality. The cells were imaged using the Olympus fluorescence microscope. The same samples

were used to measure the intensity of the fluorescence signal using the developed fluorometer. The experimental setup is shown in Fig. 4.4.
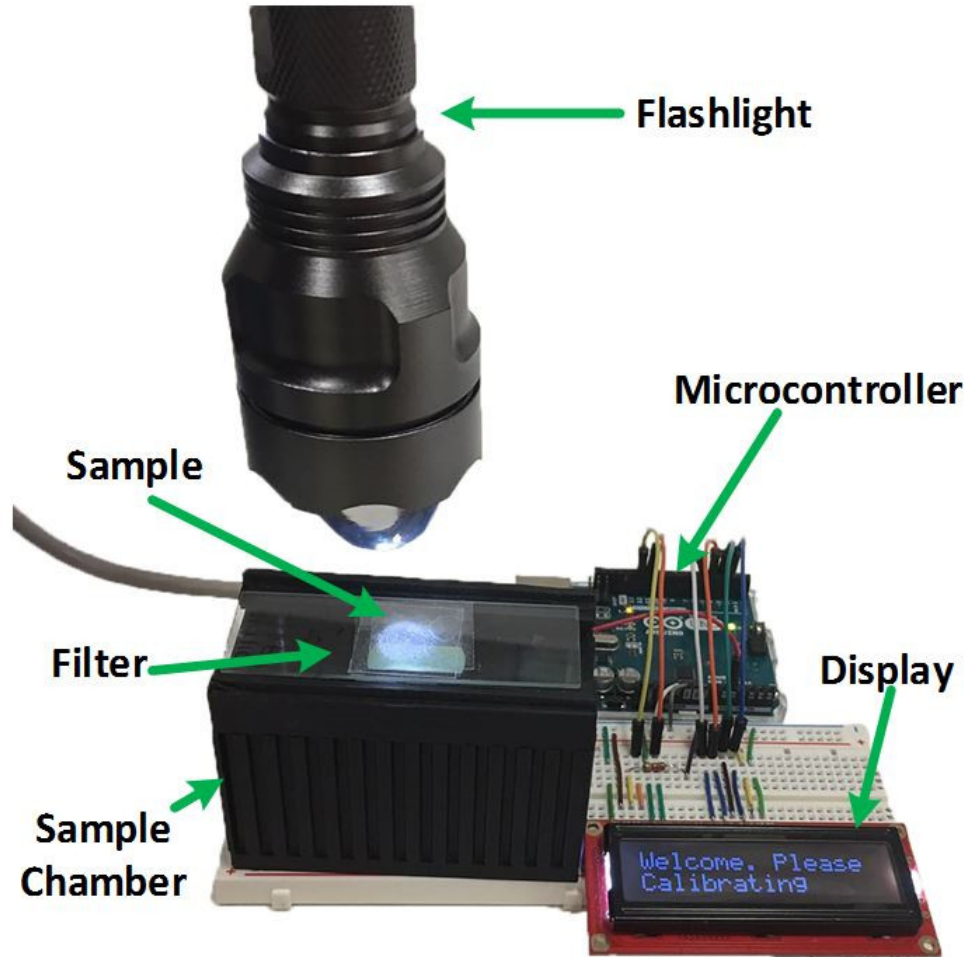
Figure 4.4 Experimental setup

4.3 Results and Discussion

Figs. 4.5(a) and 4.5(b) shows the cultured MDA-MB 231 expressing GFP when viewed under a commercial imaging system (Olympus IX51). The same cell line is then used with our prototype to detect the emitted fluorescent signal and hence confirm whether the cultured cells are fluorescent or not. The excitation and emission maximum of GFP fluorophore is 495nm

and 519nm respectively as shown in Fig. 4.5(c). The filter, light source as well as photodiode were chosen carefully to cover the excitation and emission region of this fluorophore.

Absorbance/emission spectra of the sample

(a)   (b)   (c)
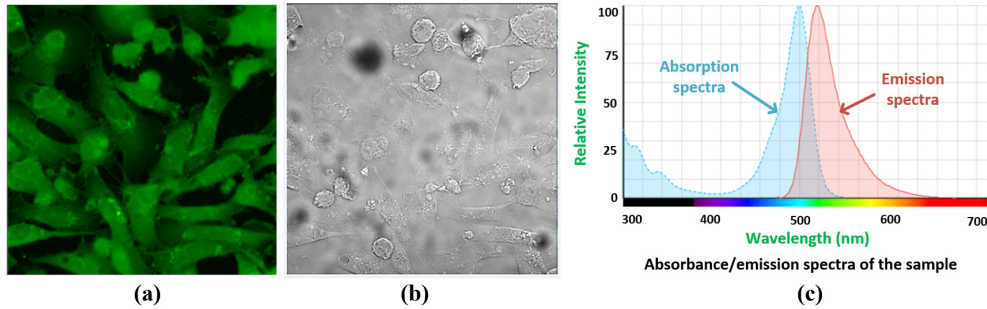
Figure 4.5 (a) Shown here is a representative image of the MDA-MB 231 breast cancer cell line visualized under a commercial fluorescence microscope (Olympus IX51 inverted microscope) (b) The same field of view of the breast cancer cells was visualized in bright field (light microscopy) using the same microscope (c) Absorption and emission spectra of Green Fluorescent Protein: This figure shows the absorption and emission spectra of the Green Fluorescent Protein where the peak absorption and peak emission of the cultured sample is 495nm and 519nm respectively (Adapted from [C4.23]).

The confluency of cultured cells on coverslip can also affect the readings of the proposed device. In order to evaluate the minimum level of confluency that is required for the device to successfully determine if the cultured cells were control cells or the cells with GFP, the cells of varying confluency were cultured on different coverslips and were finally seeded on the glass slide. The cultured cells were distributed uniformly throughout the coverslip. The cell confluency were varied as 30%, 40%, 50%, 60%, 70%, 80%, 90% and 95%. 8 samples of each concentration were made and then tested with our device. It was found that a minimum of 60% confluency is required to be able to differentiate with this device successfully. Although the device was able to detect the cells that were less than 60% confluent, the obtained readings from fluorometer were variable and the difference between the cancer cell with GFP and without GFP was less than 700mV. Since, the readings were not consistent, the result were not determined as conclusive. It is important to note that the distance between the excitation

source and the sample was kept at 2cm while taking the measurements. After taking these measurements, it is confirmed that this device will be able to differentiate between the cancer cells with GFP and control cells that are minimum of 60% confluent. Thus, all the samples that are used in the measurement, hereafter, are at least 60% confluent.

The developed prototype is a compact and portable fluorometer which provides an alternative to conventional fluorescent microscope. The visible light from flashlight excites the sample with GFP and a fluorescent signal is generated. The emitted fluorescent signal is detected with photodiode which is placed just below the emission filter inside the sample chamber. An emission filter (520nm) is placed in between photodiode and the sample, so that only the emitted fluorescent light from the sample reaches the photodiode, eliminating false detection. The emission filter was selected so that it matches the emission wavelength of GFP, hence ensuring that mainly the emitted fluorescent wavelength is allowed to pass through it. This is to ensure that the light that is received at the photodiode is from the cell line and not from the flashlight. This is confirmed when the GFP expressing cell line is replaced with the control cell and no signal is received at the receiving end. Although, popular approach is to use excitation light source along with dichroic mirror or excitation filter [4,5,22], this work shows that these filters can be omitted without affecting the performance of this device as it was also shown in [C4.25], if the set-up is done carefully.

A microcontroller (Arduino Uno) is used to control and power the complete system. It controls the detected signal and communicates the measured signal to the display. The analog signal generated by the photodiode is converted by a high-precision 10-bit analog to digital converter which is embedded in the microcontroller. Fig. 4.6 shows the flowchart of the working of the proposed device. The microcontroller is programmed in C language using the Arduino IDE compiler. At first, the device is initialized. After the initial boot is successful and the device is on, a sample of control cell is placed in the holder port of sample chamber. Then the device starts reading. This reading is performed 10 times in order to minimize the errors that can be caused due to movement or interference. An average of measurement is performed by the microcontroller and the value obtained is saved and displayed on the LCD module which will be used later in the calculation. It is to be noted that it is important to hold the flashlight/excitation source on top of the sample. Moving the flashlight away from the sample

or not focusing on the desired area will affect the result. The user might need some practice in order to get it right. The next step is to remove the control cell and replace it with cancer cell expressing GFP and the reading is performed again. As in the earlier case, 10 measurements will be taken and averaged. The averaged value is then subtracted from the value obtained from the previously stored value. If the difference is greater than 700mV, "Cancercell found" is displayed. Otherwise, "No Cancer cell" is displayed. The user is then prompted to repeat the process again.

```
                          ┌─────────┐
                          │  Start  │
                          └─────────┘
                               │
                  ┌────────────────────────────┐
                  │ Initialize GPIO pins (ADC) of│
                  │        Arduino Uno          │
                  └────────────────────────────┘
                               │         ┌──────────────────────────┐
                               │◄────────│ Insert Cancer cell without│
                  ┌────────────────────────────┐  Fluorophore        │
                  │   Read data N times and     │◄─────────────────────
                  │     calculate average       │
                  └────────────────────────────┘
                               │
                  ┌────────────────────────────┐
                  │  Save Average Value as Base │
                  │            Value            │
                  └────────────────────────────┘
                               │         ┌───────────────────────────┐
                               │◄────────│ Remove the previous sample and│
                  ┌────────────────────────────┐ insert Cancer cell with Fluorophore│
                  │   Again, Read ADC N times   │
                  └────────────────────────────┘
                               │
                  ┌────────────────────────────┐
                  │  Obtain the average value of│
                  │        ADC readings         │
                  └────────────────────────────┘
                               │
                  ┌────────────────────────────┐
                  │    Substract the value      │
                  │    Measure to the Zero      │
                  └────────────────────────────┘
                               │
                      Significant Difference
                            detected?
              Yes                          No
       ┌──────────────────────┐    ┌──────────────────────┐
       │ Display "Cancer Cell │    │ Display "No Cancer Cell│
       │     Detected"        │    │  Detected, Try again" │
       └──────────────────────┘    └──────────────────────┘
               │
          ┌─────────┐
          │   END   │
          └─────────┘
```

Figure 4.6 Operating procedure of the system

79
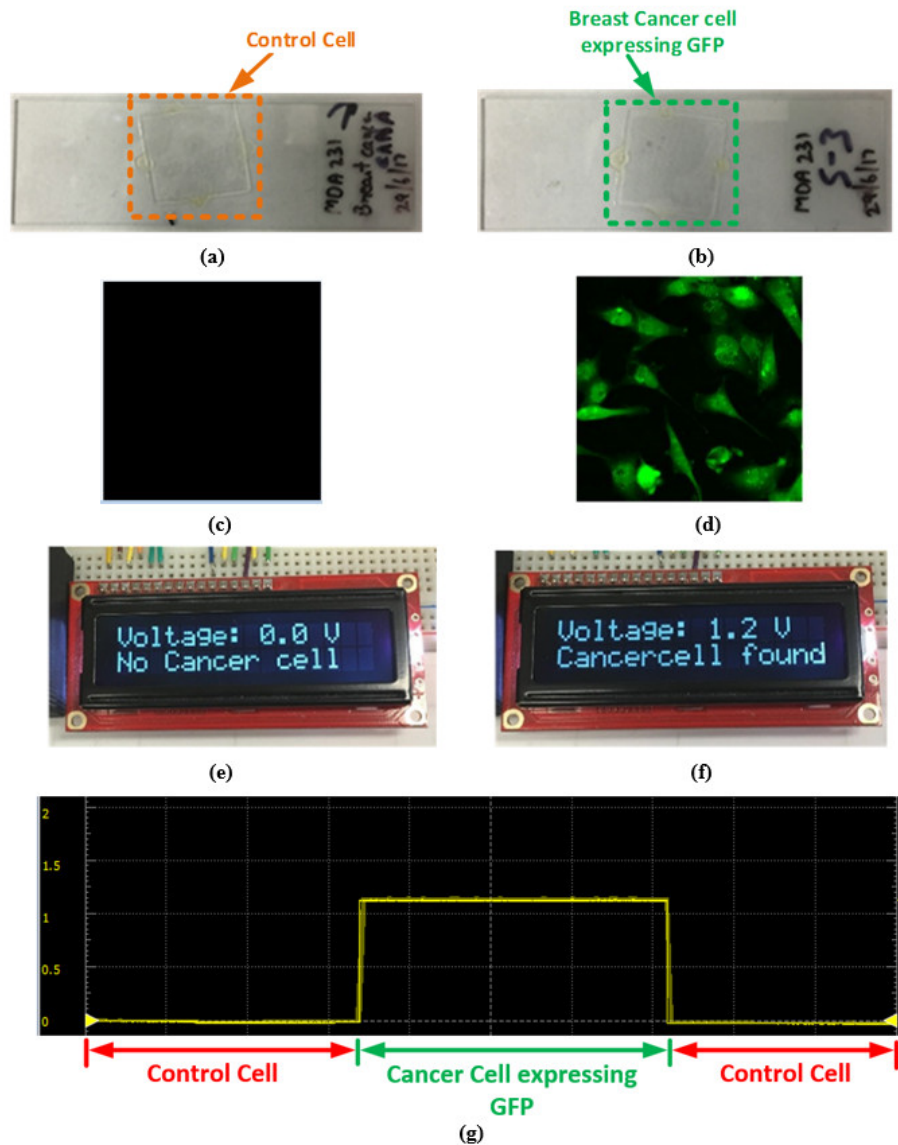
Figure 4.7 Results (a) Breast cancer cell without GFP (Control cell) cultured on a glass slide (b) Breast cancer cell conjugated with GFP fluorophore cultured on a glass slide (c) Control cell visualized under commercial microscope (d) Breast cancer cell conjugated with GFP fluorophore visualized under commercial microscope (Olympus IX51) (e) No cancer cell detected with Control cell with the proposed fluorometer (f) Cancer cell detected with Conjugated breast cancer cell with the proposed fluorometer (g) Reading on a waveform oscilloscope.

Figs. 4.7(a) and 4.7(b) shows the control breast cancer cells and the GFP expressing breast cancer cells. It can be observed that it is not possible to distinguish between these cells with naked eye. However, when the same cell lines are used with the proposed device, we are able to distinguish between these cells as can be seen in Figs. 4.7(e) and 4.7(f). The data from same samples were also read with the help of Waveform Oscilloscope on a computer as shown in Fig. 4.7(g). The oscilloscope helps in visualization of the difference in the voltage obtained when monitoring cancer cell that are conjugated with GFP and with control cell. The control cells and the breast cancer cells conjugated with fluorophore are visualized in Figs. 4.7(c) and 4.7(d) respectively with the help of a commercial fluorescent microscope [C4.1].

To evaluate the performance/effectiveness of the developed device, we employed four measurements that are commonly used in classification. These includes sensitivity, specificity, accuracy and precision. They are calculated as follows:

$$Sensitivity = \frac{TP}{TP + FN} \tag{4.1}$$

$$Specificity = \frac{TN}{TN + FP} \tag{4.2}$$

$$Accuracy = \frac{TP + TN}{TP + TN + FP + FN} \tag{4.3}$$

$$Precision = \frac{TP}{TP + FP} \tag{4.4}$$

where, TP is the number of true positives (cancer cells recognized correctly as cancer cells) and TN is the number of true negatives (i.e., control cells recognized correctly as control cells). FP is the number of false positives (i.e., Cancer cells classified incorrectly as control cells) and FN is the number of false negatives (i.e., Control cells classified incorrectly as cancer cells).

Twenty samples (ten of cancer cell expressing GFP and ten of control cell) with confluency greater than 60% were cultured on the glass slide and they were tested first with conventional fluorescent microscope [C4.1] and then with our prototype. Fig. 4.8 shows the confusion matrix drawn from the measurements obtained using the developed prototype. As it can be seen in Fig. 4.8, the proposed device was able to detect all of the control cell from the samples accurately. On the other hand, the fluorometer detected 9 out of 10 cancer cells with GFP correctly. The sensitivity, specificity, accuracy, and precision of measurement with our device were found out to be 1, 0.91, 0.95 and 1 respectively. False negative reading in this case can be related to inhomogeneous confluency in the field of coverslip. Therefore, uniform confluency of cultured cells is important in successful working of this device.

		Cancer Cell with GFP	Control Cell
Predicted Class	Cancer Cell with GFP	9 True Positive	1 False Positive
	Control Cell	0 False Negative	10 True Negative
		True Class	

Figure 4.8 Confusion Matrix

The list of major components as well as the cost that is needed to assemble this device is shown in Table 1. The total cost of this device can further be reduced by using low cost filter which can provide similar accuracy. Also, the cost can be significantly reduced if the components are bought in bulk. Table 2 shows the comparison of proposed device with other devices that are under research or are already available commercially in relation with weight, size, target of interest, cost, unit (Standalone/requires a personal computer) and power source requirement. The table is divided into two categories based on the sensing mechanism used: image based and signal based. The devices mentioned in image based category detects tuberculosis [C4.5, C4.24], imaging assays [C4.26], breast cancer [C4.4] and living cells

[C4.27] while the devices that are presented in the signal based category detects chlorophyll [C4.28–C4.30]and Escherichia [C4.32]. In addition to these devices, we have also included commercial microscope/fluorometer for comparison. These commercial devices [C4.1, C4.31] are equipped with sensitive parts and are loaded with many features. However, these devices are expensive and not portable. Hasan et al. [C4.4] detected the same breast cancer cell line that was used with the proposed device by using excitation, emission as well as dichroic mirror. Although this device has imaging capability, the use of sensitive optical filters made this microscope costly when compared with the proposed device. The developed device is lightweight (0.16kg), small in size (8cm x 4cm x 3.2cm) and costs less than other similar devices as can be seen in Table 2. By replacing the light source, optical filters and detector, this device may also be used to detect other types of cancer. These components will be selected based on the fluorophore that is conjugated with the target cancer cell. To the best of authors' knowledge, this is the first fluorometer of its kind that has been developed to detect breast cancer cells.

Table 4.1 List of major components needed to assemble this device

Components used	Model/specifications	Estimated Cost (USD)
Emission filter	520nm	75
3D printed sample chamber	Printed with CR-10	30
LCD	HC1624, 5V, 16x2	3.90
Breadboard with wires	Microtivity	6
Microcontroller	Arduino Uno R3	16.90
Flashlight	UltraFire C8	6.58
	Total Cost	**138.38**

Table 4.2 Comparison with other devices that are available in the market or are in research

Work		Weight (kg)	Dimension (cm)	Cost (USD)	Target of interest	Standalone/ Requires pc with Software	Power Source
Image Based	Miller *et al.* [C4.5, C4.24]	1	7.5x13x18	$480	Tuberculosis	Standalone	Battery Powered
	Nunez *et al.* [32]	Not known	17x18.7x31	$250	Imaging Assays	Needs PC for analysis	AC powered
	Hasan *et al.* [22]	0.13	11x6.5x15	$358	Breast Cancer	Needs PC for visualization	Battery Powered
	Babbit *et al.* [33]	Not known	Not known	$772.93*	Living cells	Standalone	Battery Powered
	Commercial microscope [C4.1]	20.5	56.5x29x57.8	$23,300	Multiple	Standalone/ needs pc for post-processing	AC powered
Signal Based	Lamb *et al.* [35]	Not known	4x4^a	$3300	Chlorophyll	Needs auxiliary component	AC powered
	Hoadley *et al.* [36]	Not known	Not known	$712.44	Chlorophyll	Standalone/ needs pc for post-processing	AC powered
	Blockstein *et al.*[37]	Not known	7.6x7.6x12.7	< $500	Chlorophyll	Needs a pc with software	AC powered
	Commercial fluorometer [38]	55	104x59x32	Not known	Multiple	Needs pc with software	AC powered
	Martin *et al.* [39]	Not known	22x100x5.3	> $170^b	Escherichia	Standalone	AC/ Battery powered
	Proposed Device	0.16	8x4x3.2^c	$138.38	Breast Cancer	Standalone	AC/ Battery powered

^{a}Height is not reported

^{b}Not reported in detail; so we calculated total cost based on the list of equipment provided in the corresponding paper

^{c}not including flashlight

This device also removes the need of expensive cameras. The sample chamber occupies only a space of 4x8 cm making it a perfect candidate for bench-top experiments. This device is very easy to use with the instruction displayed on the LCD screen for each step after it is powered on with a 5V supply or USB from a computer through Arduino Uno microcontroller. Alternatively, this device can also be connected to the serial port of the computer via USB port to enable control by the computer and thus, control input and output operations via computer through serial communication. The user needs to manually adjust the flashlight on the sample. As the focusing of the excitation light on the sample is critical in successful working of this device, the user needs some practice to efficiently use this device, hence ensuring that the readings are without error. In future, this limitation can be removed by using a mechanical system which will hold the flashlight on top of the sample at the desired position. This will ensure that the flashlight is held at correct distance and position, further ensuring the consistency of reading across all samples.

We tested functionality of our fluorometer by using this device to detect fluorescence emitted from human breast cancer cells genetically engineered to express the green fluorescence protein. These cells served as a biologically appropriate and technically convenient clinical proxy of patient tissue for the fluorescence-based selective-detection of breast cancer cells. This study involves quantifying the fluorescence signal from cancer cells cultured in vitro. This significantly differs from the morphological and physiological characteristics of cancers found to grow as "tumors" (3D culture of cells) in the human body. Our fluorometer prototype was designed to detect fluorescence emitted from cancer cells cultured in vitro. Since the morphology of the cancer cells as well as the dimensions of glass slides and coverslips used in this study were uniform, these parameters did not have an impact on the fluorometer output. However, in future, further testing may be performed to see the effect on the fluorometer output by varying the thickness of sample. As proof of principle, we first imaged the breast cancer cells using a conventional high-performance inverted fluorescence microscope (at a cost of USD 23,300) procured commercially from Olympus. As shown in Figs. 4.5(a) and 4.5(b), the microscope enabled the acquisition of high-resolution images clearly allowing visualization of green fluorescence emitted by the green fluorescent protein. Hence, this device is further simplified when compared with a regular fluorescence microscope [C4.4, C4.5, C4.22] or a fluorometer as it eliminates the need of additional

excitation filter as well as dichroic mirror. Furthermore, it is also small in size, costs less and lightweight when compared to those microscopes. Removing the cameras and the filter further eliminates the need of having to adjust light path settings, external arc lamp, and also removing the need of a filter cube to house the different set of filters. These characteristics makes this device attractive.

4.4 Conclusion

A low-cost, yet reliable, fluorometer is designed and developed in this work which measures the fluorescence signal emitted by cultured breast cancer cells expressing GFP. The goal of this work is to promote the access of fluorometers to medical and research laboratories where resources are limited. In this regard, we demonstrate the applicability of our fluorometer which is compact, lightweight and portable and it can be easily built with low-cost off-the-shelf components. Hence, this device can be relatively easily manufactured by a wide range of laboratories across the globe. This device can also be used to test other types of cancer by simply replacing the filter and photodiode to appropriately accommodate the desired conjugated fluorophore. Overall, our designed fluorometer is not only lightweight, easy-to-use, portable and compact but also entails low cost of operation and fabrication. This fluorometer has broad applications in the fluorescence-based detection of multiple cancer types and will foster research by the clinical and biomedical research community.

References

[C4.1]   "IX51 Inverted Microscope from Olympus | Biocompare.com." [Online]. Available: https://www.biocompare.com/19419-Inverted-Microscopes/396657-IX51-Inverted-Microscope/. [Accessed: 08-Nov-2018].

[C4.2]   "Meiji MT6000H Fluorescence Microscope with X-Y Stage & Focus Automation - New York Microscope Co." [Online]. Available: https://www.microscopeinternational.com/product/meiji-mt6000h-fluorescence-microscope-with-x-y-stage-focus-automation/. [Accessed: 08-Nov-2018].

[C4.3]   T. Sojinrin et al., "Plasmonic gold nanoparticles for detection of fungi and human cutaneous fungal infections," Anal. Bioanal. Chem., vol. 409, no. 19, pp. 4647–4658, 2017.

[C4.4]   M. M. Hasan, M. W. Alam, K. A. Wahid, S. Miah, and K. E. Lukong, "A Low-Cost digital microscope with real-Time fluorescent imaging capability," PLoS One, vol. 11, no. 12, p. e0167863, Dec. 2016.

[C4.5]   A. R. Miller et al., "Portable, battery-operated, low-cost, bright field and fluorescence microscope," PLoS One, vol. 5, no. 8, p. e11890, Aug. 2010.

[C4.6]   J. Kahle, R. Levin, W. Niles, B. Rasnow, M. Schehlein, and C. Shumate, "An Inexpensive Simple-to-Use Inverted Fluorescence Microscope: A New Tool for Cellular Analysis," J. Lab. Autom., vol. 15, no. 5, pp. 355–361, 2010.

[C4.7]   B. T. Wigton et al., "A Portable, Low-Cost, LED Fluorimeter for Middle School, High School, and Undergraduate Chemistry Labs," J. Chem. Educ., vol. 88, no. 8, pp. 1182–1187, Aug. 2011.

[C4.8]   S. Akraa et al., "A smartphone-based point-of-care quantitative urinalysis device for chronic kidney disease patients," J. Netw. Comput. Appl., vol. 115, pp. 59–69, Aug. 2018.

[C4.9]   D. V. Kornilin, V. N. Grishanov, and K. V. Cherepanov, "Pulse excitation fluorescence meter for diagnostic purposes," Proc. SPIE, vol. 10685, p. 41, 2018.

[C4.10] J. Kissinger and D. Wilson, "Portable Fluorescence Lifetime Detection for Chlorophyll Analysis in Marine Environments," IEEE Sens. J., vol. 11, no. 2, pp. 288–295, Feb. 2011.

[C4.11] Ó. Sampedro and J. R. Salgueiro, "Remote photonic sensor to detect crude and refined oil," Appl. Opt., vol. 56, no. 8, p. 2150, Mar. 2017.

[C4.12] "Breast Cancer Facts & Figures 2017-2018." [C4.Online]. Available: https://www.cancer.org/content/dam/cancer-org/research/cancer-facts-and-statistics/breast-cancer-facts-and-figures/breast-cancer-facts-and-figures-2017-2018.pdf. [Accessed: 08-Nov-2018].

[C4.13] "United States Cancer Statistics: Data Visualizations." [Online]. Available: https://gis.cdc.gov/Cancer/USCS/DataViz.html. [Accessed: 08-Nov-2018].

[C4.14] "Canadian Cancer Statistics Advisory Committee. Canadian Cancer Statistics 2018. Toronto, ON: Canadian Cancer Society; 2018," 2018. [Online]. Available: http://www.cancer.ca/Canadian-Cancer-Statistics-2018-EN. [Accessed: 08-Nov-2018].

[C4.15] S. P. Singh, S. Urooj, and A. Lay-Ekuakille, "Breast Cancer Detection Using PCPCET and ADEWNN: A Geometric Invariant Approach to Medical X-Ray Image Sensors," IEEE Sens. J., vol. 16, no. 12, pp. 4847–4855, Jun. 2016.

[C4.16] B. H. Choi, N. Choi, M. Y. Kim, J.-H. Yang, Y. B. Yoo, and H. K. Jung, "Usefulness of abbreviated breast MRI screening for women with a history of breast cancer surgery," Breast Cancer Res. Treat., vol. 167, no. 2, pp. 495–502, Jan. 2018.

[C4.17] G. Sun, W. Xing, R. Xing, L. Cong, S. Tong, and S. Yu, "Targeting breast cancer cells with a CuInS2/ZnS quantum dot-labeled Ki-67 bioprobe.," Oncol. Lett., vol. 15, no. 2, pp. 2471–2476, Feb. 2018.

[C4.18] L. Shi, L. Lu, G. Harvey, T. Harvey, A. Rodríguez-Contreras, and R. R. Alfano, "Label-Free Fluorescence Spectroscopy for Detecting Key Biomolecules in Brain Tissue from a Mouse Model of Alzheimer's Disease," Sci. Rep., vol. 7, no. 1, 2017.

[C4.19] J. P. Weichert et al., "Alkylphosphocholine analogs for broad-spectrum cancer imaging and therapy.," Sci. Transl. Med., vol. 6, no. 240, p. 240ra75, Jun. 2014.

[C4.20] "Ultrafire Cg-C8-3 mode Flashlight." [Online]. Available: https://www.amazon.co.uk/UltraFire-CG-C8-3-Mode-Flashlight-1x18650/dp/B00IWPGZGI. [Accessed: 05-Dec-2018].

[C4.21] Cree, "Product family data sheet Cree ® XLamp ® XP-E LEDs," 2013. [Online]. Available: http://www.cree.com/led-components/media/documents/XLampXPE.pdf. [Accessed: 05-Dec-2018].

[C4.22] D. C. Fingar, S. Salama, C. Tsou, E. Harlow, and J. Blenis, "Mammalian cell size is controlled by mTOR and its downstream targets S6K1 and 4EBP1/eIF4E.," Genes Dev., vol. 16, no. 12, pp. 1472–87, Jun. 2002.

[C4.23] M. Shirley, A., Handley, C., Bryant, S., Hall, W. A. Shirley, C. Handley, S. Bryant, and M. Hall, "Quantization of Immunoglobulin E Using Fluorescence Assay," Chem., vol. 2, no. 87, pp. 1–7, 2014.

[C4.24] A. R. Miller, G. Davis, M. Pierce, Z. M. Oden, and R. Richards-Kortum, "Portable, battery-operated, fluorescence field microscope for the developing world," Prog. Biomed. Opt. Imaging - Proc. SPIE, vol. 7556, 2010.

[C4.25] J. J. Lamb, J. J. Eaton-Rye, and M. F. Hohmann-Marriott, "A Cost-Effective Solution for the Reliable Determination of Cell Numbers of Microorganisms in Liquid Culture," Curr. Microbiol., vol. 67, no. 2, pp. 123–129, 2013.

[C4.26] I. Nuñez et al., "Low cost and open source multi-fluorescence imaging system for teaching and research in biology and bioengineering," PLoS One, vol. 12, no. 11, p. e0187163, Nov. 2017.

[C4.27] K. N. Babbit, G. A., Hanzlik, C. A., Busse, "Observing fluorescent probes living cells using a low-cost LED flashlight retrofitted to a common vintage light microscope," J. Microbiol. Biol. Educ., vol. 1, no. 14, pp. 121–124, 2013.

[C4.28] J. Lamb, K. Forfang, and M. Hohmann-Marriott, "A Practical Solution for 77 K Fluorescence Measurements Based on LED Excitation and CCD Array Detector," PLoS One, vol. 10, no. 7, p. e0132258, Jul. 2015.

[C4.29] K. D. Hoadley and M. E. Warner, "Use of Open Source Hardware and Software Platforms to Quantify Spectrally Dependent Differences in Photochemical Efficiency and Functional Absorption Cross Section within the Dinoflagellate Symbiodinium spp.," Front. Mar. Sci., vol. 4, p. 365, Nov. 2017.

[C4.30] L. Blockstein and O. Yadid-Pecht, "Lensless Miniature Portable Fluorometer for Measurement of Chlorophyll and CDOM in Water Using Fluorescence Contact Imaging," IEEE Photonics J., vol. 6, no. 3, pp. 1–16, Jun. 2014.

[C4.31] "FS5 Spectrofluorometer | Steady State | Edinburgh Instruments." [Online]. Available: https://www.edinst.com/us/products/fs5-spectrofluorometer/. [Accessed: 08-Nov-2018].

[C4.32] F. J. F. Martín et al., "A Novel Handheld Fluorimeter for Rapid Detection of Escherichia coli in Drinking Water," IEEE Sens. J., vol. 16, no. 13, pp. 5136–5144, 2016.

Addendum on Chapter 4

The excitation spectrum provides information about the range of wavelength at which the given solution when illuminated by the excitation source produces fluorescence and emission spectrum provides information about which wavelengths are generated from the solution when illuminated by excited light. The absorbance spectra provide information on which wavelengths are absorbed by the solution. This is done by illuminating solution with varying wavelength of the incident light with monochromator and reading the intensity of transmitted light with a detector [A1.1].

In order to obtain the excitation spectra, the wavelength of emission monochromator is fixed at a known wavelength and the wavelength of the excitation monochromator is scanned across the desired wavelength range. In order to obtain the emission spectra, the wavelength of the excitation monochromator is fixed at a known wavelength to excite the sample and the wavelength of the emission monochromator is scanned across the desired wavelength range and relative intensity of the fluorescence is plotted [A1.2]. The absorption, emission and excitation spectrum are typically measured by using a spectrofluorometer. The excitation and absorption spectrum is identical [A1.3]. Hence, these spectra are obtained by keeping the emission wavelength or excitation wavelength constant while the other spectrum range is scanned to record the information.

The difference between excitation peak and emission peak of wavelengths is called Stokes shift. The greater the Stokes shift, the easier it is to distinguish between excitation and emission light and better will be the developed device's accuracy. The intensity of emission spectra is usually lower than the excitation spectra. This is why, the sample is usually excited at the peak of the excitation spectra and detected at the peak of the emission spectra. The excitation and emission spectra can be separated by using appropriate optical filters. This is particularly important where the stokes shift is small which causes overlap in the excitation and emission spectrum. The use of optical filters also helps in reducing interference which can be caused by using a source which has a wider spectrum so that only the wavelengths of interest passes onto the sample. This is why, in this study an emission filter is used which passes the wavelength between 502 nm to 538 nm through it. This ensures that the selected filter covers the emission range of the GFP fluorophore as shown in Fig 4.5 (c). The detection circuitry, emission filter and the excitation source were

selected based on the GFP fluorophore which was conjugated with the breast cancer cell line in this study.

There was an error in reporting the definition of false negative and false positive in the manuscript. False negative refers to: cancer cells classified incorrectly as control cells and false positive refers to: control cells classified incorrectly as cancer cells. Therefore, the sensitivity, specificity, accuracy, and precision of measurement with the developed device were found out to be 0.9, 1, 0.95, and 1 respectively.

		Cancer Cell with GFP	Control Cell
Predicted Class	Cancer Cell with GFP	9 True Positive	0 False Positive
	Control Cell	1 False Negative	10 True Negative
		True Class	

Figure 4.8 Confusion Matrix (Corrected)

This study helped to realize:

(a) the potential of fluorescence imaging in detecting the cancer cells using low-cost off-the-shelf components.

(b) this study also showed that the dichroic mirror, excitation filter and filter cube can be omitted without affecting performance if the set-up is done carefully.

(c) low-weight and portable device can be used for this purpose.

(d) the selection of the detection and illumination circuitry should be based on the selected fluorophore.

(e) this study presented us with an opportunity to test the principle in detecting other cancer cell line when the fluorophore is same but conjugated with a different cancer cell line. In this case, we do not need to change the excitation and detection circuitry.

(f) this study also presented us with an opportunity when we can detect a different cell line which is conjugated with a different fluorophore. In this case, the excitation and detection circuitry should be selected based on the fluorophore as shown in Chapter 5. In Chapter 5, IRFP702 fluorophore is conjugated with the colorectal cancer cell line and the excitation

and emission circuitry is modified according the wavelength spectra of IRFP702 fluorophore to differentiate between cancer cells and the control cells.

(g) Although camera is an important part of a fluorescent microscope, a camera-less system can be used to differentiate between the cancer cell and control cell. This opened an opportunity to screen cancer with sensor-based components in a WCE system as shown in Chapter 6.

[A1.1]"Absorption, emission, and excitation" [Online]. Available: https://www.edinst.com/blog/what-are-absorption-excitation-and-emission-spectra [Accessed: 11-July-2020]

[A1.2]"OlympusFluoroexcitation"[Online]. Available: https://www.olympus-lifescience.com/en/ microscope-resource/primer/lightandcolor/fluoroexcitation [Accessed: 11-July-2020]

[A1.3] J.R. Albani, "Structure and dynamics of macromolecules: Absorption and Fluorescence Studies", Elsevier Science, 978-0-444-51449-3, 2004.

5. A Low-Cost and Portable Smart Instrumentation for Detecting Colorectal Cancer Cells

In the previous chapter, we were successfully able to differentiate between cultured control cell and the fluorescently labelled breast cancer cells. The breast cancer cells were conjugated with GFP which has excitation and emission wavelength of 495 nm and 519 nm respectively. It was tested both with fluorescent microscope and the fluorometer. The successful distinction between breast cancer cells and control cells helped us to realize the potential of the fluorescence imaging and encouraged us to test this principle in the WCE device for detecting abnormalities in GI region. Thus, in this chapter, we took the work further to test a GI cancer. The designed fluorometer was used to test the detection of colorectal cancer which was conjugated with a different fluorophore (IRFP702) whose excitation and emission wavelength is different than GFP. The emission and detection components of the designed fluorometer in Chapter 4 were changed to accommodate the excitation and emission wavelength of IRFP702 fluorophore. The excitation and emission range of IRFP702 is 673nm and 702nm respectively. The developed device is lightweight, easy-to-use, portable and compact and has the potential to foster research in many laboratories around the globe without the financial burden of the commercial instruments. The experimental results also show that the device can detect multiple types of cancer based on fluorophore by making changes in excitation and emission components.

The analysis and findings of this chapter is reported in the below mentioned published journal manuscript. The student has contributed in conceptualization, methodology, analysis, writing the original draft and revision of the manuscript.

Mohammad Wajih Alam; Khan A. Wahid; Md. Fahmid Islam; Wendy Bernhard; Clarence R. Geyer; Franco J. Vizeacoumar. A Low-Cost and Portable Smart Instrumentation for Detecting Colorectal Cancer Cells. Appl. Sci. 2019, 9, 3510.

A Low-Cost and Portable Smart Instrumentation for Detecting Colorectal Cancer Cells

Mohammad Wajih Alam, Khan A. Wahid, Md. Fahmid Islam, Clarence R. Geyer, and Franco J. Vizeacoumar

Abstract

Fluorescence imaging is a well-known method for monitoring fluorescence emitted from the subject of interest and provides important insights about cell dynamics and molecules in mammalian cells. Currently, many solutions exist for measuring fluorescence, but the application methods are complex and the costs are high. This paper describes the design and development of a low-cost, smart and portable fluorimeter for the detection of colorectal cancer cell expressing IRFP702. A flashlight is used as a light source, which emits light in the visible range and acts as an excitation source, while a photodiode is used as a detector. It also uses a longpass filter to only allow the wavelength of interest to pass from the cultured cell. It eliminates the need of both the dichroic mirror and excitation filter, which makes the developed device low cost, compact and portable as well as lightweight. The custom-built sample chamber is black in color to minimize interference and is printed with a 3D printer to accommodate the detector circuitry. An established colorectal cancer cell line (human colorectal carcinoma (HCT116)) was cultured in the laboratory environment. A near-infrared fluorescent protein IRFP702 was expressed in the colorectal cancer cells that were used to test the proof-of-concept. The fluorescent cancer cells were first tested with a commercial imaging system (Odyssey® CLx) and then with the developed prototype to validate the result in a preclinical setting. The developed fluorimeter is versatile as it can also be used to detect multiple types of cancer cells by simply replacing the filters based on the fluorophore.

Index Terms

Fluorescence imaging, fluorimeter, colorectal cancer, IRFP702, fluorescence microscopy

5.1 Introduction

The combined advancement in the field of molecular biology and optics has revolutionized the investigation methods used in the field of biology and chemistry. The progress in fluorescence microscopy and molecular tagging has also enabled the pathways to analyze the dynamics of cells with molecule-specific contrast [C5.1, 5.2]. In recent years, these fluorescent microscopes have garnered a lot of attention, as they offer multiple benefits and possibilities including live-cell imaging, high-resolution images and localization of fluorescence in cells. However, these fluorescent microscopes are expensive as they use sensitive and sophisticated equipment/parts [C5.3] making it affordable only to hospitals/institutions with sound financial resources. These microscopes also require a trained operator [C5.4] in order to utilize their functionality efficiently, such as adjusting the illumination, optical alignment, correct lens changeovers, filtration techniques and capturing images. A few low-cost fluorescent microscopes were developed recently [C5.5, 5.6, 5.7] to make it more affordable to researchers from developing countries but the low resolution still obstructs its wide application. On the other hand, fluorimeters measure fluorescent signal intensity emitted from the dyes that are attached to the biological molecules as well as naturally fluorescent molecules based on their excitation and emission wavelengths. These devices are commonly used for monitoring chlorophyll [5.8, 5.9, 5.10] in water. Monitoring these fluorescent signal helps researchers to find out the presence of specific molecules in the targets of interest [C5.11] based on signal intensity [C5.12]. A recent work [C5.12] showed the detection of breast cancer cells with the help of a fluorometer. However, these devices are often bulky and costly as well as vulnerable to inconsistent fluctuation caused due to the changing environment, sensors and instrument design, as well as calibration of the equipment/parts.

Colorectal cancer is the third most common type of cancer diagnosed in both men and women. It is also the third most leading cause of cancer-related deaths in the United States [C5.13]. However, diagnosing cancer requires the use of expensive equipment (such as magnetic resonance imaging (MRI)) as well as a trained operator, which limits its use in the developing countries. Furthermore, in many regions around the world, the resources are limited due to the high cost of instrumentation as well as lab supplies. Though colorectal cancer mortality rates have declined mainly due to the advancement in technology, early and effective screening is needed to further reduce associated mortalities. The most common clinical procedure employed for diagnosing

cancer includes colonoscopy (the gold standard) [C5.14] which is both invasive and relatively expensive. This procedure is complex and is accompanied by high costs of operation. Providing each individual with hands-on access to commercial equipment requires either multi-week training through a set of experiments or the deployment of multiple instruments, which therefore has been both cost and time prohibitive.

The use of fluorescence microscopy to visualize living cells is often achieved via specific labelling of proteins [C5.15] through antibody, bio-specific ligand or nanobody that is conjugated to a fluorophore. Fluorescent labelling is usually achieved by using a reactive derivative of the fluorophore, which specifically binds to a selective group contained in the target molecule. Several studies have shown the detection of cancer cells by labelling the proteins of interest. In association with the recent development of biomarker sciences, fluorescence imaging is being used as a tool to detect complex human diseases based on targetable biomarkers. For example, cancer cells express many biomarkers which can be utilized to develop fluorescent probes (e.g., fluorescent antibodies) and detect cancer tissues with fluorescent microscopy or imaging instruments [C5.16, C.17]. Although these techniques utilize ultrasensitive imaging instruments for monitoring the fluorescent signal, these modern systems are costly and need dedicated software as well as sophisticated hardware. Hence, it is a need that a low-cost device is developed which can help to differentiate between the fluorescent cancer cells and control cells (colorectal cancer cell which does not express IRFP702 fluorophore). In this work, we designed and developed a portable fluorimeter utilizing off-the-shelf components which is not only low-cost but also sensitive enough to distinguish between the IRFP702 conjugated cancer cells and control cells.

5.2 Materials and Methods

Most substances absorb light. The substances which absorb light at a particular wavelength and energy but emit light at a longer wavelength but lower energy are called fluorescence substances and the principle is called fluorescence. Fluorescent dyes or quantum dots are most commonly used as fluorescence substance. Hence, when a light of sufficient intensity is incident upon samples which are conjugated with a fluorophore dye, these samples absorb light and emit at a longer wavelength. However, these are of low intensity. The proposed

97

device exploits this principle of fluorescence to detect colorectal cancer cells. Fig. 5.1a shows the working principle of a typical fluorescence microscope [C5.7], whereas Fig. 5.1b shows the working principle of the proposed fluorimeter. In this paper, IRFP702 is used as a dye which is conjugated with colorectal cancer cells (human colorectal carcinoma (HCT116)). The peak absorption and emission wavelength of infrared protein (IRFP702) are 673 nm and 702 nm respectively. As can be seen in Fig. 5.1b, the excitation light (in the visible range) from the flashlight is focused on the top of the sample. The emitted light at a longer wavelength from the sample is then passed through a hard-coated longpass filter (Edmund Optics, Stock# 62-980) whose longpass wavelength is 700 nm. The fluorescent light is detected by the photodiode. The photodiode is placed inside a custom-built sample chamber which is black in color to minimize the interference from the ambient light. The microcontroller reads the data from the photodiode and displays it on a liquid crystal display (LCD).

(a)   (b)
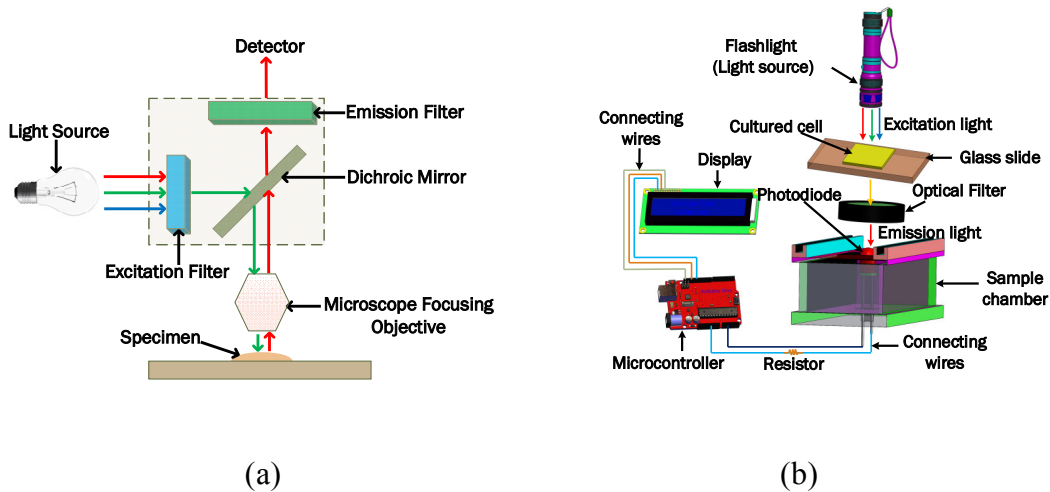
Figure 5.1 Fluorescence imaging: (a) working principle of a typical fluorescence microscope and (b) a three-dimensional illustration of the proposed fluorimeter.

The proposed device is comprised of a flashlight (Ultrafire C8) [C5.18], a photodiode (OSRAM Opto Semiconductors SFH 203) [C5.19, C.20], a microcontroller (Arduino UNO REV3 (surface-mount device) SMD version) [C5.21] and a LCD (Basic 16 × 2 Character LCD—White on Black 3.3 V version) screen [C5.22] as major components. The photodiode is used to detect fluorescent signal while the microcontroller is used to read and transmit data

detected from the photodiode to the LCD display. The chosen photodiode has a short switching time of 5 ns while its responsivity lies in the range of 400–1100 nm and is available in a 5 mm LED plastic packaging. The relative spectral sensitivity of this photodiode at 702 nm is 0.82 and it has a radiant sensitive area of 1 mm^2. This wide spectral characteristic of the photodiode makes it versatile and an ideal candidate to be used in the designed fluorimeter. The overall working principle is shown in Fig. 5.1b where it is clear that the flashlight is placed in a straight line on top of the sample. The sample is placed in between the longpass filter and flashlight. The optical longpass filter/high pass filter is designed to transmit wavelengths greater than the cut-on wavelength of the filter and block the lower wavelengths. The detector circuitry is placed inside the sample chamber. The received signal from the photodiode is processed with the help of an Arduino Uno microcontroller and displayed on an LCD display. The major components that are required to assemble the fluorimeter are shown in Fig. 5.2. The chosen flashlight has a dimension of 14.5 cm × 4.5 cm × 4.5 cm and can operate in three modes: strobe, low and high. It is operated with a rechargeable 3.7 li-ion battery and has a 3000 mAh current rating. For this experiment, the flashlight was operated in high mode. It uses a Cree XR-E Q5 type emitter, which has a luminous flux of 200 lm [C5.23]. The sample chamber is designed with SolidworksTM and printed with the help of a 3D printer (CR-10), which is black in color in order to reduce unwanted noise. The complete dimension of the custom-built sample chamber is shown in Fig. 5.3. To further minimize the interference, a longpass filter is used to pass only the fluorescence wavelengths while filtering out the unwanted spectrum from the flashlight. This longpass filter is placed between the sample and the photodiode. The measured signal is then processed using the microcontroller.
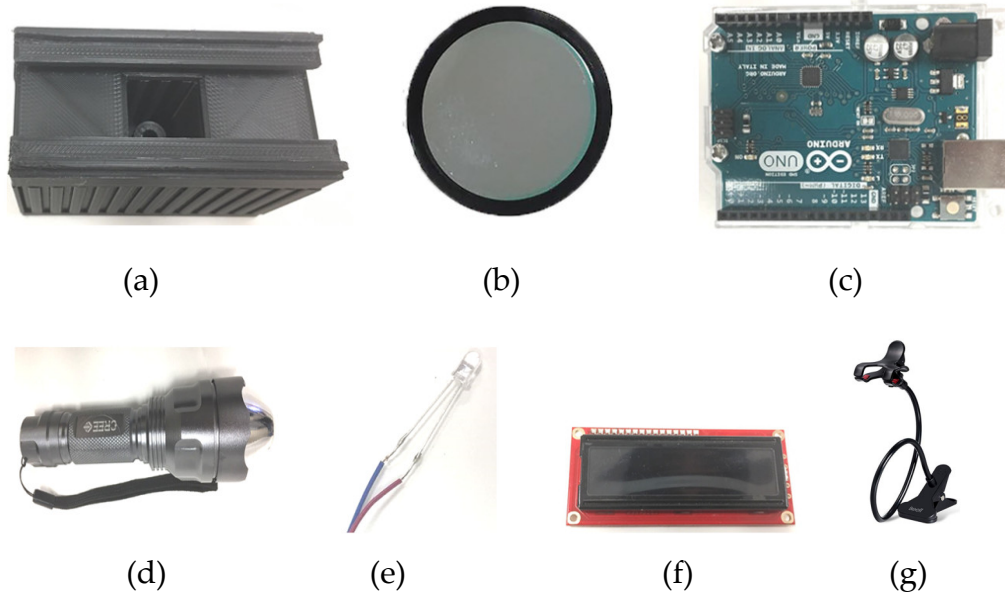
Figure 5.2 Off-the-shelf commercial components used to construct the prototype: (a) 3D printed sample chamber, (b) longpass filter, (c) microcontroller (Arduino Uno), (d) flashlight, (e) photodiode, (f) LCD display, and (g) holder (images are not to scale).
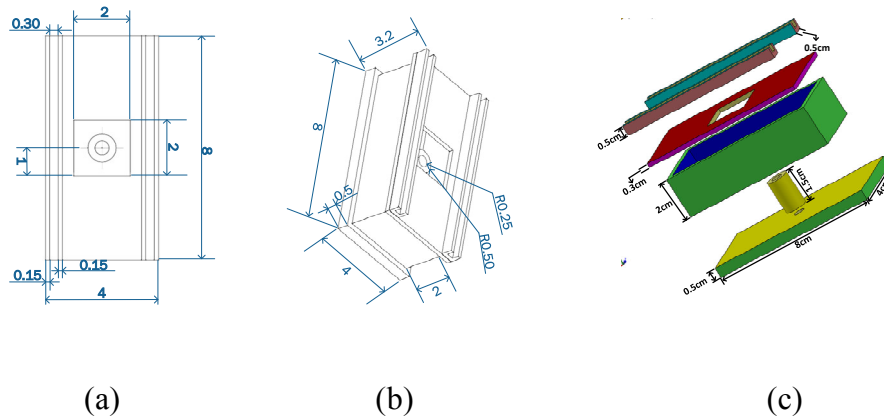
Figure 5.3 Dimension of custom-built sample chamber printed with 3D printer which houses detector circuitry (CR-10): (a) top view, (b) isometric view, and (c) 3-dimensional view (exploded). All dimensions in this figure are given in cm.

IRFP702 fluorophore was expressed in the colorectal cancer cells (HCT116) using the lentiviral transduction method to test the developed prototype. The gene encoding IRFP702 was cloned into the pHAGE plasmid backbone (Addgene, Watertown, MA, USA) to construct pHAGE-IRFP702. To prepare a lentivirus, 8×105 293-F (Thermo Fisher Scientific, Waltham, MA, USA) cells were plated for 24 h in 90% Dulbecco's Modified Eagle Medium (DMEM) medium (Thermo Fisher Scientific). One microgram of pHAGE-IRFP702 was mixed with 0.5 µg of pSPAX.2 (Addgene) and 0.5 µg pMD2.G (Addgene) in 100 µL of Opti-Eagles minimum essential media (Opti-MEM) (Thermo Fisher Scientific). Polyethylenimine (PEI) (Sigma-Aldrich, Saint Louis, MO, USA) was added to 100 µL of Opti-MEM to a final concentration of 120 µg/ ml. The DNA and PEI mixtures were mixed together and incubated at room temperature for 20 min to prepare a transfection mix. The transfection reaction was added to the cells drop-wise and incubated at 37 °C with 5% CO_2. The virus was collected 72 h after the transfection. For the transduction, 1.5×105 HCT116 cells (American Type Culture Collection) were plated for 24 h in HyClone™ McCoy's 5A Media (Fisher Scientific, Pittsburgh, PA, USA). The next day, the media was removed and replaced with 500 µL of 90% McCoy's 5A medium with 4 µg/mL of polybrene (Sigma-Aldrich) and incubated at 37 °C for 10 min. Five µL of the virus was added to the cells and then centrifuged at $1500 \times$ g for one hour. The cells were incubated at 37 °C with 5% CO_2 overnight. The next day, the media was replaced with 90% McCoy's 5A medium. Five days later the cells were analyzed on a Gallios flow cytometer (Beckman Coulter, Brea, CA, USA) to ensure infection. The cells that were positive for IRFP702 were sorted from the negative population on a MoFlo Astrios EQ Cell Sorter (Beckman Coulter). IRFP702 expression in the cells was confirmed via scanning and imaging in the 700 channel on the Odyssey CLx (LI-COR Biosciences, Lincoln, Nebraska, USA). For fluorescence analyses, the fluorescent cells and matching non-fluorescent cells (control) were seeded on coverslips in 6-well culture dishes and cultured overnight in McCoy's 5A Media. The commercial glass slides (Cat. # 12-552-3, Fisher Scientific, USA) and coverslips (Cat. # 12-540C, Fisher Scientifc, USA) have standard dimensions of 75 mm × 25 mm (length × width) and 25 mm × 25 mm (length × width) respectively. An EVOS Cell Imaging System (Thermo Fisher Scientific) was used to follow the growth of the cells. The cells were then fixed using 1% paraformaldehyde (PFA) (Sigma-Aldrich) on a glass slide which was used to test the prototype.

5.3 Results and Discussion

Fig. 5.4a illustrates the experimental setup of our developed prototype, while Fig. 5.4b is an image of the commercial system (Li-Cor Odyssey) used to visualize the cancer cells with and without conjugating fluorophore. The resulting device is portable, which uses less power, costs less, is small in size as well as lightweight and provides an alternative to the conventional fluorescent microscope. The photodiode is kept inside the custom-built sample chamber and the flashlight is held on top of the cultured sample. When the light from the excitation source excites the cultured sample of HCT116 cells expressing IRFP702, a fluorescent signal is produced. At the receiving end, the light is collected by the photodiode and is converted to the current, which is linearly proportional to the collected light [C5.24]. The photodiode is reverse biased with the help of Arduino Uno's 5 V pin, and the anode is connected to the ground via a resistor. The Arduino Uno has 5 analog pins (A0–A5). The photodiode is connected to the Arduino Uno through a A0 pin. When the light strikes the photodiode, it causes the current to flow through the resistor, which causes the voltage across it. The sensitivity of photodiode was adjusted by utilizing this principle.
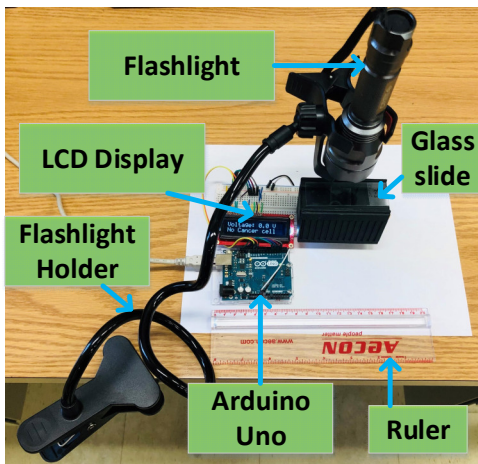
(a)   (b)

Figure 5.4 Experimental setup: (a) an overall setup of the proposed system (ruler is added in the picture to show the relative size) and (b) a commercial system: Li-Cor Odyssey.

In order to test the minimum confluency required for the proposed device to work successfully, we cultured the cells of different confluency on the coverslips. The confluency of the cells varied from 10% to 90% in 10 percent increments. The samples were distributed evenly throughout the coverslip. Four samples of each confluency were cultured on different glass slides in order to test the performance of the proposed device. A confluency of 100% was mapped to 0.3 million cells per coverslip. The other confluency level was set accordingly. It was concluded that a minimum of 60% confluency is required for the proposed device to work successfully. It is to be noted that the developed device was able to get readings from the samples that were less than 60% confluent. However, the obtained readings from these samples were not conclusive as the readings were variable. Since the readings were not consistent, the remaining experiments were performed by keeping the samples at a minimum of 60% confluent. Moreover, the distance between the sample and the flashlight was fixed at 2 cm with the help of a holder.

Fig. 5.5a shows the cultured HCT116 cells expressing IRFP702, and Fig. 5.5b is the control cells when viewed under a commercial imaging system (Odyssey CLx, LI-COR Biosciences, Lincoln, NE, USA). The same cell line that was used with the commercial system [C5.25] was then used with our prototype to validate the reading. The proposed prototype was able to detect the emitted fluorescent signal from the HCT116 colorectal cancer cells expressing IRFP702 and hence was able to distinguish between control cells and the fluorescent cells. The excitation and emission maximum of IRFP702 fluorophore is 673 nm and 702 nm respectively, as shown in Fig. 5.5d. The optical filter and light source as well as the photodiode were chosen cautiously so that they cover the excitation and emission region of this IRFP702 fluorophore. The longpass filter was selected so that it matches the emission wavelength of the IRFP702 fluorophore, thus ensuring that the emitted fluorescent wavelength passes down to the photodiode. This is to ensure that the light that is detected by the photodiode is from the cell line and not from the excitation source. Although a dichroic mirror/excitation filter is usually used in combination with the excitation light source [C5.7, C.26], this work shows that extra components can be removed if the experimental set-up is performed cautiously as it was also shown in [C5.27].
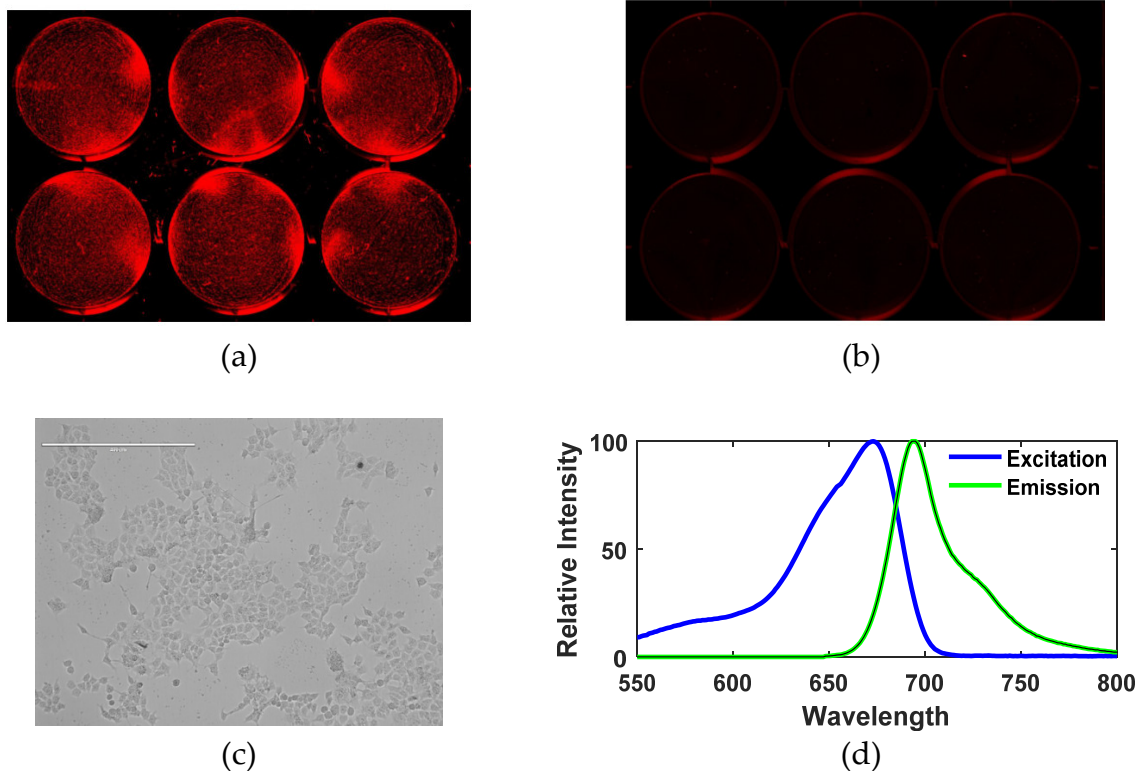
Figure 5.5 Detection of colorectal cancer cells expressing IRFP702: (a) colorectal cancer cells (HCT116) with IRFP702 fluorophore expression visualized under Odyssey CLx NIR scanner (LI-COR), (b) colorectal cancer cells (HCT116) without IRFP702 fluorophore expression visualized under Odyssey CLx NIR scanner (LI-COR), (c) colorectal cancer cells with IRFP702 fluorophore expression under EVOS Cell Imaging System, (d) excitation and emission spectra of IRFP702. This figure shows the absorption and emission spectra of the IRFP702 where the peak absorption and peak emission of the cultured sample is 673 nm and 702 nm respectively.

The complete system is powered and controlled by the help of a microcontroller (Arduino Uno). It detects the signal and transmits the measured signal to the LCD display. This microcontroller converts the analog signal generated by the photodiode using a high-precision 10-bit analog to digital converter (ADC) which is embedded inside the microcontroller. The photodiode is a semiconductor device which converts light into current [C5.28]. The current is produced when the photons are taken up by the photodiode. In Arduino Uno's ADC, the analog signal, which ranges from 0 to 5 V, is translated into a 10-bit code (1024 combinations) which corresponds to the analog value ranging from 0 to 1023. The

Arduino Uno can read a maximum input voltage of 5 V, i.e., any voltage that is higher than 5 V will be read as 5 V regardless of their actual values. To remove this limitation, resistors of different values can be used to limit the voltage within 5 V. However, in this work, the obtained readings did not go beyond the maximum limit of the Arduino Uno as the generated fluorescence signal is not very strong. Fig. 5.6 shows a flowchart which summarizes the working of the developed prototype. An Arduino IDE compiler is used to program the microcontroller. The code is written in C language. The device is initialized when it is first powered on. After the initial boot is successful, a sample of a control cell, which is cultured on a glass slide, is placed in the sample holder. The sample holder has a port which is designed to fit the cultured samples in it. After the sample placement is successful, the device starts reading. The microcontroller reads the data 10 times in order to reduce errors that may be caused due to manipulation, movement or placement of flashlight. The measured value is averaged, which is saved as a base value and displayed on the LCD display. This value will be used later in the calculation. It is to be noted that it is important to place the excitation source/flashlight on top of the sample, which is why a flashlight holder is used. The holder helps the user to hold the flashlight on top of the sample at the desired angle and distance away from the sample. After the reading of the control cell is completed, it is replaced with a sample of fluorescent colorectal cancer cell (HCT116 conjugated with IRFP702). As in the earlier case, the reading is performed again 10 times. This reading is averaged and compared with the previously measured value from the control cell. If the difference in voltage measurement obtained from the control cell and the fluorescent cell is greater than 700 mV, "CancerCell Found" is displayed. Otherwise, "No CancerCell" is displayed.
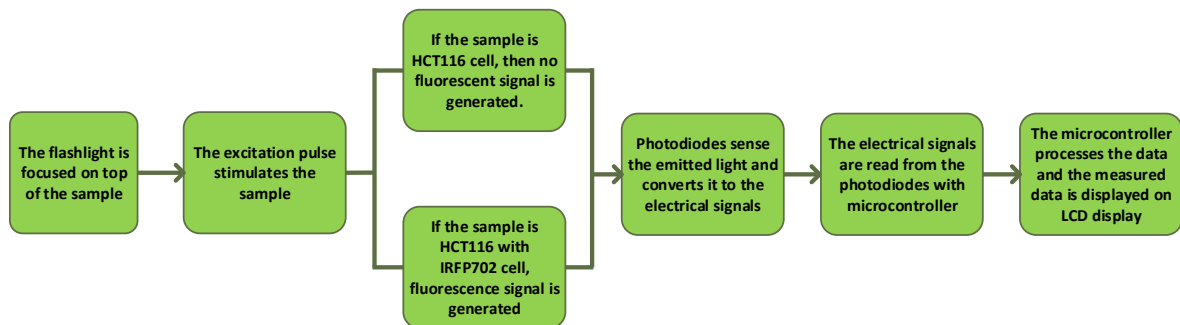
Figure 5.6 Flowchart showing the operating procedure of the device.

Figs. 5.7a, 5.7b show the control colorectal cancer cells and the IRFP702 expressing colorectal cancer cells on a glass slide respectively. Figs. 5.7c, 5.7d show the control cells and the IRFP702 expressing colorectal cancer cells visualized with the help of a commercial system [C5.25] respectively. From Figs. 5.7a, 5.7b, it can be construed that it is difficult to differentiate between these cultured samples with the naked eye. However, when these same cultured colorectal cancer cells are used with our developed device, we are able to differentiate between these cells, as can be seen in Fig. 5.7e. These readings from the samples were visualized with the help of waveform oscilloscope on a computer. In order to evaluate the effectiveness/performance of the proposed device, we applied four measurement techniques that are commonly used in classification. These measurements include sensitivity, accuracy, specificity and precision, where sensitivity = TP/(TP + FN), accuracy = (TP + TN)/(TP + TN + FP + FN), specificity = TN/(TN + FP) and precision = TP/(TP + FP). As shown in Fig. 5.8a, the fluorescence intensity is proportional to the number of cells.

Figure 5.7 Results: (a) control colorectal cancer cell, (b) colorectal cancer cell expressing IRFP702 fluorophore, (c) control cell visualized with commercial system, (d) colorectal cancer cell expressing IRFP702 visualized with commercial system, and (e) reading on a waveform oscilloscope.

(a)   (b)
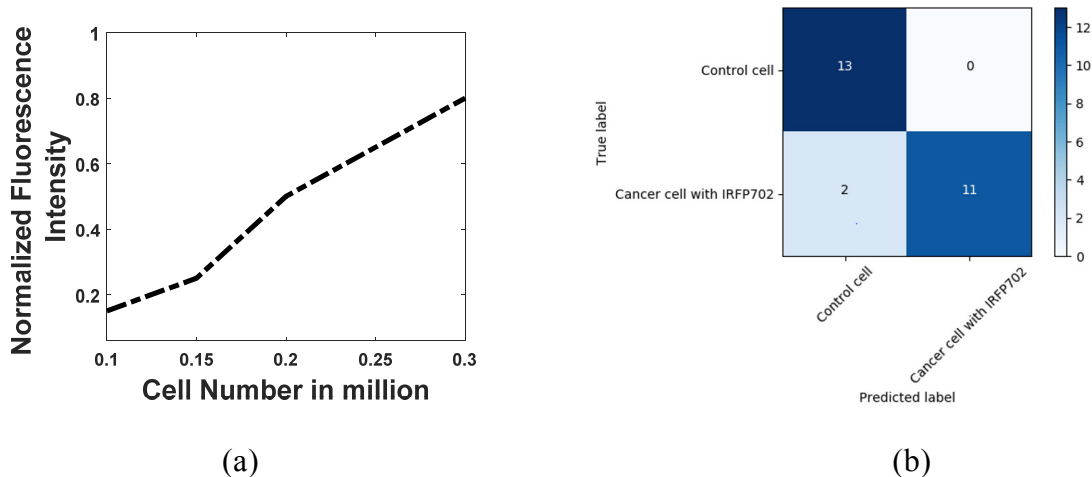
Figure 5.8 (a) Fluorescence intensity vs cell-number (b) Confusion matrix
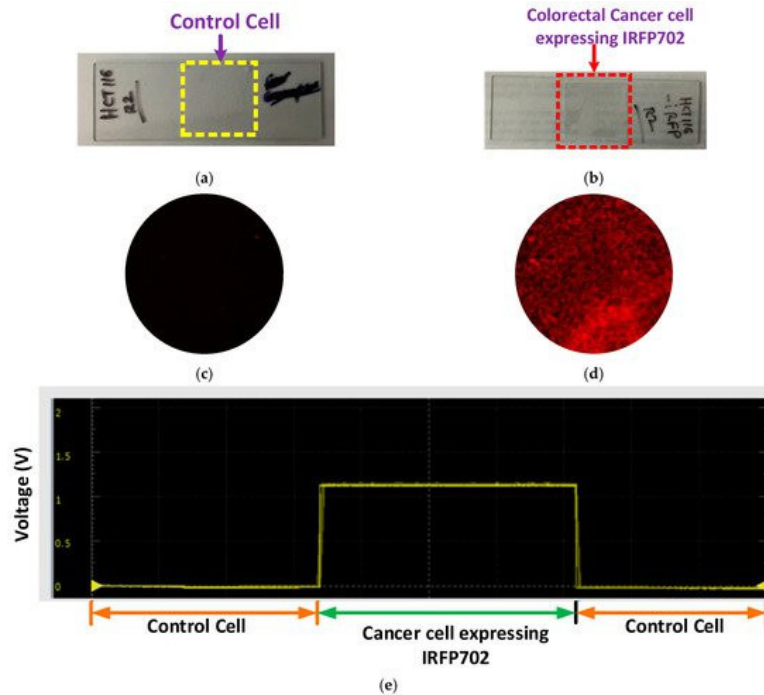
Twenty-six samples (thirteen of cancer cell expressing IRFP702 and thirteen of control cell) were cultured on the glass slide with a confluency greater than 60%, and they were examined first with the Odyssey system and then with the developed prototype. Fig. 5.8b shows the confusion matrix. As can be seen in Fig. 5.8b, the proposed device was able to detect all of the control cells from the samples accurately. On the other hand, the fluorimeter detected 11 out of 13 cancer cells with IRFP702 correctly. The sensitivity, accuracy, specificity and precision were found out to be 0.85, 0.92, 1 and 1 respectively.

Table 5.1 shows the list of major components that were used to build this device along with the individual and aggregate cost. The total cost of this device can further be reduced by using a low-cost filter which can provide similar accuracy. The presented device is again simplified with respect to a regular fluorescence microscope [C5.7] as it eliminates the requirement of an additional dichroic mirror as well as excitation filter. Moreover, it is small in size, compact, costs less and is lightweight when compared to most commercial as well as research microscopes, as shown in Table 5.2. In addition to these advantages, removing the filter and camera also offers additional advantages, such as it eliminates the need of having to adjust light path settings and the external arc lamp. This device also obviates the need of having a filter cube in these devices to house the different set of filters. In addition, this device also removes the need for using expensive cameras.

Table 5.1 List of major components required to construct the proposed device.

Components used	Model/specifications	Estimated Cost (USD)
Filter [5.29] [40]	700nm	150
3D printed chamber	Printed with CR-10	30
16x2 LCD display [C5.22]	HC1624, 5V, 16x2	3.90
Breadboard with wires [C5.30]	Microtivity	6.09
Microcontroller [C5.21]	Arduino Uno R3	16.90
Flashlight [C5.18]	UltraFire C8	6.58
Photodiode [C5.19]	Mouser , 720-SFH203	0.94
Flashlight holder [C5.31]	Any cell phone holder with clip	10
	Total	**224.37**

The sample chamber takes up a space of 4×8 cm which makes this experimental setup a perfect candidate for benchtop experiments. This device is user-friendly as the instruction is displayed on the LCD screen guiding the user for each step in the detection process. Alternatively, this developed device can also be connected via the serial port of a computer with a USB to enable control by the computer and hence control input and output operations via the computer through serial communication.

Table 5.2 Comparison of the developed device with other devices in market or in research

Work		Weight (kg)	Dimension (cm)	Cost (USD)	Target of interest	Standalone/ Needs pc with Software	Power Source
Image Based	Tapley *et al.* (2013) [C5.3]	3	20x20x10	Not known	Tuberculosis	Needs PC	Battery Powered
	Nunez *et al.* (2017) [C5.30]	Not known	17x18.7x31	$250	Imaging Assays	Needs PC for analysis	AC powered
	Hasan *et al.* (2016) [C5.7]	0.13	11x6.5x15	$358	Breast Cancer	Needs PC for visualization	Battery Powered
	Babbit *et al.* (2013) [C5.31]	Not known	Not known	$772.93 *	Living cells	Standalone	Battery Powered
	Commercial microscope (2019) [C5.25]	33	93.98x134.62x157.48	$50,055.42 [C5.34]	Multiple	Needs PC	AC powered
Signal Based	Lamb *et al.* (2015) [C5.33]	Not known	4x4**	$3300	Chlorophyll	Needs auxiliary component	AC powered
	Hoadley *et al.* (2017) [C5.36]	Not known	Not known	$712.44	Chlorophyll	Standalone/ needs pc for post-processing	AC powered
	Blockeistein *et al.* (2014) [C5.35]	Not known	7.6x7.6x12.7	< $500	Chlorophyll	Needs a pc with software	AC powered
	Commercial fluorometer (2019) [C5.38]	55	104x59x32	Not known	Multiple	Needs pc with software	AC powered
	Martin *et al.* (2016) [C5.39]	Not known	22x100x5.3	> $170*	Escherichia	Standalone	AC/ Battery powered
	Kim *et al.**** (2017) [C5.11]	0.108	5.2 x 3.5 2.5	Not known	Cyanobacteria	Standalone	9V supply
	Proposed Device	0.16	8x4x3.2	$224.37	Colorectal Cancer	Standalone	AC/ Battery powered

*Not reported in detail. The total cost was calculated based on the list of equipment provided in the manuscript.
**height is not mentioned in the manuscript.
*** Weight and dimension is without considering laser source or sample vial.

We first tested the functionality of the developed fluorimeter by using it to detect fluorescence emitted from human colorectal cancer cells which were genetically engineered to express the fluorescence protein. These cultured cells functioned both as a biologically appropriate as well as technically convenient clinical proxy of colorectal cancer cells for the fluorescence-based selective-detection process. As proof of principle, the cultured colorectal cancer cells (with and without IRFP702) were imaged using a conventional Odyssey CLx imaging system obtained commercially from Odyssey and the same cultured cells (with and without IRFP702) were then tested with our developed prototype to validate the result.

5.4 Conclusion

In this paper, we proposed an alternative low-cost fluorimeter which can differentiate between cultured control cell and the fluorescent colorectal cancer cell. The choice of the light source, optical filter and the sensor is critical in the successful implementation of this device. The device can be minimized further to make it more portable, appealing and lightweight. The Arduino Uno used in this project contains an Atmega chip, which can be programmed and the unnecessary component or pins can be removed while keeping only the necessary components that are required for this device [C5.40]. In addition to this, the flashlight can be replaced with another light source which works in the same range but is lightweight and portable. Following this process will make this device smaller as well as portable. Alternatively, the Arduino Uno can be replaced by other boards which are relatively smaller in size [C5.41]. This research aims to construct a fluorimeter and make it accessible to medical and research laboratories where resources are limited. This goal is realized as we demonstrate the functionality of this device using low-cost, easily available off-the-shelf components. Hence, the manufacturing of this device is possible by a wide range of laboratories across the globe. This device can be used to detect other types of cancer cells by simply replacing the optical filter and detector circuitry, which must be selected according to the conjugated or expressed fluorophores [C5.12]. Moreover, this device can also be tested to detect other targets in the future with slight modifications, such as chlorophyll, Escherichia and cyanobacteria. The lightweight, easy-to-use, portable and compact design of this device, as well as the potential for measurement of multiple types of cancer in the near future, will foster research

in many laboratories around the globe without the financial burden of the cumbersome commercial instrument.

References

[C5.1]   W. E. Moerner and D. P. Fromm, "Methods of single-molecule fluorescence spectroscopy and microscopy," *Rev. Sci. Instrum.*, vol. 74, no. 8, pp. 3597–3619, Aug. 2003.

[C5.2]   D. Cole, G. Young, A. Weigel, A. Sebesta, and P. Kukura, "Label-Free Single-Molecule Imaging with Numerical-Aperture-Shaped Interferometric Scattering Microscopy," *ACS Photonics*, vol. 4, pp. 211–216, 2017.

[C5.3]   A. Tapley *et al.*, "Mobile Digital Fluorescence Microscopy for Diagnosis of Tuberculosis," *J. Clin. Microbiol.*, vol. 51, no. 6, pp. 1774–1778, 2013.

[C5.4]   B. Kim, Y. J. Lee, J. G. Park, D. Yoo, Y. K. Hahn, and S. Choi, "A portable somatic cell counter based on a multi-functional counting chamber and a miniaturized fluorescence microscope," *Talanta*, vol. 170, pp. 238–243, Aug. 2017.

[C5.5]   S. Akraa *et al.*, "A smartphone-based point-of-care quantitative urinalysis device for chronic kidney disease patients," *J. Netw. Comput. Appl.*, vol. 115, pp. 59–69, Aug. 2018.

[C5.6]   J. Kissinger and D. Wilson, "Portable Fluorescence Lifetime Detection for Chlorophyll Analysis in Marine Environments," *IEEE Sens. J.*, vol. 11, no. 2, pp. 288–295, Feb. 2011.

[C5.7]   M. M. Hasan, M. W. Alam, K. A. Wahid, S. Miah, and K. E. Lukong, "A Low-Cost digital microscope with real-Time fluorescent imaging capability," *PLoS One*, vol. 11, no. 12, p. e0167863, Dec. 2016.

[C5.8] Y. Zheng, L. Zhang, T. Mi, and J. Zhao, "Portable plant chlorophyll fluorimeter based on blue LED rapid induced technology," in *2017 International Conference on Optical Instruments and Technology: Optoelectronic Measurement Technology and Systems*, 2018, vol. 10621, p. 45.

[C5.9] X. Geng, Y. Gao, C. Feng, and Y. Guan, "A facile and high sensitive micro fluorimeter based on light emitting diode and photodiode," *Talanta*, vol. 175, pp. 183–188, Dec. 2017.

[C5.10] X. Xing *et al.*, "Correction of profiles of in-situ chlorophyll fluorometry for the contribution of fluorescence originating from non-algal matter," *Limnol. Oceanogr. Methods*, vol. 15, no. 1, pp. 80–93, Jan. 2017.

[C5.11] S. H. Kim, Y. He, E. H. Lee, J. H. Kim, and S. M. Park, "Portable Fluorometer for Cyanobacteria Detection," *IEEE Sens. J.*, vol. 17, no. 8, pp. 2377–2384, 2017.

[C5.12] M. W. Alam *et al.*, "Development of a low-cost and portable smart fluorometer for detecting breast cancer cells," *Biomed. Opt. Express*, vol. 10, no. 2, pp. 399–410, Feb. 2019.

[C5.13] R. L. Siegel, K. D. Miller, and A. Jemal, "Cancer statistics, 2017," *CA. Cancer J. Clin.*, vol. 67, no. 1, pp. 7–30, Jan. 2017.

[C5.14] J. J. Estrada, A. M. Bedon, J. P. Kaminski, G. Rodriguez, M. Ali, and A. Albert, "Direct access screening colonoscopy as a safe and effective approach to increasing colorectal cancer screening.," *J. Clin. Oncol.*, vol. 35, no. 4_suppl, pp. 540–540, Feb. 2017.

[C5.15] A. Gautier and A. G. Tebo, "Fluorogenic Protein-Based Strategies for Detection, Actuation, and Sensing," *BioEssays*, vol. 40, no. 10, p. 1800118, Oct. 2018.

[C5.16] R. R. Zhang *et al.*, "Beyond the margins: real-time detection of cancer using targeted fluorophores," *Nat. Rev. Clin. Oncol.*, vol. 14, no. 6, pp. 347–364, Jun. 2017.

[C5.17] T. E. McCann, N. Kosaka, P. L. Choyke, and H. Kobayashi, "The Use of Fluorescent

Proteins for Developing Cancer-Specific Target Imaging Probes," Humana Press, Totowa, NJ, 2012, pp. 191–204.

[C5.18] "UltraFire CG-C8 Flashlight." [Online]. Available: https://www.amazon.co.uk/UltraFire-CG-C8-3-Mode-Flashlight-1x18650/dp/B00JA9EMLK. [Accessed: 25-Feb-2019].

[C5.19] "SFH 203 OSRAM Opto Semiconductors | Mouser." [Online]. Available: https://www.mouser.com/ProductDetail/OSRAM-Opto-Semiconductors/SFH-203?qs=sGAEpiMZZMtWNtIk7yMEsZEKXNTNxzvbCuJXkQkukYk%3D. [Accessed: 25-Feb-2019].

[C5.20] "SFH 203 Photodiode." [Online]. Available: https://media.osram.info/media/resource/hires/osram-dam-2495935/SFH 203.pdf. [Accessed: 25-Feb-2019].

[C5.21] "Arduino Uno Rev3 SMD." [Online]. Available: https://store.arduino.cc/usa/arduino-uno-smd-rev3. [Accessed: 25-Feb-2019].

[C5.22] "Basic 16x2 Character LCD - LCD-09052, Sparkfun." [Online]. Available: https://www.sparkfun.com/products/9052. [Accessed: 25-Feb-2019].

[C5.23] Cree, "Product family data sheet Cree ® XLamp ® XP-E LEDs," 2013. [Online]. Available: http://www.cree.com/led-components/media/documents/XLampXPE.pdf. [Accessed: 05-Dec-2018].

[C5.24] M. W. Alam, T. Sultana, and M. S. Alam, "A heartbeat and temperature measuring system for remote health monitoring using wireless body area network," *Int. J. Bio-Science Bio-Technology*, vol. 8, no. 1, pp. 171–190, Feb. 2016.

[C5.25] "Odyssey." [Online]. Available: https://www.licor.com/bio/products/imaging_systems/odyssey/. [Accessed: 19-Nov-2018].

[C5.26] R. Witte *et al.*, "Concepts in Light Microscopy of Viruses," *Viruses*, vol. 10, no. 4, p.

202, Apr. 2018.

[C5.27]   J. J. Lamb, J. J. Eaton-Rye, and M. F. Hohmann-Marriott, "A Cost-Effective Solution for the Reliable Determination of Cell Numbers of Microorganisms in Liquid Culture," *Curr. Microbiol.*, vol. 67, no. 2, pp. 123–129, 2013.

[C5.28]   M. I. Das, Choton Kanti; Alam, Mohammad Wajih; Hoque, "A wireless heartbeat and Temperature Monitoring System for Remote Patients," in *Proceedings of the International Conference on Mechanical Engineering and Renewable Energy 2013 (ICMERE2013)*, 2013, pp. 1–6.

[C5.29]   "700nm High Performance Longpass Filter, Edmund Optics." [Online]. Available: https://www.edmundoptics.com/p/700nm-125mm-dia-high-performance-longpass-filter/17597/. [Accessed: 25-Feb-2019].

[C5.30]   "Microtivity IB401." [Online]. Available: https://www.amazon.com/microtivity-400-point-Experiment-Breadboard-Jumper/dp/B004RXKWDQ. [Accessed: 25-Feb-2019].

[C5.31]   "Cell Phone Holder." [Online]. Available: https://www.amazon.com/dp/B01H8RDAX6. [Accessed: 03-Mar-2019].

[C5.32]   I. Nuñez *et al.*, "Low cost and open source multi-fluorescence imaging system for teaching and research in biology and bioengineering," *PLoS One*, vol. 12, no. 11, p. e0187163, Nov. 2017.

[C5.33]   K. N. Babbit, G. A., Hanzlik, C. A., Busse, "Observing fluorescent probes living cells using a low-cost LED flashlight retrofitted to a common vintage light microscope," *J. Microbiol. Biol. Educ.*, vol. 1, no. 14, pp. 121–124, 2013.

[C5.34]   "General Services Administration, Federal Supply Service, 2012." [Online]. Available: https://www.gsaadvantage.gov/ref_text/GS24F1183C/0LJVOV.2LOISL_GS-24F-1183C_TERMSCONDITIONS1183C.PDF. [Accessed: 19-Nov-2018].

[C5.35]   J. Lamb, K. Forfang, and M. Hohmann-Marriott, "A Practical Solution for 77 K Fluorescence Measurements Based on LED Excitation and CCD Array Detector," *PLoS One*, vol. 10, no. 7, p. e0132258, Jul. 2015.

[C5.36]   K. D. Hoadley and M. E. Warner, "Use of Open Source Hardware and Software Platforms to Quantify Spectrally Dependent Differences in Photochemical Efficiency and Functional Absorption Cross Section within the Dinoflagellate Symbiodinium spp.," *Front. Mar. Sci.*, vol. 4, p. 365, Nov. 2017.

[C5.37]   L. Blockstein and O. Yadid-Pecht, "Lensless Miniature Portable Fluorometer for Measurement of Chlorophyll and CDOM in Water Using Fluorescence Contact Imaging," *IEEE Photonics J.*, vol. 6, no. 3, pp. 1–16, Jun. 2014.

[C5.38]   "FS5 Spectrofluorometer | Steady State | Edinburgh Instruments." [Online]. Available: https://www.edinst.com/us/products/fs5-spectrofluorometer/.   [Accessed: 08-Nov-2018].

[C5.39]   F. J. F. Martín *et al.*, "A Novel Handheld Fluorimeter for Rapid Detection of Escherichia coli in Drinking Water," *IEEE Sens. J.*, vol. 16, no. 13, pp. 5136–5144, 2016.

[C5.40]   "How to Make a Permanent Circuit Board to Shrink Arduino Projects | Arduino | Maker Pro." [Online]. Available: https://maker.pro/arduino/tutorial/how-to-make-a-permanent-circuit-board-to-shrink-arduino-projects. [Accessed: 01-Aug-2019].

[C5.41]   "PICO: The world's smallest Arduino compatible board! by MellBell Electronics — Kickstarter." [Online]. Available: https://www.kickstarter.com/projects/melbel/pico-the-worlds-smallest-arduino-board/faqs. [Accessed: 27-Jul-2019].

Addendum on Chapter 5

In Chapter 4, breast cancer cell line (MDA-MB-231) was conjugated with GFP. The excitaiton and emission peak of GFP is 495 nm and 519 nm respectively. The emission filter, detection circuitry and the excitation source in Chapter 4 was selected based on GFP. Similarly, in Chapter 5, colorectal cancer cell line (HCT116) was conjugated with IRFP702. The excitation and emission peak of IRFP702 fluorophore is 673 nm and 702 nm respectively. The long pass filter in this chapter is selected so that only the wavelengths above 700 nm will be able to pass onto the detector circuitry. The emission filter in both studies are selected in such a way that it covers the emission spectra range of the conjugated fluorophore to reduce interference from other light sources. This ensures that the fluorescent signal from the fluorophore reaches to the detector.

This chapter helped us realize that by changing the excitation and detection circuitry, a different fluorophore can be detected. The fluorophore can be conjugated with other cancer cell line. If the same fluorophore is conjugated with other cancer cell line, same excitation and detector circuitry can be used to detect that cell line. Similarly, if a different fluorophore is conjugated with the cancer cell line, the excitation and detector circuitry should be modified according to the excitation and emission spectra of the fluorophore. This study opens the opportunity to detect multiple cancers with a single set-up.

6. A Fluorescence based Wireless Capsule Endoscopy System for Detecting Colorectal Cancer

Utilizing the knowledge, principle and experimental results discussed in Chapter 3, 4, and 5, a fluorescence based WCE system prototype is designed, developed and discussed in this chapter which is able to automate the detection of colorectal cancer. This device removes camera and utilizes minimum components to detect fluorescence. AS7262 sensor is used to detect the varying level of fluorescence. The prototype capsule consists of four major blocks: optical block (consists of detection and illumination components), microcontroller block (controls the processes), telemetry (for transmitting and receiving information), and power module. There is also an external data logger to receive the data sent by the capsule. The developed capsule is tested ex-vivo on swine intestine, liquid phantom and on a minced meat. It improves the diagnostic as well as screening procedure. In addition to being non-invasive, the capsule presents us with an opportunity to enable automatic detection of abnormality. The device is able to detect varying level of fluorescence emitted from the fluorophore. The device enables early detection of cancer possible with selective and specific detection, paving the way to perform targeted endoscopy. It will also make mass-screening possible through a pain-less procedure while improving survival rate of patients. Since the detection sensor used in this device can detect 6 different wavelength range, detection of multiple cancer using a single WCE device may be possible in future.

The analysis and findings of this chapter is reported in the below mentioned submitted journal manuscript. The student has contributed in conceptualization, methodology, analysis, writing the original draft and revision of the manuscript.

Mohammad Wajih Alam, Seyed Shahim Vedaei, and Khan A. Wahid, "A fluorescence-based wireless capsule endoscopy system for detecting colorectal cancer," Cancers 2020, 12, 890.

A Fluorescence Based Wireless Capsule Endoscopy System for Detecting Colorectal Cancer

Mohammad Wajih Alam, Seyed Shahim Vedaei, and Khan A. Wahid

Abstract

Wireless capsule endoscopy (WCE) has been widely used in gastrointestinal (GI) diagnosis that allows the physicians to examine the interior wall of the human GI tract through a pain-free procedure. However, there are still several limitations of the technology, which limits its functionality, ultimately limiting its wide acceptance. Its counterpart, the wired endoscopic system is a painful procedure that demotivates patients from going through the procedure, and adversely affects early diagnosis. Furthermore, the current generation of capsules is unable to automate the detection of abnormality. As a result, physicians are required to spend longer hours to examine each image from the endoscopic capsule for abnormalities, which makes this technology tiresome and error-prone. Early detection of cancer is important to improve the survival rate in patients with colorectal cancer. Hence, a fluorescence-imaging-based endoscopic capsule that automates the detection process of colorectal cancer was designed and developed in our lab. The proof of concept of this endoscopic capsule was tested on porcine intestine and liquid phantom. The proposed WCE system offers great possibilities for future applicability in selective and specific detection of other fluorescently labelled cancers.

Index Terms

Wireless capsule endoscopy; Fluorescence; Colorectal cancer; Non-invasive

6.1 Introduction

The wireless capsule endoscopy (WCE) system is becoming increasingly popular for examining the entire human gastrointestinal (GI) tract, as this method eases patients' discomfort and pain compared to other endoscopy methods [C6.1]. However, there are still many challenges (such as image quality, frame rate, battery life, automatic detection of abnormalities, localization, etc.) associated with this promising technology, and these limit its use in modern day healthcare system [C6.2, C6.3]. These tiny swallowable capsules are designed to reach the areas where access is limited without performing surgery. However, the frame rate and image quality of the currently available WCE devices are insufficient for optimal screening [C6.4].

A typical WCE system consists of a pill-shaped electronic capsule, a data recorder with radio frequency (RF) antenna, and a workstation computer with software, as shown in Figure 6.1. The capsule is integrated with an image sensor, illumination source, batteries, communication module, and other components [C6.5, C6.6]. Once the capsule is active and swallowed by the patient, it starts capturing images and sending the captured images to the data recorder via the RF transmitter. The data recorder (which is usually attached to the patient's waist using a strap) receives and saves the data. After 24 h, the patient returns the data logger to the physician who then downloads the images from the data logger to a computer, where the images are examined using the vendor's software [C6.7]. The software labels the frames suspected to include abnormalities, which would then be examined by the physician [C6.7]. This entire process is labor-intensive and time-consuming [C6.8]. The accuracy of the detection software and human error make this technology prone to diagnostic errors. Such errors can also be a result of inexperience, lack of training and subjective interpretation of the data [C6.9], hampering the wide acceptance of this technology. Although the conventional WCE system, which uses white light imaging, can now provide high-resolution images, proper diagnosis depends on the characteristics captured by the capsule, which varies due to morphological changes of the GI wall [C6.10]. Such morphological changes often appear very late, thus hampering the overall diagnostic as well as prognosis.
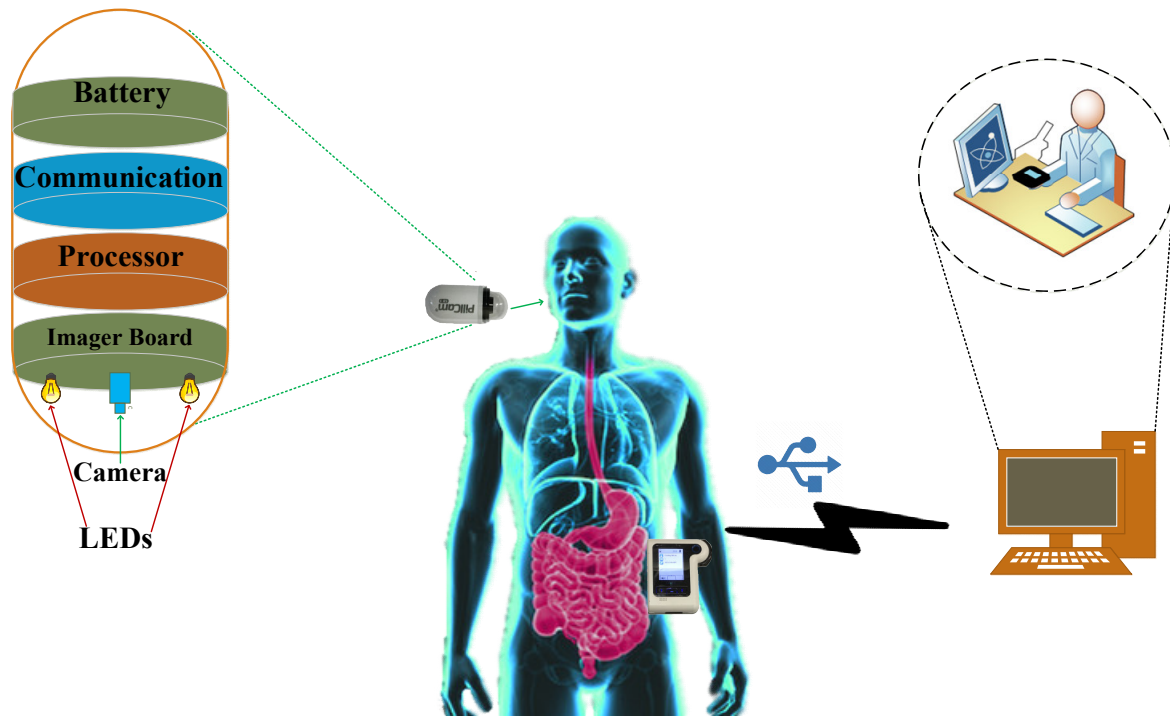
Figure 6.1 Illustration of a typical wireless capsule endoscopy (WCE) system.

Colorectal cancer is the third commonest type of cancer diagnosed in both men and women. It is also the third commonest cause of cancer-related deaths in the United States [C6.11]. About 1 million new cases of colorectal cancer are diagnosed each year, among which about 72% of cases arise in the colon, and the remaining 28% in the rectum, which collectively make it the leading cause of cancer-related deaths worldwide. The stage at which the cancer is first diagnosed is an important factor in determining the prognosis and survival of patient [C6.12]. Early detection of cancer is essential for improving the survival rate of cancer patients [C6.13]. There are different state-of-art methods that are currently used in the healthcare system for diagnosing colorectal cancer: computed tomography colonography [C6.14, C6.15], flexible sigmoidoscopy [C6.16, C6.17], double contrast barium enema [C6.18], stool DNA test [C6.19], fecal occult blood testing [C6.20], and the colonoscopy (the gold standard) [C6.21]. Although these state-of-art methods are popular among physicians, they are not very comfortable for the patients. Moreover, the patients are afraid of invasiveness, pain and embarrassment, which makes them not want to go through the conventional procedure unless it is entirely necessary. This effects early detection adversely. Despite a tremendous advancement in therapeutic and diagnostic possibilities, colorectal cancer in

patients are often detected in the advanced stage, and the survival rate for such patients is only 14%. However, if the same cancer was diagnosed at an early stage, the chances of survival can increase up to 90% [C6.22].

Fluorescence imaging is a technique which is widely used in medicine, biology, and biochemistry. It is the process which visualizes fluorescent dyes or proteins as labels to study the biological molecules and phenomena [C6.23]. The visualization of these tissues are usually achieved by labelling the proteins via a nanobody, antibody or bio-specific ligand [C6.24]. Fluorescent labelling [C6.25] binds fluorescent dyes covalently to biomolecules, such as proteins, so that they can be differentiated from non-fluorescent (non-bound) biomolecules. Fluorescence can be detected by using autofluorescence or specific labelling of proteins. It has been used to detect various physiological abnormalities for many decades as a non-invasive procedure. For instance, fluorescein has been used to detect ophthalmic pathologies since 1960. This method has also proven to be useful in successful detection of cancer. Attaching the fluorophore to a targeting agent enables the functionality of fluorescence imaging in the clinical environment, thereby increasing the specificity and sensitivity of detection. The combination of fluorophores with targetable cancer biomarkers have led to increased interest of both researchers and the medical industry in the area of fluorescence-guided surgery. Clinical trials were first introduced in early 2010. They use various fluorophores along with a range of targeting strategies (such as, antibodies, molecules, peptides, activatable fluorophores and multimodal fluorophores).

Autofluorescence is the process of detecting fluorescence emissions arising from endogenous fluorophores. Various tumor types are detectable both by autofluorescence techniques as well as by the use of exogenous fluorescent markers [C6.26]. Tumor-specific fluorescent imaging agents [C6.27] help surgeons with real-time intraoperative feedback on the location of tumors. The accurate detection or demarcation between tumor, inflammation and normal tissue is often difficult due to the lack of visual distinction among them. Targeted fluorescence imaging is therefore helpful in this regard, and can help solve this problem by providing real-time tumor detection or visualization [C6.28]. Thus, conjugating fluorescent dye to specific tumor-recognizing ligands (such as peptides or antibodies) enhances the specificity of tumor detection considerably. Various tumor-specific agents have already shown feasibility in early phase clinical trials. It is important to choose biomarkers which express strong fluorescence several fold higher

than the surrounding normal tissues in order to provide better selectivity and sensitivity. Previously, we have proposed a low-cost fluorometer which worked on the principle of fluorescence to detect breast cancer cells [C6.29] and colorectal cancer cells [C6.30].

In this work, a complete WCE system is designed based on the principle of fluorescence to detect colorectal cancer. This system has potential to automate the detection process and improve the overall efficiency and accuracy of diagnosis.

6.2 Materials and Methods

a   b
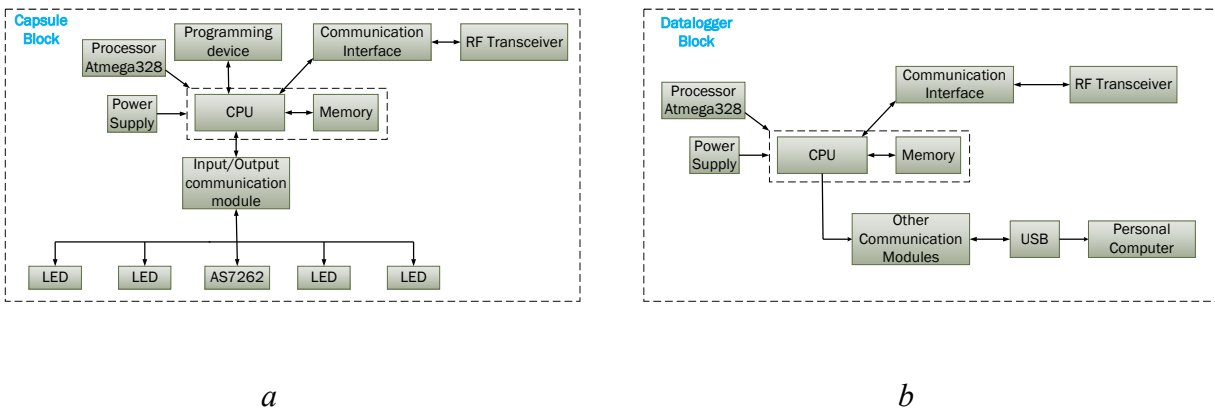
Figure 6.2 Hardware blocks of the proposed capsule prototype (a) Capsule block (b) Data logger block

The developed capsule prototype consists of the following blocks: an optical block, a microcontroller, telemetry, and a power module. The hardware diagram of the proposed system is shown in Figure 6.2. Figure 6.3a shows the internal components of the capsule. Figure 6.3b shows the 4-layered printed circuit board (PCB) design of the prototype. The components were chosen so that the capsule size remains small while optimizing the power consumption, performance, and sensitivity.

a   *b*
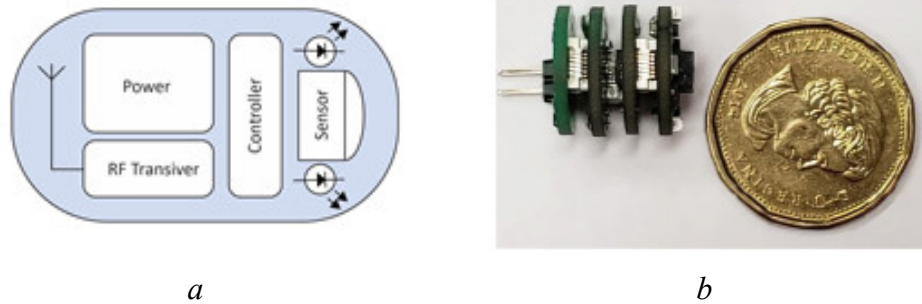
Figure 6.3 (a) Internal components; (b) Capsule prototype with 4 printed circuit board (PCB) layers (compared with a CAD $1 coin).

The proposed device consists of four main electronic printed circuit boards (PCBs): a sensor board with illumination components, a control/processor board, a telemetry board and the power module as shown in Figure 6.4. The placement of each electronic component and its associated connections was crucial in this miniaturized design. The four PCBs are connected via headers, and the design was selected as the best solution for the compact, efficient, and reliable design. Figure 6.4a shows the top layer which consists of four light emitting diodes (LEDs) arranged around the spectral sensor. These LEDs works in the ultraviolet (UV) range having a peak emission wavelength of 395 nm and excitation wavelengths ranging between 380 nm and 410 nm (Kingbright, ATS2012UV395). The sensor used for sensing the fluorescent light is an AS7262 spectral sensor manufactured by ams AG. It has 6-channel multispectral sensing capabilities, and works in the visible range between 430 nm and 670 nm with a full-width half max (FWHM) of 40 nm; i.e. 450 nm, 500 nm, 550 nm, 570 nm, 600 nm and 650 nm, each with a 40 nm FWHM. Moreover, each wavelength channel has a Gaussian filter characteristic. The spectral sensor is connected with the microcontroller via the I2C protocol. When the microcontroller is initialized at startup, the sensor is also ready to capture the spectrum. At each iteration, the microcontroller selects the wavelength channel in operation, and captures the data from the sensor accordingly. In our case, the peak excitation and emission wavelength of fluorescein is 494 nm and 521 nm respectively as shown in Figure 6.5. As such, the green channel is selected for the detection.
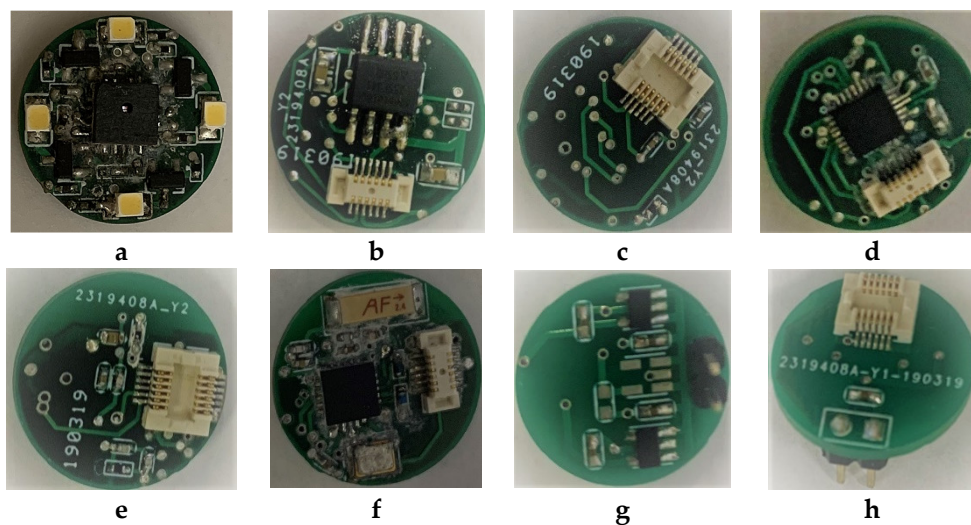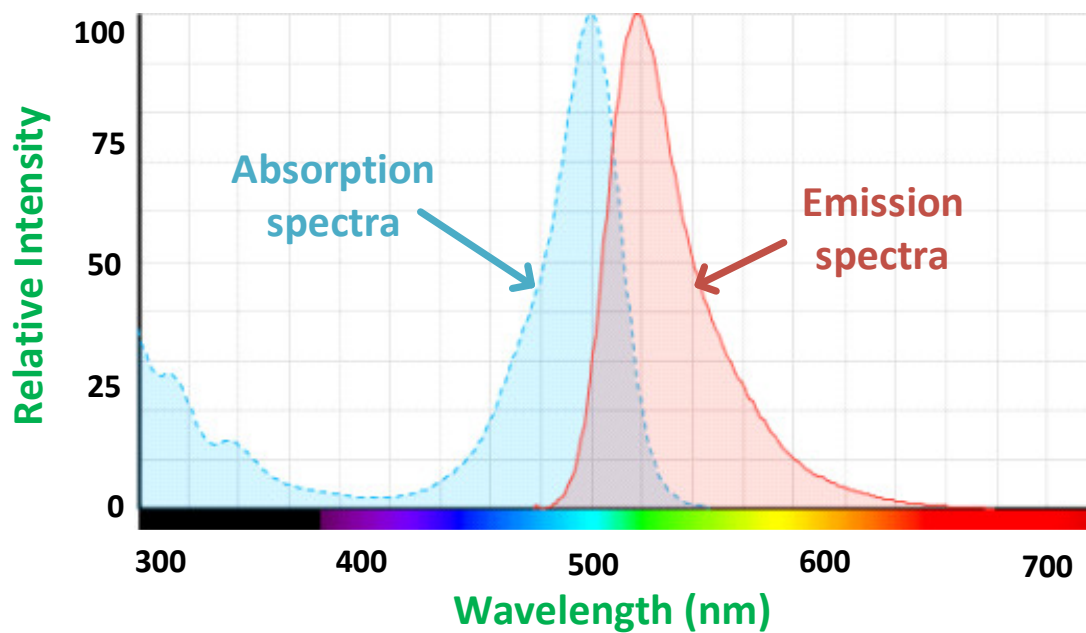
Figure 6.4 Illumination with spectral sensor: (a) top view; (b) bottom view. (ii) Control/processing unit: (c) top view; (d) bottom view. (iii) Telemetry unit: (e) top view; (f) bottom view. (iv) Power unit: (g) top view; (h) bottom view.

Figure 6.5 Absorption/emission spectra of the sample adapted from [C6.31]

A comprehensive analysis was performed before selecting the complete illumination system. The choice of these components depends upon several factors, but trade-offs were considered between power consumption, miniature size, and the light intensity that would be required for the capsule to perform efficiently. The chosen LED is 2 mm × 1.25 mm in size. Furthermore, the absorption/emission spectra of the target fluorophore were considered while selecting these components. The spectral sensor is situated in the middle of the LEDs, equidistant from all LEDs. The electrical connections with the second layer (microcontroller) were achieved through pins 23 and 24 via a 11 × 2 header that helps the board to correctly align with the optical sensor. Each LED is driven via digital pulse width modulation (PWM) pins of the microcontroller, which will help to control the brightness, if needed. Figure 6.4a,b show the sensor/illumination unit of the capsule. The control board is the heart of the capsule as it controls the processes and connects all other PCB layer. The microcontroller used in this device is an ATmega328P. This microcontroller can operate at between 1.8 and 5.5 volts. The chip has 8 analog input pins and 14 digital I/O pins, which makes interfacing with other components easy. This microcontroller receives the data from the spectral sensor and sends it to the RF transceiver.

The capsule prototype uses an nRF24L01 + radio transceiver for wireless communication. This transceiver has a good range and can communicate for a considerable distance through walls with negligible data loss. The nRF24L01 + module operates at 2.4 GHz. At this working frequency, the wireless transmission module shows the characteristics of having long transmission range and strong penetrability, which is helpful for WCE application. This module is an important bridge for wireless communication (both transmission and reception) with the external data logger. The power board contains miniature low dropout regulators (LDO), each having a rated voltage of 3.3 V and current of 150 mA. Any kind of silver oxide or Li-ion battery with a voltage range over 3.7 V could be used to power up the capsule prototype.

The data logger is based on an Atmel microcontroller, which is capable of receiving the capsule's signal and transmitting the received data to a computer. It has two modes of operation. First, when the data logger is plugged into a computer via a USB port, it detects the "software mode" operation, which means that the data logger can receive signals from the capsule and transmit them to the computer in real-time. On the other hand, when the data logger is powered up by an external power source without having connection to the computer, the device enters a "stand-

alone mode". In this mode, the data logger will still receive data from the capsule, but stores the received data in the internal memory and transmits them to the Raspberry Pi board for further processing. By connecting the data logger to the computer, our software can read the data from the memory. Figure 6.6 shows the data logger which is connected to the Raspberry Pi system.
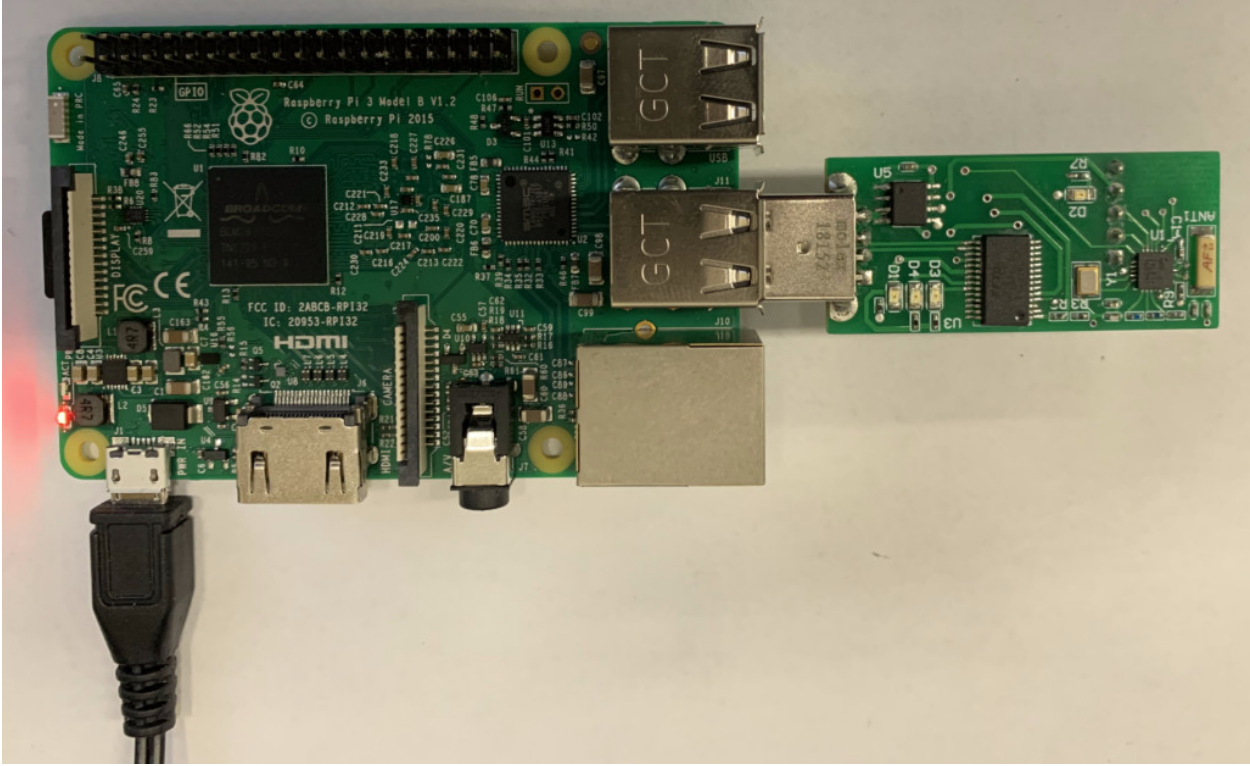
Figure 6.6 Data logger connected to Raspberry Pi system.

6.3 Results and Discussion

6.3.1 Screening Intestine

One of the major objectives of this work is to demonstrate the ability to detect the increasing levels of fluorescence emitted by the cancer cells compared with normal cells. Fluorescein is a safe-dye and commonly used in vivo. It has found increased use in many applications, such as: ophthalmology and neurosurgery [C6.32, C6.33]. Fluorescein has also been used to differentiate between cancer cells and normal cells during intraoperative surgery for different types of cancer [C6.27, C6.34, C6.35]. The fluorophore can be administered into body via different pathways: intravenously [C6.34, C6.36], intradermally [C6.35], or by spraying [C6.37]. The fluorescence intensity may vary depending on the region where the cancer is located, the time since it was injected, and on the fluorophore concentration. A fluorescein concentration of 5 mg/kg (~1.5 µM) to 20 mg/kg (~6 µM) is enough for detectable fluorescence emitting from the cancer cells when injected intravenously [C6.38, C6.39]. In this work, different concentrations of fluorescein were prepared (231 µM to 18 nM) in order to test whether the proposed capsule can detect different levels of fluorescence. Moreover, the functionality was also tested on a porcine intestine (shown in Figure 6.7a). Figure 6.7b and c show the experimental setup when the external light is on and off, respectively. As can be seen in Figure 6.7c, only the area with fluorescein glows when exposed to ultraviolet (UV) light from the developed prototype.
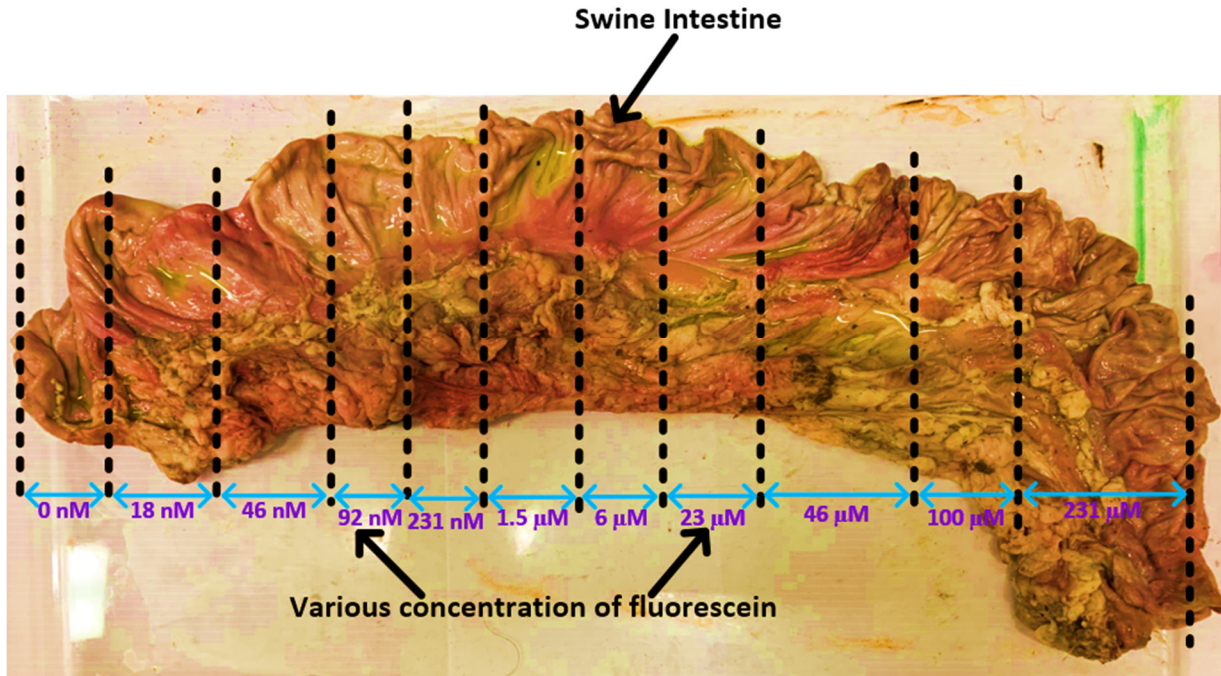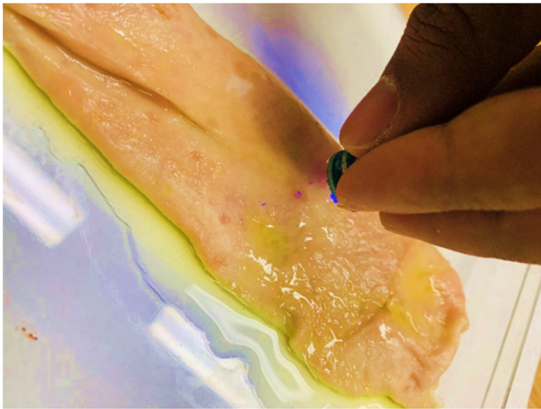
Figure 6.7 Screening of a porcine intestine by the capsule prototype: (a) various concentrations of fluorescein solution sprayed over the intestine; (b) demonstration of the capsule in working conditions; (c) demonstration of the capsule in working conditions when no external light is present.

Figure 6.8 shows the Fluorescein intensity captured by the capsule prototype for varying concentrations. The fluorescence intensity increases with increasing concentration and the device is also able to detect the concentration that emits a low level of fluorescence. It can be seen that the response from the tissue with no fluorescein and the area with fluorescein were clearly distinguished even at a low concentration (see inset of Figure 6.8). Hence, in an area of intestine with a high concentration of the biomarker (i.e., resembling cancer), a good response or signal will be found, whereas in an area without the biomarker, no fluorescence signal will be detected. Moreover, if the fluorescein is conjugated with an antibody that targets a specific antigen found in colorectal cancer cells [C6.40], targeted fluorescence-based WCE is possible. We have presented work based on this principle in previous studies [C6.29, C6.30, C6.41].
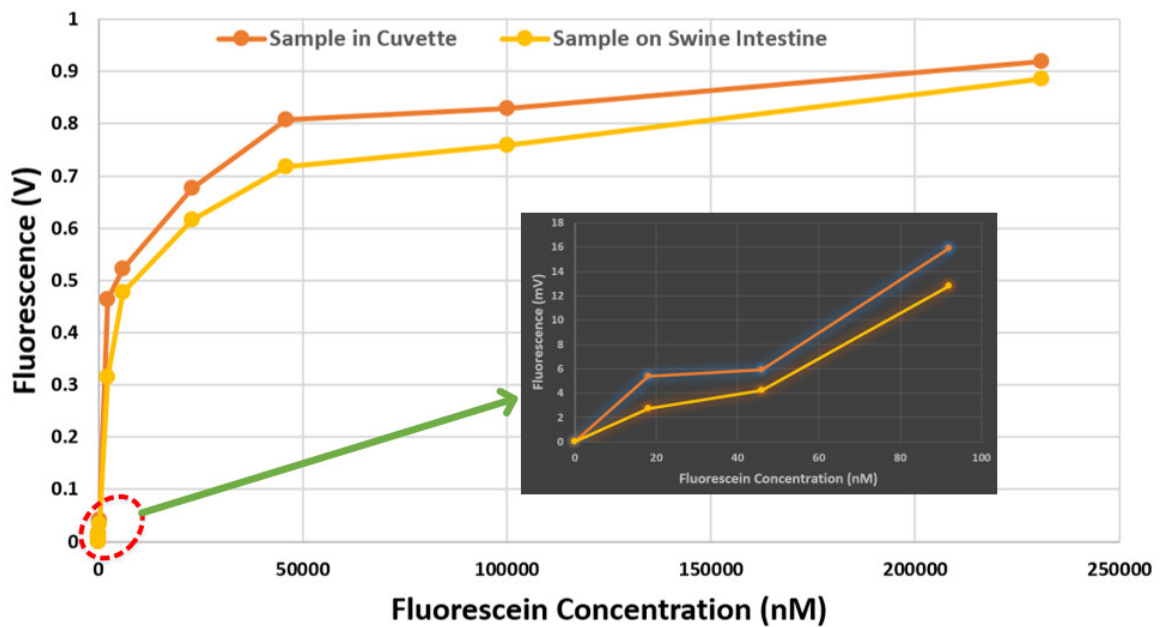
Figure 6.8 Change of fluorescence intensity with varying fluorescein concentrations. Inset: zoomed plot when the concentration is low.

In order to further assess the performance of the proposed WCE device, we used the following four indices: sensitivity, specificity, accuracy, and precision, as expressed below:

$$Sensitivity = \frac{TP}{TP+FN} \qquad (6.1)$$

$$Specificity = \frac{TN}{TN+FP} \qquad (6.2)$$

$$Accuracy = \frac{TP + TN}{TP + TN + FP + FN} \qquad (6.3)$$

$$Precision = \frac{TP}{TP + FP} \qquad (6.4)$$

where, TP is the number of true positives, TN is the number of true negatives, FP is the number of false positives, and FN is the number of false negatives. The samples were divided into three categories: 231 µM (high concentration), 1.5 µM (medium concentration) and 231 nM (low concentration). Each category contained 10 positive samples (i.e., area sprayed with fluorescein) and 10 control samples (i.e., area without fluorescein). Figure 6.9 shows the confusion matrix using the measurements. It can be seen that the prototype is able to detect the samples accurately when the fluorescein concentration varies from high to medium level. However, when the concentration was low, the results are not conclusive. The sensitivity, specificity, accuracy and precision indices for 231 µM and 1.5 µM were 1, 1, 1 and 1 respectively, and for 231 nM were 0.6, 1, 0.8 and 1 respectively. To further assess the potential use of fluorescein for the detection of tumors, the fluorescein was sprayed over the porcine intestine and the signal was measured at various time-points with 1.5 µM solution. The fluorescence intensity at different time-points is shown in Figure 6.10. For WCE applications, the fluorescence signal should be present for about 8 h.

		Positive Sample	Control Sample
Predicted Class	Positive Sample	10 True Positive	0 False Positive
	Control Sample	0 False Negative	10 True Negative
		True Class	

a

		Positive Sample	Control Sample
Predicted Class	Positive Sample	10 True Positive	0 False Positive
	Control Sample	0 False Negative	10 True Negative
		True Class	

b

		Positive Sample	Control Sample
Predicted Class	Positive Sample	6 True Positive	0 False Positive
	Control Sample	4 False Negative	10 True Negative
		True Class	

c

Figure 6.9 Confusion Matrix from sample of: (a) high concentration, 231 µM; (b) medium concentration, 1.5 µM, and; (c) low concentration, 231nM.
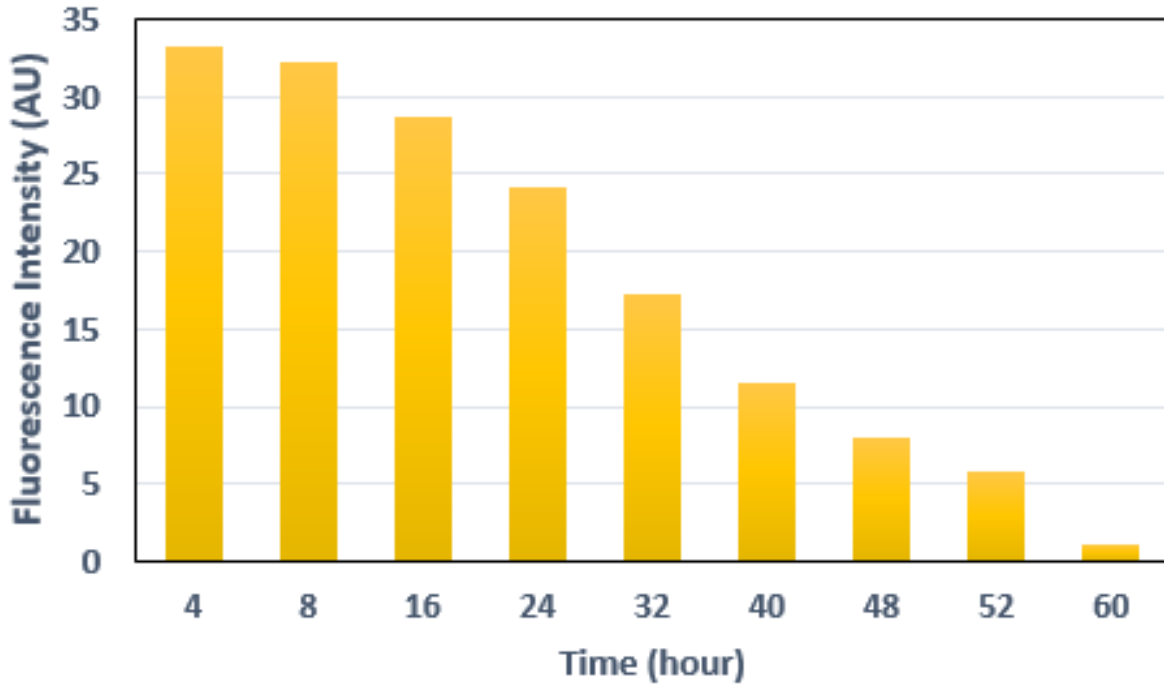
Figure 6.10 Fluorescence intensity measured at different time-points from the initial application of fluorescein

Table 6.1 Cost breakdown of the proposed capsule prototype

Component	Model/Specification	Cost ($USD)
Spectrum sensor IC	ams AS7262-BLGT	3.12
EEPROM IC	AT25SF041-SSHD-T	0.22
LED	ATS2012UV395	1.82
Microcontroller	ATMEGA328P-MMHR	1.8
Transceiver	NRF24L01	2.45
Antenna	ANT-2.45-CHPCT-ND	1.71
PCB		10
Miscellaneous cost		50
	Total Cost	**71.12**

6.3.2 Data Logger

When the capsule is turned on, it starts to sense the signal through the sensor module (AS7262) and begins to capture the data and send to the data logger via RF transceiver. The data logger receives and stores the data. The software on the data logger is a Python script which communicates through the serial port. Operational parameters, such as spectrum capture interval and capsule illumination mode can be controlled via the software. Table 6.1 shows the breakdown of the material costs of our system. The miscellaneous cost in Table 6.1 includes packaging, 3D-printing and fabrication costs. Note that labor and engineering costs are not included in the table.

6.3.3 Power Consumption

Table 6.2 shows the current consumption of the individual components in both active and inactive modes. For an average of 14.85 mA current consumption, the proposed device can run for 12 h with batteries of 178.2 mAh capacity [C6.42]. The runtime can be extended by connecting two or three batteries in series. Therefore, the lifetime is enough to cover most patient's GI transit time [C6.43, C6.44]. However, an increased battery life may be useful for patients who need a longer GI transit time (capsule retention or other chronic disease) [C6.45, C6.46].

Table 6.2 Power consumption of the capsule prototype

Component	Active Mode	Inactive mode	Total Current Consumption	Total Power Consumption
Regulators	0.08 mA	0.02 mA	0.08 mA	0.27 mW
Microcontroller	2.53 mA	0.30 mA	2.53 mA	8.35 mW
nRF24L01+	12 mA	0.41 mA	3.13 mA	10.33 mW
LEDs	5.38 mA	0 mA	2.69 mA	8.88 mW
AS7262	6.71 mA	6.32 mA	6.42 mA	21.19 mW
		Total	**14.85 mA**	**49.02 mW**

6.3.4 Wireless Communication

There are several wireless transceivers available, each having their pros and cons depending on the application. A Nordic transceiver is used in the proposed system. One of the major challenges in wireless communication is the possibility of data corruption during transmission and reception. The Nordic transceiver has a built-in capability for cyclic redundancy check (CRC)-based error detection and retry with acknowledgement (i.e., it resends the data packet until it is successfully received), which makes it a reliable choice. However, several retries may hamper the data transmission rate in a noisy environment [C6.47].

In order to verify the performance of our prototype further at 2.4 GHz [C6.48, C6.49], we performed two additional experiments using an equivalent liquid phantom and minced meat as shown in Figure 6.11. Since the nRF24L01 module has a CRC functionality (i.e., detects error bits automatically), it is not possible to measure the exact BER (bit error rate, the ratio of the number of bits received in error to the total number of bits received) in this experiment. However, considering the loss of the entire packet, we have implemented test cases to measure the number of bytes lost per test case. The results are shown in Table 6.3. The prototype was placed in a liquid phantom first, and then in 1.8 kilogram of minced meat (as shown in Figure 6.12). The liquid phantom was made from pure water, methanol and sodium chloride to mimic human GI fluid [C6.50, C6.51]. The chamber size of liquid phantom and minced meat were: 40 cm × 30 cm × 16.5 cm (length × width × height) and 26 cm × 17 cm × 7 cm (length × width × height) respectively. The capsule was placed in the middle of the chamber in all test cases. The distance between the capsule and the data logger was varied gradually from 0.3 to 10 meters, and data from the capsule were sent to the data logger. All data bits were transmitted to the data logger with no loss when the distance between the data logger and the capsule in liquid phantom was up to 5 meter. When the distance increased to 10 meters, we started to notice loss of data packets and the transmission rate was found to be 90%. In another test case, the capsule was placed in minced meat. As before, when the distance between the capsule and the data logger was varied up to 5 meters, no loss of data packets was observed. However, when the distance increased to 10 meters, we noticed that transmission rate was affected, with 80% of data successfully transmitted. Since, the data logger is wearable and generally worn around the waist in practice, the distance between a swallowed capsule and the data logger is generally about 0.3 meter [C6.52]. Therefore, we expect our prototype to work at 2.4 GHz spectrum with no loss of data during communication.
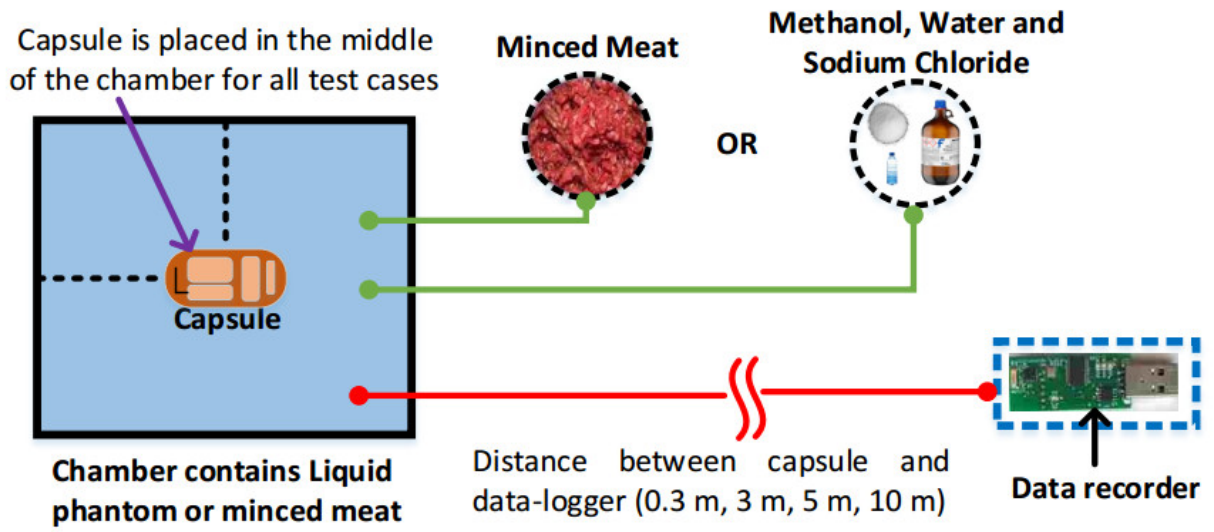
Figure 6.11 Experimental setup for testing transmission rate of the proposed prototype. A plastic storage box is used as a test chamber.

Figure 6.12 Measurement setup to test the transmission rate of the proposed capsule in: (a) liquid phantom (b) minced meat.

Table 6.3: Transmission performance of the capsule

Test Case	Distance between capsule and data logger (m)	Transmitted bytes	Received bytes	Percentage of transmitted data (%)
Liquid phantom	0.3	20	20	100
	3	20	20	100
	5	20	20	100
	10	20	18	90
Minced meat	0.3	20	20	100
	3	20	20	100
	5	20	20	100
	10	20	16	80

6.3.5 Comparison with other WCE System

Table 6.4 shows a comparison with different WCE systems which are available both commercially or are at the research stage. This table is divided into two categories: fluorescence-based capsules and non-fluorescence-based capsules. As can be seen from the table, the commercial WCE systems are non-targeted endoscopy. Most of them are camera-based, and target the small bowel region, and lack functionality for automatic detection of abnormalities. As a result, once the data is unloaded with the help of vendor's software on a computer, post-processing is required to find the frames of interest. This requires significant amount of time and labor. Furthermore, the use of camera makes the capsule expensive both cost-wise (>$500) and power-wise, ultimately affecting the battery life and its affordability.

Table 6.4 Comparison with other devices: both commercial and research prototype

	Work	TE	Region of Interest	Resolution	Camera/ Sensor	I/S	TM	RT	Cost of Capsule only (USD)	DL
Non-fluorescence based	PillCam SB [C6.47]	No	Small Bowel	256x256	1 CMOS	6 LED	RF	Yes	N.G.	Yes
	PillCam SB2 [C6.48]	No	Small Bowel	256x256	1 CMOS	4 LED	RF	Yes	~530	Yes
	PillCam SB3 [C6.49]	No	Small Bowel	256x256	1 CMOS	4 LED	RF	Yes	~500	Yes
	PillCam ESO [C6.50]	No	Esophagus	256x256	2 CMOS	6 LED	RF	Yes	N.G.	Yes
	PillCam ESO2	No	Esophagus	256x256	2 CMOS	2x4 LED	RF	Yes	~500	Yes
	PillCam ESO3	No	Esophagus	256x256	2 CMOS	2x6	RF	Yes	~570	Yes
	PillCam Colon	No	Colon	256x256	2 CMOS	2x6 LED	RF	Yes	N.G.	Yes
	PillCam Colon2 [C6.51]	No	Colon	256x256	2 CMOS	2x4 LED	RF	Yes	~550	Yes
	MiroCam [C6.52]	No	Small Bowel	320x320	1 CMOS	6	HBC	Yes	~380	Yes
	EndoCapsule [C6.53]	No	Small Bowel	1920x1080	1 CCD	6	RF	Yes	~570	Yes
	OMOM [C6.54]	No	Small Bowel	640x480	1 CMOS	4	RF	Yes	~380	Yes
	CapsoCam [C6.55]	No	Small Bowel	1920x1080	4 CMOS	16	USB	No	~380	No
	SmartPill [C6.56]	No	GI tract	N.A.	Pressure, pH & Temperature	None	RF	Yes	~530	Yes
	CorTemp [C6.57]	No	GI tract	N.A.	Temperature	None	RF	Yes	~40	Yes
	VitalSense [C6.58]	No	GI tract	N.A.	Jonah core temperature	None	RF	Yes	~68	Yes
	e-Celsius [C6.59]	No	GI tract	N.A.	Temperature	None	RF	Yes	~65	Yes
Fluorescence based	Al-Rawhani Et al. [C6.60]	No	Small bowel	N.A.	SPAD, ASIC chip	1 LED	RF	Yes	N.G.	Yes
	Demosthenous et al. [C6.61][C6.62]	Yes	Small bowel	N.A.	6 photodiodes	6 laser diodes	SPI	No	~500	No
	Kfouri et al. [C6.63]	No	GI tract	640x480	1CCD	8 LED	RF	Yes	N.G.	No

Table 6.4 (continued)

Fluorescence based	Nemiroski et al. [C6.64]	No	GI Bleeding	N.A.	1 photodiode	1 LED	Zigbee	Yes	~110	No
	Ryou et al. [C6.65]	No	GI bleeding	N.A.	N.G.	N.G.	RF	Yes	N.G.	No
	Proposed Device	Yes	Colorectal Cancer	N.A.	Spectral sensor	4 LED	RF	Yes	71.12	Yes

TE= targeted endoscopy; I/S= illumination source; TM = transmission mode; RT= realtime; "-"= not mentioned; DL= data logger; N.A. = Not applicable; N.G. = Not Given

This is the material cost of lab prototype as shown in Table 6.1.

Moreover, the frame rate and resolution of the GI image in the existing system is not optimal for proper diagnosis of GI abnormalities. There are few non-camera based WCE systems which can measure different physiological parameters, such as pH, temperature and pressure. Removing the cameras will significantly increase the battery life of the capsule and reduce the cost. In addition, there are other capsules at the research stage which aim to detect bleeding and automate the detection of a cancer. Some of them utilize the property of autofluorescence to automate the detection process. However, autofluorescence comes with reduced specificity and sensitivity in automating cancer detection. As a result, this technique does not provide enough contrast when compared to normal and abnormal cells, because the signal from the cancerous cells are often buried under the autofluorescence of healthy cells. In addition, the intensity of autofluorescence is dependent on diet [C6.72]. To the best of our knowledge, there is no work which proposes fluorescence-based targeted WCE system for detecting colorectal cancer.

6.4 Summary and Outlook

Targeted fluorescence-based WCE systems have the advantage of improving specificity and sensitivity over the current generation of conventional WCE systems. They improve the diagnostic as well as screening procedures of the entire GI tract. In addition to being non-invasive, these capsules present us with an opportunity to enable automatic detection of abnormalities. One of the main challenges in designing such a system is to make these devices small enough that a

patient can swallow it. The components used to build the proposed prototype are available off-the-shelf. The developed capsule size is 16 mm × 34 mm. Further miniaturization can be done by using custom-designed components. Moreover, this device also removes the need for bulky components (such as optical filters and a mounting holder) which reduces the cost of the device.

Most colon cancers begin as pre-cancerous polyps. Therefore, screening for cancer in a timely manner will allow physicians to find and treat different types of cancer at an early stage before they cause symptoms. This will lower the burden on both the patient and the healthcare system. After the screening procedure is completed and a positive sign of cancer is suspected, other confirmatory tests (such as CT, PET-CT, MRI, or ultrasound scans) can be performed to confirm the findings and locate the cancerous cell [C6.73]. The follow-up treatment usually depends upon location, stage and type of the cancer. Moreover, researchers have been working on monoclonal antibodies that can recognize and attach to specific proteins which are produced by cells. Each monoclonal antibody can target only a specific protein. Different antibodies differ in functionality and are selected based on the type of protein that they are targeting. Some of these antibodies block the protein that aids in the growth of the cancer, while others detach cancer cells from the blood supply, prohibiting growth [C6.74]. The main treatments for early-detected cancers are surgery and chemotherapy. Other treatments include radiotherapy and targeted cancer drugs [C6.75]. These treatment strategies are based on the stage at which the cancer is detected.

Due to the invasive characteristics of the traditional endoscopic system, most patients are reluctant to go through the procedure, adversely affecting the early-detection process and the possibility of efficient treatment. Therefore, the non-invasive WCE technology can help with early detection. The proposed device can detect multiple fluorescence signals from multiple fluorophores; therefore, it may be possible to detect other types of cancers by using different fluorophores that would bind to the specific antigen of a specific cancer cell. The development of a single WCE device for detecting multiple cancers may be possible in the future.

In the future, a camera can also be placed on the other end of the WCE device which will only turn on to capture the GI images when an increased level of fluorescence is detected. This would help the physicians examine the abnormality visually, thereby increasing the efficiency, as well as the reliability of the system. The battery life of the proposed capsule can be improved by using the adaptive illumination technique [C6.76]. Moreover, we have previously tested the

139

PillCam SB3 capsule on horses [C6.77]. It would be interesting to see the application of this technology in veterinary medicine.

In order to provide the best and most effective healthcare, the Internet of Things (IoT) offers new ways of improving the system by presenting novel facilities and enhancing the functionalities of the existing system. It is estimated that the hospital-centered healthcare system will be transformed to a home-centered system by 2030 [C6.78]. Thus, it is imperative that the IoT is introduced into the WCE system as well. The existing WCE systems cannot yet offer real-time detection as the diagnosis is mainly done offline [C6.6]. In addition, a self-data analyzing intelligent system could be helpful, which can select useful data for transmission and save transmission cost, bandwidth, and energy. To develop an IoT-based system, features like intelligence, heterogeneous network connectivity, real-time sensing, and security may be incorporated into the system

6.5 Conclusion

WCE has enabled a pathway towards pain-free diagnosis and screening of the entire GI tract. This system has encouraged patients to go through the examinations, ultimately paving the way for mass screening and enabling early diagnosis of GI abnormalities. The current generation of WCE systems has several limitations which restrict its wide application. Hence, in this paper, we have presented the design and development of a complete WCE system, which utilized the principle of fluorescence imaging, capable of performing targeted endoscopy. The developed capsule consists of four major units: illumination, processor, transceiver and power. Each of these units was separately tested before integrating into a complete system. Initial experiments with various solutions and phantoms have demonstrated that the proposed device is capable of selective and specific detection of abnormal colorectal cancerous cells.

.

References

[C6.1]   Pomerai, D.D.; Daniells, C.; David, H.; Allan, J.; Duce, I.; Mutwakil, M.; Thomas, D.; Sewell, P.; Tattersall, J.; Jones, D.; et al. Wireless capsule endoscopy. Nature 2000, 405, 417–418.

[C6.2]   Alam, M.W.; Hasan, M.M.; Mohammed, S.K.; Deeba, F.; Wahid, K.A. Are Current Advances of Compression Algorithms for Capsule Endoscopy Enough? A Technical Review. IEEE Rev. Biomed. Eng. 2017, 10, 26–43.

[C6.3]   El-Matary, W. Wireless Capsule Endoscopy: Indications, Limitations, and Future Challenges. J. Pediatr. Gastroenterol. Nutr. 2008, 46, 4–12.

[C6.4]   Pan, G.; Xin, W.; Yan, G.; Chen, J. A video wireless capsule endoscopy system powered wirelessly: Design, analysis and experiment. In Proceedings of the Measurement Science and Technology; Institute of Physics Publishing: Bristol, UK, 2011; Volume 22.

[C6.5]   Li, B.; Meng, M.Q.H. Computer-based detection of bleeding and ulcer in wireless capsule endoscopy images by chromaticity moments. Comput. Biol. Med. 2009, 39, 141–147.

[C6.6]   Alam, M.W.; Sohag, M.H.A.; Khan, A.H.; Sultana, T.; Wahid, K.A. IoT-Based Intelligent Capsule Endoscopy System: A Technical Review. In Intelligent Data Analysis for Biomedical Applications; Hemanth, J., Gupta, D., Balas, V.E., Eds.; Elsevier: Amsterdam, The Netherlands, 2019; pp. 1–20, ISBN 978-0-12-815553-0.

[C6.7]   Iakovidis, D.K.; Koulaouzidis, A. Software for enhanced video capsule endoscopy: Challenges for essential progress. Nat. Rev. Gastroenterol. Hepatol. 2015, 12, 172–186.

[C6.8]   Suman, S.; Hussin, F.; Malik, A.; Ho, S.; Hilmi, I.; Leow, A.; Goh, K.-L. Feature Selection and Classification of Ulcerated Lesions Using Statistical Analysis for WCE Images. Appl. Sci. 2017, 7, 1097.

[C6.9]   Gray, M.; Moore, J.M.; Brock, A. A re-review of caspule endoscopies of patients referred for deep enteroscopy changes their management. Gastrointest. Interv. 2014, 3, 89–92.

[C6.10]   Levinthal, G.N.; Burke, C.A.; Santisi, J.M. The accuracy of an endoscopy nurse in interpreting capsule endoscopy. Am. J. Gastroenterol. 2003, 98, 2669–2671.

[C6.11]   Siegel, R.L.; Miller, K.D.; Jemal, A. Cancer statistics, 2017. CA Cancer J. Clin. 2017, 67, 7–30.

[C6.12]   WHO | Early Diagnosis and Screening. Available online: https://www.who.int/cancer/prevention/diagnosis-screening/en/ (accessed on 1 February 2020).

[C6.13]   Why is early diagnosis important? | Cancer Research UK. Available online: https://www.cancerresearchuk.org/about-cancer/cancer-symptoms/why-is-early-diagnosis-important (accessed on 1 February 2020).

[C6.14]   CT Colonography. Available online: https://www.radiologyinfo.org/en/info.cfm?pg=ct_colo (accessed on 25 January 2020).

[C6.15]   Ginnerup Pedersen, B.; Rosenkilde, M.; Christiansen, T.E.M.; Laurberg, S. Extracolonic findings at computed tomography colonography are a challenge. Gut 2003, 52, 1744–1747.

[C6.16]   Holme, Ø.; Løberg, M.; Kalager, M.; Bretthauer, M.; Hernán, M.A.; Aas, E.; Eide, T.J.; Skovlund, E.; Lekven, J.; Schneede, J.; et al. Sigmoidoscopy Screening for Colorectal Cancer. Ann. Intern. Med. 2018, 168, I-24.

[C6.17]   Burki, T. Flexible sigmoidoscopy screening for colorectal cancer. Lancet. Oncol. 2018, 19, e291.

[C6.18]   Glick, S. Double-Contrast Barium Enema for Colorectal Cancer Screening. Am. J. Roentgenol. 2000, 174, 1529–1537.

[C6.19]   Imperiale, T.F.; Ransohoff, D.F.; Itzkowitz, S.H.; Levin, T.R.; Lavin, P.; Lidgard, G.P.; Ahlquist, D.A.; Berger, B.M. Multitarget Stool DNA Testing for Colorectal-Cancer Screening. N. Engl. J. Med. 2014, 370, 1287–1297.

[C6.20]   Wieten, E.; Schreuders, E.H.; Grobbee, E.J.; Nieboer, D.; Bramer, W.M.; Lansdorp-Vogelaar, I.; Bruno, M.J.; Kuipers, E.J.; Spaander, M.C.W. Incidence of faecal occult blood test interval cancers in population-based colorectal cancer screening: A systematic review and meta-analysis. Gut 2019, 68, 873–881.

[C6.21]   Howard, R.; Machado-Aranda, D. Frailty as a Predictor of Colonoscopic Procedural Risk: Robust Associations from Fragile Patients. Dig. Dis. Sci. 2018, 63, 3159–3160.

[C6.22]   American Society of Clinical Oncology Colorectal Cancer: Statistics | Cancer.Net. Available online: https://www.cancer.net/cancer-types/colorectal-cancer/statistics (accessed on 1 February 2020).

[C6.23]   Haustein, E.; Schwille, P. Trends in fluorescence imaging and related techniques to unravel biological information. HFSP J. 2007, 1, 169–180.

[C6.24]   Gautier, A.; Tebo, A.G. Fluorogenic Protein-Based Strategies for Detection, Actuation, and Sensing. BioEssays 2018, 40, 1800118.

[C6.25]   Schneider, A.F.L.; Hackenberger, C.P.R. Fluorescent labelling in living cells. Curr. Opin. Biotechnol. 2017, 48, 61–68.

[C6.26]   Borisova, E.G.; Angelova, L.P.; Pavlova, E.P. Endogenous and exogenous fluorescence skin cancer diagnostics for clinical applications. IEEE J. Sel. Top. Quantum Electron. 2014, 20, doi:10.1109/JSTQE.2013.2280503.

[C6.27]   Van Dam, G.M.; Themelis, G.; Crane, L.M.A.; Harlaar, N.J.; Pleijhuis, R.G.; Kelder, W.; Sarantopoulos, A.; De Jong, J.S.; Arts, H.J.G.; Van Der Zee, A.G.J.; et al. Intraoperative tumor-specific fluorescence imaging in ovarian cancer by folate receptor-α targeting: first in-human results. 2011, 17, 1315–1319.

[C6.28]   Luo, S.; Zhang, E.; Su, Y.; Cheng, T.; Shi, C. A review of NIR dyes in cancer targeting and imaging. Biomaterials 2011, 32, 7127–7138.

[C6.29]   Alam, M.W.; Wahid, K.A.; Goel, R.K.; Lukong, K.E.; Alam, M.W.; Wahid, K.A.;
           Goel, R.K.; Lukong, K.E. Development of a low-cost and portable smart fluorometer
           for detecting breast cancer cells. Biomed. Opt. Express 2019, 10, 399–410.

[C6.30]   Alam, M.W.; Wahid, K.A.; Fahmid Islam, M.; Bernhard, W.; Geyer, C.R.;
           Vizeacoumar, F.J. A Low-Cost and Portable Smart Instrumentation for Detecting
           Colorectal Cancer Cells. Appl. Sci. 2019, 9, 3510.

[C6.31]   Fluorescein   (FITC/DTAF)—Jackson   ImmunoResearch.   Available
           online: https://www.jacksonimmuno.com/technical/products/conjugate-
           selection/fitc (accessed on 25 March 2020).

[C6.32]   Yannuzzi, L.A.; Rohrer, K.T.; Tindel, L.J.; Sobel, R.S.; Costanza, M.A.; Shields, W.;
           Zang, E. Fluorescein Angiography Complication Survey. Ophthalmology 1986, 93,
           611–617.

[C6.33]   Lipson, B.K.; Yannuzzi, L.A. Complications of intravenous fluorescein injections.
           Int. Ophthalmol. Clin. 1989, 29, 200–205.

[C6.34]   Acerbi, F.; Broggi, M.; Schebesch, K.M.; Höhne, J.; Cavallo, C.; De Laurentis, C.;
           Eoli, M.; Anghileri, E.; Servida, M.; Boffano, C.; et al. Fluorescein-guided surgery
           for resection of high-grade gliomas: A multicentric prospective phase II study
           (FLUOGLIO). Clin. Cancer Res. 2018, 24, 52–61.

[C6.35]   Spiguel, L.; Shaw, C.; Katz, A.; Guo, L.; Chen, H.-C.; Lee, B.T.; Singhal, D.
           Fluorescein Isothiocyanate. Ann. Plast. Surg. 2017, 78, S296–S298.

[C6.36]   Xiao, S.Y.; Zhang, J.; Zhu, Z.Q.; Li, Y.P.; Zhong, W.Y.; Chen, J.B.; Pan, Z.Y.; Xia,
           H.C. Application of fluorescein sodium in breast cancer brain-metastasis surgery.
           Cancer Manag. Res. 2018, 10, 4325–4331.

[C6.37]   Kiesslich, R.; Neurath, M.F. Endoscopic detection of early lower gastrointestinal
           cancer. Best Pract. Res. Clin. Gastroenterol. 2005, 19, 941–961.

[C6.38]   Belykh, E.; Martirosyan, N.L.; Yagmurlu, K.; Miller, E.J.; Eschbacher, J.M.;
           Izadyyazdanabadi, M.; Bardonova, L.A.; Byvaltsev, V.A.; Nakaji, P.; Preul, M.C.
           Intraoperative Fluorescence Imaging for Personalized Brain Tumor Resection:

Current State and Future Directions. Front. Surg. 2016, 3, doi:10.3389/fsurg.2016.00055.

[C6.39]   Chen, B.; Wang, H.; Ge, P.; Zhao, J.; Li, W.; Gu, H.; Wang, G.; Luo, Y.; Chen, D. Gross Total Resection of Glioma with the Intraoperative Fluorescence-guidance of Fluorescein Sodium. Int. J. Med. Sci 2012, 2012, 9.

[C6.40]   Pèlegrin, A.; Folli, S.; Buchegger, F.; Mach, J.-P.; Wagnières, G.; Van Den Bergh, H. Antibody–fluorescein conjugates for photoimmunodiagnosis of human colon carcinoma in nude mice. Cancer 1991, 67, 2529–2537.

[C6.41]   Hasan, M.M.; Alam, M.W.; Wahid, K.A.; Miah, S.; Lukong, K.E. A Low-Cost digital microscope with real-Time fluorescent imaging capability. PLoS ONE 2016, 11, e0167863.

[C6.42]   AZ13DP-8 Energizer Battery Company | Battery Products | DigiKey. Available online: https://www.digikey.ca/products/en/battery-products/batteries-non-rechargeable-primary/90?k=coin-i-battery&k=&pkeyword=coin-i-battery&sv=0&pv1989=0&pv33=164442&sf=0&FV=-8%7C90&quantity=&ColumnSort=0&page=1&pageSize=25 (accessed on 24 November 2019).

[C6.43]   Voska, M.; Zavoral, M.; Grega, T.; Majek, O.; Martinek, J.; Tacheci, I.; Benes, M.; Vojtechova, G.; Drastich, P.; Bures, J.; et al. Accuracy of colon capsule endoscopy for colorectal neoplasia detection in individuals referred for a screening colonoscopy. Gastroenterol. Res. Pract. 2019, 2019, doi:10.1155/2019/5975438.

[C6.44]   Sieg, A.; Friedrich, K.; Sieg, U. Is PillCam COLON capsule endoscopy ready for colorectal cancer screening a prospective feasibility study in a community gastroenterology practice. Am. J. Gastroenterol. 2009, 104, 848–854.

[C6.45]   Rácz, I.; Jánoki, M.; Saleh, H. Colon Cancer Detection by 'Rendezvous Colonoscopy': Successful Removal of Stuck Colon Capsule by Conventional Colonoscopy. Case Rep. Gastroenterol. 2010, 4, 19–24.

[C6.46]   D'Haens, G.; Löwenberg, M.; Samaan, M.A.; Franchimont, D.; Ponsioen, C.; van den Brink, G.R.; Fockens, P.; Bossuyt, P.; Amininejad, L.; Rajamannar, G.; et al. Safety and Feasibility of Using the Second-Generation Pillcam Colon Capsule to Assess Active Colonic Crohn's Disease. Clin. Gastroenterol. Hepatol. 2015, 13, 1480–1486.

[C6.47]   Chen, C.; Pomalaza-Ráez, C. Design and Evaluation of a Wireless Body Sensor System for Smart Home Health Monitoring. In Proceedings of the GLOBECOM—IEEE Global Telecommunications Conference, Honolulu, HI, USA, 30 November–4 December 2009.

[C6.48]   Li, R.; Guo, Y.X.; Du, G. A Conformal Circularly Polarized Antenna for Wireless Capsule Endoscope Systems. IEEE Trans. Antennas Propag. 2018, 66, 2119–2124.

[C6.49]   Liu, C.; Guo, Y.X.; Xiao, S. Circularly polarized helical antenna for ISM-band ingestible capsule endoscope systems. IEEE Trans. Antennas Propag. 2014, 62, 6027–6039.

[C6.50]   Lee, S.H.; Lee, J.; Yoon, Y.J.; Park, S.; Cheon, C.; Kim, K.; Nam, S. A wideband spiral antenna for ingestible capsule endoscope systems: Experimental results in a human phantom and a pig. IEEE Trans. Biomed. Eng. 2011, 58, 1734–1741.

[C6.51]   Means, D.L.; Chan, K.W. Evaluating Compliance with FCC Guidelines for Human Exposure to Radiofrequency Electromagnetic Fields Additional Information for Evaluating Compliance of Mobile and Portable Devices with FCC Limits for Human Exposure to Radiofrequency Emissions; Office of Engineering and Technology Federal Communications Commission: Washington, DC, USA, 2001.

[C6.52]   Khan, T.H.; Wahid, K.A. An advanced physiological data logger for medical imaging applications. Eurasip J. Embed. Syst. 2012, 2012, 1–14.

[C6.53]   Cave, D.R.; Fleischer, D.E.; Leighton, J.A.; Faigel, D.O.; Heigh, R.I.; Sharma, V.K.; Gostout, C.J.; Rajan, E.; Mergener, K.; Foley, A.; et al. A multicenter randomized comparison of the Endocapsule and the Pillcam SB. Gastrointest. Endosc. 2008, 68, 487–494.

[C6.54]   Aasen, T.D.; Wilhoite, D.; Rahman, A.; Devani, K.; Young, M.; Swenson, J. No significant difference in clinically relevant findings between Pillcam ® SB3 and Pillcam ® SB2 capsules in a United States veteran population. World J. Gastrointest. Endosc. 2019, 11, 124–132.

[C6.55]   PillCamTM SB 3 System | Medtronic. Available online: https://www.medtronic.com/covidien/en-us/products/capsule-endoscopy/pillcam-sb-3-system.html (accessed on 3 February 2020).

[C6.56]   Eisen, G.M.; Eliakim, R.; Zaman, A.; Schwartz, J.; Faigel, D.; Rondonotti, E.; Villa, F.; Weizman, E.; Yassin, K.; de Franchis, R. The Accuracy of PillCam ESO Capsule Endoscopy Versus Conventional Upper Endoscopy for the Diagnosis of Esophageal Varices: A Prospective Three-Center Pilot Study. Endoscopy 2006, 38, 31–35.

[C6.57]   PillCamTM COLON 2 System | Medtronic. Available online: https://www.medtronic.com/covidien/en-us/products/capsule-endoscopy/pillcam-colon-2-system.html (accessed on 3 February 2020).

[C6.58]   MiroCam. Available online: http://www.medivators.com/products/gi-physician-products/mirocam-capsule-endoscope (accessed on 24 June 2017).

[C6.59]   Capsule Endoscopy | ENDOCAPSULE 10 System | Olympus Medical Systems. Available online: https://www.olympus-europa.com/medical/en/Products-and-Solutions/Products/Product/ENDOCAPSULE-10-System.html (accessed on 21 November 2019).

[C6.60]   OMOM Capsule Endoscopy, JINSHAN Science & Technology. Available online: http://english.jinshangroup.com/capsuleendoscopy.html (accessed on 3 February 2020).

[C6.61]   CapsoCam Plus® | CapsoVision. Available online: https://www.capsovision.com/products/capsocam-plus (accessed on 3 February 2020).

[C6.62]   SmartPillTM   Motility   TestingSystem| Medtronic.   Available
          online: https://www.medtronic.com/covidien/en-us/products/motility-
          testing/smartpill-motility-testing-system.html (accessed on 3 February 2020).

[C6.63]   CorTemp, HQ Inc. Available online: https://hqinc.net/ (accessed on 3 February
          2020).

[C6.64]   Philips   Respironics | VitalSense.   Available   online:
          http://www.actigraphy.com/solutions/vitalsense/ (accessed on 3 February 2020).

[C6.65]   e-Celsius   Performance, Bodycap.   Available   online:
           http://www.bodycap-medical.com/en/product/ecelsius-performance (accessed on 3
          February 2020).

[C6.66]   Al-Rawhani, M.A.; Chitnis, D.; Beeley, J.; Collins, S.; Cumming, D.R.S. Design and
          implementation of a wireless capsule suitable for autofluorescence intensity detection
          in biological tissues. IEEE Trans. Biomed. Eng. 2013, 60, 55–62.

[C6.67]   Demosthenous, P.; Pitris, C.; Georgiou, J. Infrared Fluorescence-Based Cancer
          Screening Capsule for the Small Intestine. IEEE Trans. Biomed. Circuits and
          Systems, 2016, 10(2), 467-476.

[C6.68]   Demosthenous, P.; Georgiou, J. Towards a fluoroscopic cancer screening capsule for
          the small intestine. 2014 36th Annual International Conference of the IEEE
          Engineering in Medicine and Biology Society, Chicago, IL, USA, 2014; pp. 3122–
          3125.

[C6.69]   Kfouri, M.; Marinov, O.; Quevedo, P.; Faramarzpour, N.; Shirani, S.; Liu, L.W.C.;
          Fang, Q.; Deen, M.J. Toward a miniaturized wireless fluorescence-based diagnostic
          imaging system. IEEE J. Sel. Top. Quantum Electron. 2008, 14, 226–234.

[C6.70]   Nemiroski, A.; Ryou, M.; Thompson, C.C.; Westervelt, R.M. Swallowable
          fluorometric capsule for wireless triage of gastrointestinal bleeding. Lab. Chip 2015,
          15, 4479–4487.

[C6.71]   Ryou, M.; Nemiroski, A.; Azagury, D.; Shaikh, S.N.; Ryan, M.B.; Westervelt, R.M.;
          Thompson, C.C. An implantable wireless biosensor for the immediate detection of

148

upper GI bleeding: A new fluorescein-based tool for diagnosis and surveillance (with video). Gastrointest. Endosc. 2011, 74, 189–194.

[C6.72]   Inoue, Y.; Izawa, K.; Kiryu, S.; Tojo, A.; Ohtomo, K. Diet and Abdominal Autofluorescence Detected by in Vivo Fluorescence Imaging of Living Mice. Mol. Imaging 2008, 7, doi:10.2310/7290.2008.0003.D. De Pomerai et al., "Wireless capsule endoscopy," Nature, vol. 405, no. May, pp. 417–418, 2000.

[C6.73]   Tests to Stage | Bowel Cancer | Cancer Research UK. Available online: https://www.cancerresearchuk.org/about-cancer/bowel-cancer/getting-diagnosed/tests-stage (accessed on 17 March 2020).

[C6.74]   Weiner, G.J. Building better monoclonal antibody-based therapeutics. Nat. Rev. Cancer 2015, 15, 361–370.

[C6.75]   Types of Cancer Treatment—National Cancer Institute. Available online: https://www.cancer.gov/aboutcancer/treatment/types (accessed on 17 March 2020).

[C6.76]   Shrestha, R.; Mohammed, S.K.; Hasan, M.M.; Zhang, X.; Wahid, K.A. Automated Adaptive Brightness in Wireless Capsule Endoscopy Using Image Segmentation and Sigmoid Function. IEEE Trans. Biomed. Circuits Syst. 2016, 10, 884–892.

[6.77]   Montgomery, J.B.; Bracamonte, J.L.; Alam, M.W.; Khan, A.H.; Mohammed, S.K.; Wahid, K.A. Is there an application for wireless capsule endoscopy in horses? Can. Vet. J. 2017, 58, 1321–1325.

[6.78]   Qu, Y.; Nosouhi, M.R.; Cui, L.; Yu, S. Privacy Preservation in Smart Cities. In Smart Cities Cybersecurity and Privacy; Elsevier: Amsterdam, The Netherlands, 2019; pp. 75–88.

Addendum on Chapter 6

Most WCE systems are image-based. The imaging capability in a WCE system is an attractive choice as it provides an important functionality of visualization of GI tract. However, it comes with several limitations as discussed in Chapter 1 and 2. The image-based capsule generates a minimum of 144,000 frames during its lifetime when it captures at 4 frame per second. These capsule lacks the functionality of automatic detection of abnormalities, which is why, the physicians are required to go through each frame in search of abnormality. The post-processing of such endoscopic procedure heavily relies on the expertise of a physician. Such analysis requires the patient to have distinct morphological changes in order to be diagnosed accurately. These morphological changes often appear late, which hampers the overall diagnostic procedure which is discussed in section 6.4. This is why, the principle of fluorescence is used in the developed WCE system to screen colorectal cancer.

In the targeted fluorescence endoscopy system, the fluorescence signal from the cancerous cells labelled with the exogenous fluorophores is more than the surrounding healthy tissues which results in an increased detection rate. Antigen with the labelled fluorophores binds to the target tumor in the GI tract leading to the generation of a stronger signal which is detected with the AS7262 sensor of the developed capsule. Utilizing this technique enhances sensitivity and specificity of the developed device as well. For this, a fluorophore (fluorescein) was selected which is FDA approved to be used in humans. The peak excitation and emission wavelength of fluorescein is 494 nm and 521 nm respectively. It is to be noted that although the peak excitation wavelength is 494 nm, the fluorescein can be excited by illuminating in the UV region as well in order to get emitted fluorescent signal. Also, the greater the difference between excitation and emission spectra, the lesser is the probability of false positive detection caused due to the interference of excitation source. For this region, the excitation source is chosen in such a way that the fluorescein is illuminated in the UV region and the detection is performed in green channel. This ensures that there is no overlap between excitation source and the detection sensor. The excitation source (UV LED) and the detection source (green channel of AS7262 sensor) was chosen based on the fluorophore (fluorescein). The fluorescence signal measured by the AS7262

sensor is in raw 16-bit integer format. The AS7262 sensor contains 16-bit ADC. Thus, the voltage is measured by the following formula:

$$\frac{Resolution\ of\ the\ ADC}{System\ Voltage} = \frac{ADC\ reading}{voltage\ measured} \tag{6.5}$$

This device also removes the need of extra components such as dichroic mirror, excitation mirror and filter cube which is usually present in fluorescent microscope as shown in Figure 5.1. It has been previously shown in Chapter 4 and 5 that by careful selection of the excitation source, detection sensor, and emission filter, it is possible to remove other components (dichroic mirror, excitation filter, filter cube) without affecting performance. Moreover, the AS7262 sensor was selected for this study because this sensor has built-in filters which ensures that the detected signals are coming from the fluorophore and not from other light sources. Removing the extra components (such as dichroic mirror, excitation filter, external emission filter and filter cube) helps in keeping the size smaller while reducing the weight and the complexity of the developed system. The distance between the intestine and the capsule was kept at 1 cm while screening intestine in this study. Further experiment also needs to be performed to detect multiple cancers with a single device in the scenario where the patient has multiple cancer.

As shown in Table 6.4, the imaging capsule has low frame rate and resolution which hampers the diagnostic process. The higher frame rate leads to increased in the number of captured images which leads to more work for physicians. The lack of automatic detection of abnormality further makes this technology unpopular. As discussed in Chapter 3, the use of cameras adds an important functionality of visualization but comes with several limitations. The use of cameras hampers the battery life which leads to the decrease in completion rates, especially in those patients who has GI complications. The cost of the image-based capsules is also higher than the capsules which are sensor based. The battery life is found to be lower and the demand of transmission power is higher in image-based capsule. The image-based capsule also requires a complex system architecture, higher on-chip memory and efficient compression algorithm. When compared to image-based capsule, the sensor-based capsules are simple, consumes less power, has higher battery life, requires low data-rate, low bandwidth and is cheaper. Since the sensor-based capsule has higher battery life, multiple sensors can be used to monitor vital signals making it an attractive choice as well.

7. Conclusion and Future Direction

7.1 Summary and Conclusion

In this thesis, a fluorescence based WCE system for early-stage automated detection of colorectal cancer is presented. The development of such device which screens the GI tract and detects low-level of fluorescence emitted by fluorophore conjugated cancer cells, presents a novel, pain-free, non-invasive screening method for early-stage detection of colorectal cancer. We envision that the final fluorescence based WCE system will be able automate the detection of multiple types of cancer using a single electronic capsule. In implementing this prototype, a number of unique features were tested that were used in other applications:

- Design and development of low-cost fluorescent microscope for selective detection of breast cancer cells.
- Design and development of fluorometer for detecting colorectal cancer and breast cancer cells.
- Design and development of a complete WCE system to screen colorectal region.
- Reducing power consumption, avoiding unnecessary data collection, while providing a way to scan entire GI tract.
- Proposed the principle to diagnose multiple cancer with one capsule.
- Early-stage cancer detection, promoting mass screening and ultimately improving the survival rate of such patients.

In Chapter 3, various WCE systems and their compression algorithms were reviewed. It was concluded that an extensive research work is still needed to achieve higher compression ratio while maintaining acceptable quality of image. The advancement of camera in today's world has made capturing of high-quality images possible. However, transmitting such image would adversely affect the power consumption of the capsule. Hence, there is a need to compress the captured image so that the capsule can work for at least 8 hours for screening the GI tract. However, the available compression algorithms are lossy and requires complex system architecture and on-chip memory. These also affect the power consumption. When compression algorithm is applied to the captured images, it affects its quality. If the image is of low resolution, the diagnostic is

152

error-prone. Increasing frame rate and maintaining image quality will help in efficient diagnosis but at the cost of higher power consumption and reduced battery life of the capsule. Hence, alternative ways were needed to be explored in order to screen colorectal cancer. As such, we worked towards a WCE system based on fluorescence.

Fluorescence imaging is widely used in the field of biology for selective and specific detection of objects of interest. This technique is commonly used to view, localize, and track fluorescing particles in a wide selection of organic and inorganic structures. Also, the intrinsic fluorescent products (such as GFP) allows biologists to genetically tag protein of living beings which leads us into a new era of fluorescence microscopy. For optimal and efficient use of fluorescence microscopy and to determine the feasibility of this technique in WCE system, it was important to have basic knowledge of strengths and weaknesses of different approaches as well as an understanding of the elementary trade-offs of the variables related to it. In Chapter 4, we used off-the-shelf components to build a fluorometer in order to differentiate breast cancer cells conjugated with GFP with the control cells. The excitation and emission maximum of GFP fluorophore is 495 nm and 519 nm respectively. The filter, light source and photodiode were carefully chosen to cover the excitation and emission region of this fluorophore. MDA-MB-31 breast cancer cells expressing GFP were tested with the developed fluorometer. The results were validated with a commercial microscope (Olympus IX51). This worked helped us realize the potential of fluorescence imaging and its probable use in the WCE device for detecting GI abnormalities. Hence, the next step was to target GI cancer.

In Chapter 5, the developed fluorometer was used to detect colorectal cancer. An established colorectal cancer cell line (human colorectal carcinoma (HCT116)) was cultured and a near-infrared fluorescent protein IRFP702 was expressed in the colorectal cancer cells. These cells were used to test the proof-of-concept. The developed fluorometer distinguished the fluorescently labelled cells with control cells successfully. The cells were then tested with a commercial imaging system (Odyssey CLx) to validate the result. The developed fluorometer is versatile as multiple types of cancer can be detected by changing the filters, excitation and emission source. The observed readings from this chapter confirmed that it was possible to detect fluorescence using off-the-shelf components with specific and selective detection.

In Chapter 6, utilizing the concepts developed in earlier chapters, a WCE prototype was developed. The capsule prototype is comprised of four main printed circuit boards (PCBs): the sensor board with illumination components, control/processor board, telemetry board and the power module. The illumination and detection source were selected based on the target fluorophore. The peak excitation and emission wavelength of fluorescein is 494 nm and 521 nm respectively. In order to validate the working of the developed prototype, it was tested on porcine intestine, liquid phantom and minced meat. The distance between the capsule and the intestine was kept at 1 cm for all measurements. The developed system is able to successfully detect the varying level of fluorescence and send it to the data logger, making early detection possible. The results are promising and we strongly believe that it is possible that the capsule can automate the detection of multiple cancer in near future.

7.2 Future Research Direction

It would be interesting to further develop the capsule for commercial use. One of the hindrances is the size. The size and power of the capsule could be reduced by using custom components so that the capsule is swallowable and can last longer for increased diagnostic completion rates. These can also be used to increase fluorescence detection sensitivity. This study performed initial testing with small sample size. Further testing and analysis (such as Receiver Operating Characteristics curve) with higher sample size and different concentration is needed to further test the efficiency of this device. The proof-of-concept to screen colorectal cancer is shown in this thesis. The capsule can be further modified to detect multiple types of cancer by placing multiple sensor at both end of capsule. Further experiment also needs to be performed to detect multiple cancers with a single device in the scenario where the patient has multiple cancer. There is no denying that the camera will continue to be a popular choice in the WCE world as it offers an important functionality of visualization of abnormalities as shown in Table 6.4. This is why, the camera can also be placed at the other end which would only turn on when the required spike in fluorescence is measured, allowing to visualize and confirming the detection. This will ensure that both image and sensor-based functionality exists in a single capsule while allowing for visual functionality and ensuring that the capsule will run for more than 8 hours. A series of in-vivo testing on animal models is required. This will help to prove the feasibility of using these capsules

to detect multiple cancers in living beings in near future. Although the space and computing resources were limited in the proposed capsule, one can imagine that a more complex system can be developed in the future for cancer diagnosis such that the tumors could be treated on the spot without having to undergo uncomfortable and painful colonoscopies or surgery. Other biosensors such as pH, temperature, etc. can be integrated in the capsule to monitor other parameters and relate it to the data to improve efficiency. Works can also be done on localization of the capsule. In future, functionality such as, drug delivery, tissue sampling and robotic legs can be integrated into the platform. Other future directions are also presented in a published book chapter [Appendix A1, publication no. 3].

Appendix

A1. Other Publications:

These publications are also published which are related to my doctoral program but are not included in this dissertation as chapters.

[1] Md. Mehedi Hasan, Mohammad Wajih Alam, Khan. A. Wahid, Sayem Miah, and Kiven Erique Lukong, "A Low-Cost digital microscope with real-Time fluorescent imaging capability," PLoS One, vol. 11, no. 12, p. e0167863, Dec. 2016.

[2] Julia B. Montgomery, Jose L. Bracamonte, Mohammad Wajih Alam, Alimul H. Khan, Shahed K. Mohammed, Khan A. Wahid. Is there an application for wireless capsule endoscopy in horses?. Can Vet J. 2017;58 (12):1321–1325.

[3] Mohammad Wajih Alam, Mohammad Hanif Ali Shohag, Alimul Haque Khan, Tanin Sultana, Khan A. Wahid. IoT-Based Intelligent Capsule Endoscopy System: A Technical Review. In Intelligent Data Analysis for Biomedical Applications; Hemanth, J., Gupta, D., Balas, V.E., Eds.; Elsevier, 2019; pp. 1–20.